

-Modeling and Design of Pultruded FRP Members-

-Swapnil Dwivedi-

A Dissertation Submitted to
Indian Institute of Technology Hyderabad
In Partial Fulfillment of the Requirements for
The Degree of Master of Technology



भारतीय प्रौद्योगिकी संस्थान हैदराबाद
Indian Institute of Technology Hyderabad

Department of {civil} Engineering

July, 2018

Declaration

I declare that this written submission represents my ideas in my own words, and where others' ideas or words have been included, I have adequately cited and referenced the original sources. I also declare that I have adhered to all principles of academic honesty and integrity and have not misrepresented or fabricated or falsified any idea/data/fact/source in my submission. I understand that any violation of the above will be a cause for disciplinary action by the Institute and can also evoke penal action from the sources that have thus not been properly cited, or from whom proper permission has not been taken when needed.

Swapnil

(Signature)

SWAPNIL DWIVEDI

(- Student Name -)

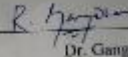
CEIS MITECH 110251

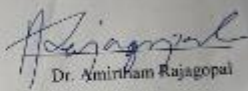
(Roll No)

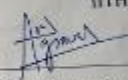
Approval Sheet

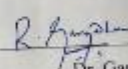
Approval Sheet

This thesis entitled **Modeling and Design of Pultruded FRP Members** by Swapnil Dwivedi is approved for the degree of Master of Technology


Dr. Gangadharan R
Examiner
Dept. of Mechanical Engg.
IITH


Dr. Amirtham Rajagopal
Examiner
Dept. of Civil Engg.
IITH


Dr. Anil Agarwal
Adviser
Dept. of Civil Engg.
IITH


Dr. Gangadharan R
Chairman
Dept. of Mechanical Engg.
IITH

Acknowledgements

I would like to thank my advisor Dr. Anil agarwal whose guidance helped me to complete my research project. His guidance and efforts helped me to complete objectives of research. His investment of time and efforts on my research helped me to counter all difficulties. Because of his guidance I always developed new skills required to complete the research. I am grateful to him for shaping my career and for all the help during the research.

I would like to thank Prof. K V L Subramaniam, Dr. Anil Agarwal, Dr. A Rajagopal Dr.Surendra Nadh Somala and Dr. Mahendra Kumar Madhavan for providing me the knowledge during the course work. I would like to thank Dr. Ramji Manoharan for allowing me to perform experimental work in material characterization lab of central workshop. I would like to thank Naresh reddy, Matta Seshadri, P. raju for helping and guiding me in experimental work performed in in material characterization lab of central workshop.

I would like to thank all my research group members whose constant help and support helped me to complete my research work. I would like to thank Mr. Girish, Mr. Raju, Mr. Gopal, Mr. Laxman, Mr. Prashanth, Mr. Venkatesh for helping me in the experimental work.

I would like to thank my family members whose constant support and believe in me helped me to achieve my goals.

Dedicated to

My family

Abstract

Pultruded glass fiber reinforced plastics were tested experimentally and modeled using Finite element software Abaqus. Coupon testing was done for material characterization. Coupons were tested in tension, compression, bearing and provisions of respective ASTM codes were followed while performing experiments. Youngs modulus, Maximum load and Maximum stress of coupon specimens under tension and compression were determined.

Experimental testing of short hollow tubes (230mm diameter,6mm thick and 300mm long) was performed under axial compression. Maximum load, Maximum stress and Youngs modulus of all specimens were determined. A comparison of Youngs modulus obtained from coupon testing as well as from short hollow tubes was done.

Numerical modeling of pultruded H beams was done in abaqus and correlation between mid-span deflection obtained from experiments and numerical modeling was determined.

Optimization studies on seven-meter-long pole was done. Fiber orientation in mats and number of rovings were varied keeping volume fraction same to see the effect on stiffness of GFRP pole. Longitudinal fibers behaved better than any other fibers in stiffness determination

To study shear effects a 0.5 meter GFRP pole was modeled with same stacking sequence as that of seven-meter-long GFRP pole. As expected fibers in +45 and -45 directions behaved better than other fibers in stiffness determination.

Four composite plates were prepared by hand layup technique. One composite plate was made with 10 mats and in other plates number of rovings and mats were varied.

Nomenclature

(V_{fbL})	-	volume of fiber in a layer
w_L	-	width of mat
L_L	-	length of mat
ρ_f	-	Density of glass fiber
V_{TL}	-	total volume of laminate
V_f	-	Total volume fraction
t_L	-	thickness of layer(ply)
V_r	-	volume of rovings
L_L	-	Length of roving
n	-	number of rovings
λ	-	Slenderness Ratio of coupon
L_c	-	Length of coupon
r	-	Radius of gyration of coupon
t_c	-	Thickness of coupon
Λ_{tube}	-	Slenderness ratio of short hollow tube (230 mm diameter,300 mm height)
L_{tube}	-	Length of short hollow tube (230 mm diameter,300 mm height)
r_{tube}	-	Radius of gyration of short hollow tube (230 mm diameter,300 mm height)
I_{tube}	-	Moment of inertia of short hollow tube (230 mm diameter,300 mm height)
A_{tube}	-	Area of short hollow tube (230 mm diameter,300 mm height)

Table of Contents

1. Introduction.....	2
1.1 General.....	2
1.2 Types of Fibers and Resin	3
1.2.1 Glass fiber.....	3
1.2.2 Resin.....	3
1.3. Methods of production of GFRP	4
1.3.1 Filament winding.....	4
1.3.2 Hand Layup	4
1.3.3 Resin transfer molding	5
1.3.4 Autoclave molding	5
1.3.5 Pultrusion.....	6
1.4 Material.....	7
1.4.1 Rovings.....	7
1.4.2 Continuous filament mat	8
1.4.3 Glass fiber fabrics.....	9
1.4.4 Matrix	10
1.5 Pipe and Channel sections	11
1.6 Stacking sequence.....	12
1.7 Volume fraction	14
1.8 Problem Statement.....	14
1.9 Objective.....	15
2. Literature Review	17
3. Experimental Program	24
3.1 General.....	24
3.2. Tensile coupon testing	24
3.2.1. Dimensions of specimens according to ASTM D 638	25
3.2.2 Dimensions of tested specimens (TYPE ONE)	26
3.2.3 Speed of testing	27
3.2.4 Procedure.....	27
3.2.5 Fixture.....	28
3.2.6 Dimensions of tested specimens (TYPE FOUR).....	28
3.2.7 Tension testing of type four specimen.....	29
3.3 Compression testing.....	30

3.3.1 Specimen Preparation	30
3.3.2 Dimensions of specimens according to ASTM D 695	31
3.3.3 Dimensions of specimens used for compression testing	31
3.3.4 Speed of testing	32
3.3.5 Procedure	32
3.3.6 Fixture.....	33
3.4 Bearing Test.....	33
3.4.1 Dimensions of specimens according to ASTM D 953	33
3.4.3 Speed of testing	35
3.4.3 Fixture.....	35
3.4.4 Procedure	36
3.5 Compression test on short hollow tubes	37
3.5.1 General	37
3.5.2 Equipment used	37
3.5.3 Speed of test	37
3.5.4 Fixture.....	37
3.5.5 Dimensions of specimens	38
3.5.6 Orientation of strain gauges.....	38
3.5.7 Procedure.....	40
3.6 Compression test with jig	41
3.6.1 General	41
3.6.2 Speed of test	41
3.6.3 Dimensions of specimens	41
3.6.4 Fixture.....	41
3.6.5 Procedure.....	42
3.7 Preparation of plates by hand layup technique	42
3.7.1 General	42
3.7.2 Volume fraction calculation	43
3.7.3 Stacking sequence	43
4.Numerical studies	48
4.1 Modeling of H beams (validation study)	48
4.1.1 H beam 1.....	48
4.1.2 H beam 2.....	50
4.2 Optimization studies for seven-meter pole	52
4.2.1 Modeling of seven-meter-long pole with original stacking sequence	53

4.2.2 Using different stacking sequences to optimize pole stiffness	57
4.3.3 Removing mats and adding more rovings to increase pole stiffness	59
4.4 Modeling of 500 mm short pole (to study shear effects)	60
4.4.1 Modeling of 500 mm short pole with original stacking sequence (MAT 1)	60
4.5 Analysis of support plates proposed for experimental set up	62
4.5.1 Analysis of top plate	62
4.5.2 Analysis of bottom plate	65
4.6 Modeling of tension coupon specimen	67
4.6 Modeling of coupon specimen under compression	68
4.7 Modeling of coupon specimen under compression (for stiffness determination)	70
5.RESULTS AND DISCUSSION	72
5.1 Corrections in graph and toe compensation	72
5.1.1 Toe compensation done in tensile testing of coupons	72
5.1.2 Stiffness correction done during tensile testing	74
5.1.3 Negative strain correction in compression(strength)test	75
5.1.4 Strain correction in compression (modulus) test	76
5.1.5 Stiffness correction in compression (modulus test)	77
5.1.6 Strain correction in compression test of short hollow circular tube	78
5.1.7 Correction for displacement during compression test of short hollow circular tube	79
5.2 Results of tensile coupon testing	80
5.2.1 Results for tension test of channel section specimens (Type one)	81
4.2.2 Results for tension test of channel section (Type 4)	83
5.2.3 Results for tension test of pipe section specimens (type one)	85
5.2.4 Results for tension test of pipe section specimens (type four)	86
5.3 Results of compression coupon testing	87
5.3.1 Results of compression strength test of channel section specimens	87
5.3.2 Results of compression modulus test of channel section specimens	89
5.3.3 Results of compression strength test of pipe section specimens	90
5.3.4 Results of compression modulus test of pipe section specimens	91
5.4 Bearing strength test results	92
5.5 Axial compression test on short hollow circular tubes	94
5.5.1 Axial compression test on specimen1	94
5.5.2 Axial compression test on specimen2	98
5.5.3 Axial compression test on specimen3	101

5.6 Validation study of two H beams in abaqus	105
5.7 Reaction force for different mats	107
5.8 Determination of stiffness for 0.5 m GFRP pole	109
5.9 Analysis of plates for experimental setup.....	110
5.10 Experimental results for compression test with jig.....	111
5.10 Modeling of coupon specimen under tension	112
5.11 Modeling of coupon specimen under Compression	112
5.12 Modeling of coupon specimen under Compression	113
6.CONCLUSIONS	114

LIST OF FIGURES

Figure 1 Stairs and decking in Brazil(left) and transmission pole(right)	2
Figure 2 Hand layup technique	5
Figure 3 Pultrusion process	6
Figure 4 Glass rovings.....	8
Figure 5 Chopped fibers.....	9
Figure 6 Stitched Glass fiber fabric.....	10
Figure 7 Pipe used for cutting coupon specimens	11
Figure 8 Preformer used for making pipe specimens	11
Figure 9 Channel section used for cutting coupon specimens.....	12
Figure 10 Stacking sequence followed for pipe section	12
Figure 11 Stacking sequence for specimens cut from channel section	13
Figure 12 Presence of imperfection in pipe section	14
Figure 13 Load vs displacement (left) Stress vs strain graphs for coupon specimens(right) (Ernesto Guades, Thiru Aravinthan, Md Mainul Islam (2014)	17
Figure 14 Load vs displacement (left) Stress vs strain graphs (right) for square hollow tube specimens (Ernesto Guades, Thiru Aravinthan, Md Mainul Islam (2014).	18
Figure 15 Flow chat explaining experimental program	24
Figure 16 Different types of specimen according to ASTM D 638.....	25
Figure 17 Standard specimen dimensions according to ASTM D638	26
Figure 18 Standard speeds for different types of specimens ASTM D 638.....	27
Figure 19 Fixture used for tension coupon testing	28
Figure 20 Flow chart showing experimental testing for compression test.....	30

Figure 21 Specimen prepared for strength test(left), Specimen prepared for modulus test (right)	31
Figure 22 Compression platens	33
Figure 23 Dimensions of specimen for bearing strength test according to ASTM D 953	34
Figure 24 Side view(left) and Front view (right) of tension fixture	36
Figure 25 Fixture for compression test of short hollow GFRP tubes	38
Figure 26 Orientation of strain gauges for specimen one	39
Figure 27 Orientation of strain gauge for specimen two	39
Figure 28 Orientation of strain gauges for specimen three	40
Figure 29 Fixture for compression test of coupons with jig.....	42
Figure 30 Stacking sequence followed for composite plate 1.....	43
Figure 31 Stacking sequence followed for composite plate 2.....	44
Figure 32 Stacking sequence followed for composite plate 3.....	44
Figure 33 Stacking sequence followed for composite plate 4.....	44
Figure 34 Placing of mat in plastic film.....	45
Figure 35 Application of resin in mats	45
Figure 36 Tensioning of rovings done with help of steel rods.....	46
Figure 37 Composite plate with no rovings and with 10 mat.....	46
Figure 38 Composite plate with 165 rovings and 6 mats	47
Figure 39 Composite plate with 255 rovings and 4 mats	47
Figure 40 Composite plate with 345 rovings and 2 mats	47
Figure 41 Stacking sequence of H beam 1 (Barbero et.al)	49
Figure 42 Stacking sequence of H beam 1 used in abaqus (composite layup)....	49
Figure 43 Load and boundary conditions used for H beam 1	50
Figure 44 Stacking sequence of H beam2 (Barbero et.al)	51
Figure 45 Stacking sequence of H beam 2 used in abaqus (composite layup)....	51
Figure 46 Load and boundary conditions used for H beam2.....	52

Figure 47	Preformer used for manufacturing GFRP pole.....	53
Figure 48	Original stacking sequence used for pipe section in industry.....	54
Figure 49	Seven-meter-long pole modeled in abaqus	55
Figure 50	Assigning local coordinates to pole	55
Figure 51	Composite layup used for pole	56
Figure 52	Displacement of 1050mm applied at one end of pole	57
Figure 53	90-0 mat used with rovings in between	57
Figure 54	0-90-chop mat used with rovings in between.....	58
Figure 55	Mats removed and rovings increased (for original stacking sequence)	59
Figure 56	Mats removed and rovings increased (for MAT 2)	60
Figure 57	500 mm long short pole modeled in abaqus.....	61
Figure 58	Load applied to 500 mm short pole.....	61
Figure 59	Mesh for 500 mm short pole	62
Figure 60	Dimensions of plate used at top of GFRP pole.....	62
Figure 61	Solid part created for top plate.....	63
Figure 62	Rigid body constraint used to tie bolt with washer.....	63
Figure 63	Pressure load applied to top plate.....	64
Figure 64	Fixed boundary conditions given to corner holes.....	64
Figure 65	Mesh created for top plate.....	65
Figure 66	Solid part created for bottom plate.....	65
Figure 67	Loading applied to bottom plate.....	66
Figure 68	Mesh created for bottom plate.....	67
Figure 69	Tension coupon created in abaqus	67
Figure 70	Load and boundary conditions applied to coupon specimen.....	68
Figure 71	Mesh for coupon specimen	68
Figure 72	Composite layup used for modeling coupon specimen.....	68
Figure 73	Coupon(strength) specimen modeled in abaqus.....	69

Figure 74	Load and boundary conditions of coupon (strength) specimens	69
Figure 75	Mesh created for coupon (strength)specimen	70
Figure 76	Coupon(stiffness) specimen modeled in abaqus.....	70
Figure 77	Coupon(stiffness) specimen modeled in abaqus.....	71
Figure 78	Mesh of coupon (stiffness) specimen in abaqus	71
Figure 79	Toe compensation recommended by ASTM D 638.....	72
Figure 80	Stress vs strain graph having toe region.....	73
Figure 81	Stress vs strain graph after toe compensation.....	73
Figure 82	Stress vs strain curve without and after stiffness correction	74
Figure 83	Stress vs strain curve during compression strength test (before correction)	75
Figure 84	Stress vs strain curve during compression strength test (after correction)	75
Figure 85	Stress vs strain curve during compression modulus test (before correction)	76
Figure 86	Stress vs strain curve during compression modulus test(after correction)	76
Figure 87	Stress vs strain curve for machine and strain gauge (before correction)	77
Figure 88	Stress vs strain curve for machine and strain gauge (after correction)	78
Figure 89	Stress vs strain curve for short hollow tube under axial compression (without correction).....	78
Figure 90	Stress vs strain curve for short hollow tube under axial compression (with correction)	79
Figure 91	Load vs displacement for short hollow tube under axial compression (without correction).....	79
Figure 92	Load vs displacement for short hollow tube under axial compression (with correction)	80
Figure 93	Stress vs strain graph for channel section specimens (Type one)	81
Figure 94	Shear rupture and delamination failure in channel section specimens (type one)	82

Figure 95 Shear plane rupture occurring in channel section specimens (type one)	82
Figure 96 Delamination occurring in channel section specimens (type one)	82
Figure 97 Stress vs strain graph for channel section specimens (type four)	83
Figure 98 Shear plane fracture and delamination in channel section specimens (type four)	83
Figure 99 Delamination and debonding in channel section specimens (type four)	84
Figure 100 Delamination in channel section specimens (type four)	84
Figure 101 Stress vs strain graph for pipe section specimens (Type one)	85
Figure 102 Stress vs strain graph for pipe section specimens (Type four)	86
Figure 103 Shear plane rupture and delamination for pipe section specimens (type four)	86
Figure 104 Shear plane rupture for pipe section specimens (type four)	86
Figure 105 Delamination in pipe section specimens (type four)	87
Figure 106 Stress vs strain graph of compression strength test of channel section specimens	87
Figure 107 Delamination in compression strength test for channel section specimens	88
Figure 108 Rupture occurring in compression strength test for channel section specimens	88
Figure 109 Stress vs strain graph for compression modulus test of channel section specimens	89
Figure 110 Delamination observed during compression modulus test of channel section specimens	89
Figure 111 Rupture observed during compression modulus test of channel section specimens	90
Figure 112 Stress vs strain graph for compression strength test of pipe section specimens	90
Figure 113 Delamination occurred during compression strength test of pipe section specimens	91
Figure 114 Stress vs strain graph for compression modulus test of pipe section specimens	91

Figure 115 Delamination in compression strength test of pipe section specimens	92
Figure 116 Stress-strain graph for bearing strength test(HRB series)	92
Figure 117 Shear out failure observed in HRB3.....	93
Figure 118 Bearing failure observed in HRB2	93
Figure 119 Stress vs strain graph for bearing strength test (B series))	93
Figure 120 Shear out failure observed in b4	94
Figure 121 Bearing failure observed in b1	94
Figure 122 Orientation of strain gauges on specimen 1	94
Figure 123 Load vs displacement graph for specimen1	95
Figure 124 Stress vs strain graph for specimen1	95
Figure 125 Comparison with coupon specimen PL12	96
Figure 126 Failure mode in specimen 1(front side)	97
Figure 127 Failure mode in specimen 1(back side).....	97
Figure 128 Orientation of strain gauges on specimen 2	98
Figure 129 Load vs displacement graph for specimen2	98
Figure 130 Stress vs strain graph for specimen2	99
Figure 131 Comparison with coupon specimen PL12	99
Figure 132 Delamination occurring in Specimen2.....	100
Figure 133 Orientation of strain gauges on specimen 3	101
Figure 134 Load vs displacement graph for specimen3	101
Figure 135 Stress vs strain graph for specimen 3	102
Figure 136 Comparison with coupon specimen PL12	102
Figure 137 Failure through strain gauge 4(left) and through strain gauge 3 (Right).....	103
Figure 138 Presence of material imperfection and failure near stain gauge 4 and 5 (inside view)	104
Figure 139 Presence of material imperfection and failure near stain gauge 1 and 2 (inside view).....	104

Figure 140 Deflection at midspan (abaqus) for H beam 1	105
Figure 141 Deflection at midspan (abaqus) for H beam 2	106
Figure 142 Reaction force determined at fixed end for MAT1	107
Figure 143 Reaction force determined at fixed end (90-0 mat) MAT2	107
Figure 144 Reaction force determined at fixed end (0-90-chop mat) MAT3....	108
Figure 145 Deformation obtained from short pole.....	109
Figure 146 No plastic strain for top plate	110
Figure 147 No plastic strain for bottom plate	110
Figure 148 Stress vs strain results for coupons tested in compression with jig	111
Figure 149 Stress determination for coupon specimen	112
Figure 150 Compressive stress determined for coupon specimen.....	112
Figure 151 Compressive stress determined for coupon specimen	113

LIST OF TABELS

Table 1 g/m ² for each layer of GSM551 mat	8
Table 2 g/m ² for each layer of GSM688 mat	9
Table 3 g/m ² for each layer of GSM936 mat	9
Table 4 Dimensions of specimens cut from pipe section (type one).....	26
Table 5 Dimensions of specimens cut from channel section (type one)	27
Table 6 Dimensions of TYPE four specimens cut from pipe section	29
Table 7Dimensions of TYPE four specimens cut from channel section	29
Table 8Dimensions of specimen for bearing strength test (ASTM D 953)	34
Table 9 Dimensions of specimens used for bearing strength test.....	35
Table 10Dimensions of Fixture used for bearing strength test (tension loading)	36
Table 11Dimensions of coupons used for compression testing with jig	41
Table 12Material properties of Hbeam2 (Barbero et.al)	50
Table 13showing overall volume fraction and for individual glass fibers.....	55
Table 14 showing overall volume fraction and for individual glass fibers.....	58
Table 15 showing overall volume fraction and for individual glass fibers.....	58
Table 16Comparison of deflection values for H beam 1	105
Table 17Comparison of deflection values for H beam 2	106
Table 18Comparison of load values for different mats	108
Table 19 comparison of stacking sequence (shear case).....	109

Chapter 1

1. Introduction

1.1 General

GFRP (Glass Fiber Reinforced Polymers) are in high demand these days because of their extraordinary properties such as light weight, corrosion resistance, high specific strength and low maintenance cost. Hence it has become a suitable alternative for traditional materials such as concrete, steel and timber in construction industry. GFRP (Glass fiber reinforced plastics) are mostly used in aerospace, automotive, marine, O&G (oil and gas) and civil construction industries. namely (fiberglass structures): ladders, platforms, handrail systems tank, pipe and pump supports. Commercial use of GFRP started back in 1940 for naval industry. After that speed of production increased globally. GFRP also has other advantages such as: high strength to weight ratio, high durability and fabrication adaptability



Figure 1Stairs and decking in Brazil(left) and transmission pole(right)

1.2 Types of Fibers and Resin

1.2.1 Glass fiber

Glass fibers are used as a reinforcement to plastic (polymer) material. There are different types of glass fibers that are commercially available. Some of the common available types are A glass, AR glass, C glass, D glass, E glass, R glass and S glass. These differ from each other in terms of the presence of alkali and silicates in their composition. In E glass, E stands for electrical as it was made for electrical applications but now it is most commonly used in structural applications. S in S glass stands for higher amount of silica and it carries its strength even at higher temperature as compared to E glass and has higher fatigue strength. It is used for aerospace applications. C in C glass stands for corrosion and is used for structures in adverse chemical environments such as storage tanks. R (reinforcement) glass is used in construction. D (dielectric) glass is used for applications that require low dielectric constants. A (appearance) glass is used for improving surface appearance. A combination of the above-stated glass also exists like: E (electrical)-CR (corrosion resistant) glass and AR (alkali resistant) glass.

E glass is most commonly used glass fiber used in fiber-reinforced polymer industry and is known for its strength and electrical resistance properties.

1.2.2 Resin

Resin used in fiber-reinforced plastics can also be referred to as 'polymers'. Resins can be classified as thermoplastic or thermosetting. Thermoplastic resin softens, melts on heating and hardens with cooling. Material properties of thermoplastics remain the same during softening. Some thermoplastics are nylon, polypropylene. Thermosetting resins are mixed with hardener/catalyst and undergo a non-reversible reaction to form a hard, infusible product. Unlike thermoplastics, thermosets never return to their initial state. Above a certain temperature (Glass transition temperature) their mechanical properties change. It changes from a rigid crystalline structure to a more flexible structure. Some commonly used thermosetting resins are polyester and epoxy. Thermosetting resins are better than thermoplastics as below glass transition temperature they retain their strength as well as shape that is useful for production of permanent shapes. Most commonly polyester and epoxy are used for structural applications. Advantages of polyester are low cost, ability to be made translucent. Its drawbacks are brittleness and high shrinkage during curing. Advantages of epoxy are high mechanical strength and good bonding to metal and glasses. Its drawback includes high cost and difficulty in processing.

1.3. Methods of production of GFRP

1.3.1 Filament winding

Fibers are impregnated with resin and wound over a rotating mandrel in specific directions. Curing can be done either at normal or elevated temperature. Later in the process mandrel is removed leaving behind the desired shape. Sometimes mandrel also becomes integral part of assembly. In filament winding tensioning of fibers is critical as too much tensioning can cause breaking and fracture of fibers. Fiber tensioning affects fraction of fiber and porosity in composite. Advantages of this method are less labor involvement as it is an automated process, degree of uniformity in fibers orientation and distribution is more and size of composite is not limited. Disadvantages of this method includes high capital investment, precise control is needed for uniform orientation and distribution of fibers and sometimes cost of mandrel can be high adding to total cost.

1.3.2 Hand Layup

It is one of the most economical method for GFRP production as infrastructural requirement is less. In this method mold are used for fabrication of GFRP. First step in the process is spreading of release gel over mold surface to avoid any sticking of resin on surface. Plastic sheets are placed on top and bottom of mold to get good finish. Reinforcement fibers are cut according to size of mold and are placed at surface of mold. Then resin with hardener is poured on reinforcing fiber. Other layers if fibers are then placed according to stacking sequence and roller is moved over fiber-resin to remove any entrapped air. Then curing is done at normal or some specified temperature. After that mold is opened and composite is taken out and used for further processing. This method is suitable for thermosetting polymers (like epoxy and polyester) based composites. High volume fractions are difficult to obtain in this method.

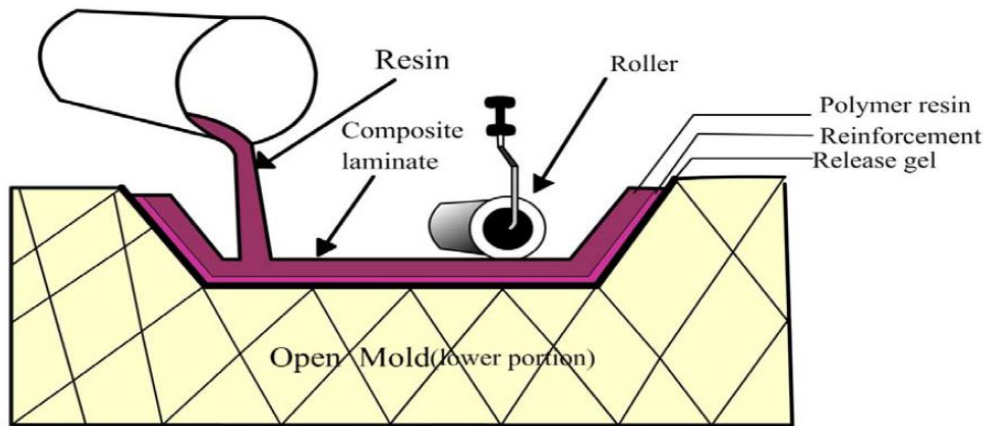


Figure 2 Hand layup technique

1.3.3 Resin transfer molding

Resin is transferred over already placed reinforcement. It is closed molding process. Mold has upper and lower half. Reinforcement is placed on surface of lower mold. Gel is applied for easy removal of composite. Mold is closed and clamped. Resin is sent to the mold through ports and air is removed through vents. Uniformity in flow of resin can be increased by the use of catalyst as accelerator. Resin and catalyst are mixed in mixing chamber. Resin injector is used inject mixture to mold cavity. After curing is completed mold is opened and composite is taken out. Process can be automated to reduce time taken. For highly viscous resins pressure required is more which can cause displacement of fibers known as fiber wash. This process is useful for production of hollow and complex structural shapes. Disadvantages of this method includes high tool cost and limitation on size of composites.

1.3.4 Autoclave molding

In this method an autoclave is used to heat and apply pressure to FRP during curing. In this method prepregs are used. Prepregs are ready made tape consisting of fibers in polymer matrix. In this method prepregs are stacked in a particular sequence and spot welding is done to prevent relative movement between layers. Vacuum is used to remove entrapped air and after that assembly is sent to autoclave. Autoclave is used to apply heat and pressure. Now matrix is uniformly distributed and close contact between fibers and matrix is ensured. Then cooling of assembly is done and composite is taken out of the mold. Advantages of this method are: Composites with higher volume fraction can be obtained, contact between fibers and matrix is good, no void content and method is applicable for both thermoplastic

and thermosetting resins. Disadvantages of this method includes limitation on part size which depends on autoclave size, it is a costly technique and it requires skilled labor.

1.3.5 Pultrusion

Pultrusion is continuous automated composite manufacturing process. Mechanism of pultrusion is similar to metal extrusion process, only difference is that in metal extrusion process material is pushed through the dies, while in pultrusion it is pulled through dies. First step in the process is tensioning of reinforcement through creels. After tensioning fibers are guided to resin bath, where fibers are impregnated with resin in resin bath. After resin bath it is passed through preform plates where excess resin and fillers (if used) are removed from the fibers. Also preformer plates guides and aligns the reinforcement to heated die. Then it is guided through heating die where curing is done as well as desired shape is given. Cured composite profile (coming from hot die) is pulled through a pulling mechanism. Finally, pultruded profiles are cut with a saw which is inbuilt after pulling mechanism.

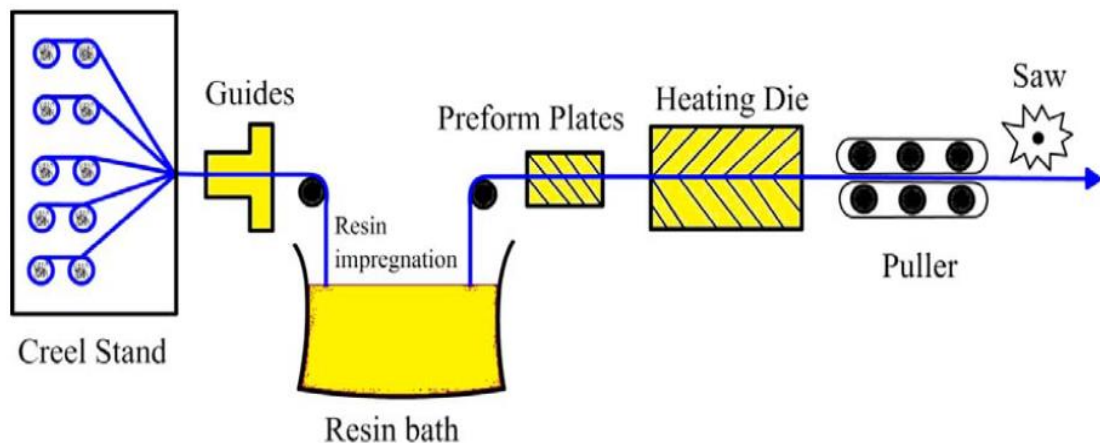


Figure 3 Pultrusion process

Advantages of the process are: high production rate as it is a continuous production process, simple process that does not require additional labor skills and the quality and finish of the product is better as compared to other methods. Disadvantages of the process are: the process is good only for constant cross sections, tapered and complex shapes are difficult to produce by this method, control of fiber orientation is difficult in this method and thin wall products are difficult to produce.

Products with a wide range of cross sections like C section, box section, angle section, I section and even omega cross section can be easily manufactured with pultrusion. Products

such as solid rods, tubing, flat sheets can be produced with much ease. Pultruded products give tough competition to other products in market of electrical, corrosion, construction, transportation, as well as aerospace and defense. The products fabricated by this method are transformer air duct spacer sticks, ladders, bus bar supports, fuse tubes, cable support trays, fishing rods, antennas, skate boards, tool handles, ski poles, golf shafts, bridges and platforms stairs, pipes and tubes, leaf springs, seating, bus luggage racks, etc. Pultruded products are also used for making tool handles for high voltage work and rail covers for subways. Pultrusion products are also very useful as floor grating.

In this study pultrusion process for producing Gfrp sections was adopted because through pultrusion high volume fractions of fibers about 60% can be achieved and sections of constant can be produced with good surface finish.

1.4 Material

Material required in this work for pultrusion process consists of reinforcement and matrix. Reinforcement includes rovings, continuous filament mat. Again mat consisted of woven fabrics (+45/-45), 90 degree fibers and chop (that was randomly oriented). Matrix used is polyester which is a thermosetting resin.

1.4.1 Rovings

Individual glass filaments when bundled without twist into multifilament strands are used in pultrusion process. Rovings are aligned along the direction of pultruded part along the lengthwise direction of composite material. This direction is also known zero-degree direction of the material. Due to alignment of rovings along the lengthwise direction it is very strong in strength and stiffness. They provide pultruded part most of its axial, flexural strength and stiffness. While impregnating roving bundles with resin it should be ensured that each fiber is wet out with resin otherwise it will create dry fiber areas in product that are highly undesirable. In this study rovings of 40, 60 numbers as well as 100 numbers were used. A preformer having required number of holes was used in industry to ensure rovings are present in requisite number in the final product. In this study rovings of 4800 tex i.e. 4.8 gram/meter are used.

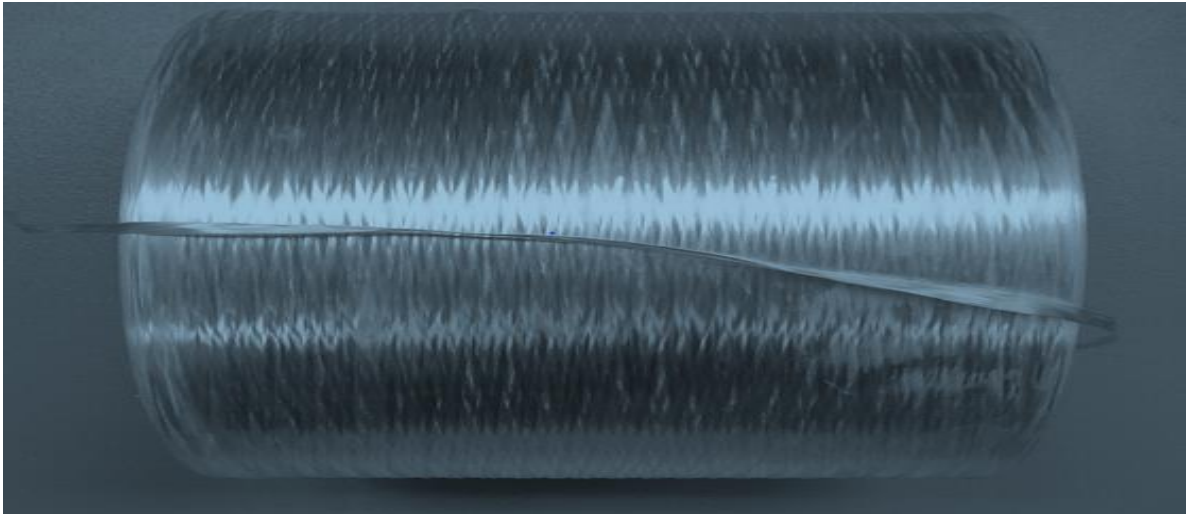


Figure 4 Glass rovings

1.4.2 Continuous filament mat

It is also known as continuous strand mat; it is the second most widely used glass fiber in industry. It is used to provide crosswise or transverse strength and stiffness. It consists of continuous, swirled, random and very long fibers held together by resin. In this study mat consisted of woven fabrics (+45/-45) and 90 degree fibers and chop (that was randomly oriented). Continuous filament mat help rovings to be in proper position as it moves through die. In chop fibers due to the random orientation of the fibers in the plane of the continuous mat it can be assumed to have equal properties in all directions (i.e., isotropic properties).

In this study mat-45/90/45/chop of 551GSM i.e. 551 g/m², mat of 90/0 of 688GSM i.e.688g/m² and a mat of 0/90/chop of 936GSM i.e. 936 g/m² are used.

LAYER	g/m ²
-45	100
90	283
45	100
chop	60
Sewing	≤10

Table 1 g/m² for each layer of GSM551 mat

LAYER	g/m ²
90	342
0	336
sewing	10

Table 2 g/m² for each layer of GSM688 mat

LAYER	g/m ²
0	100
90	283
chop	100
sewing	60

Table 3 g/m² for each layer of GSM936 mat

GSM551 has chop fibers stitched with -45/90/45, GSM688 is a bidirectional mat that has fibers only in 0 and 90 and GSM 936 has chop fibers stitched with 0 and 90.

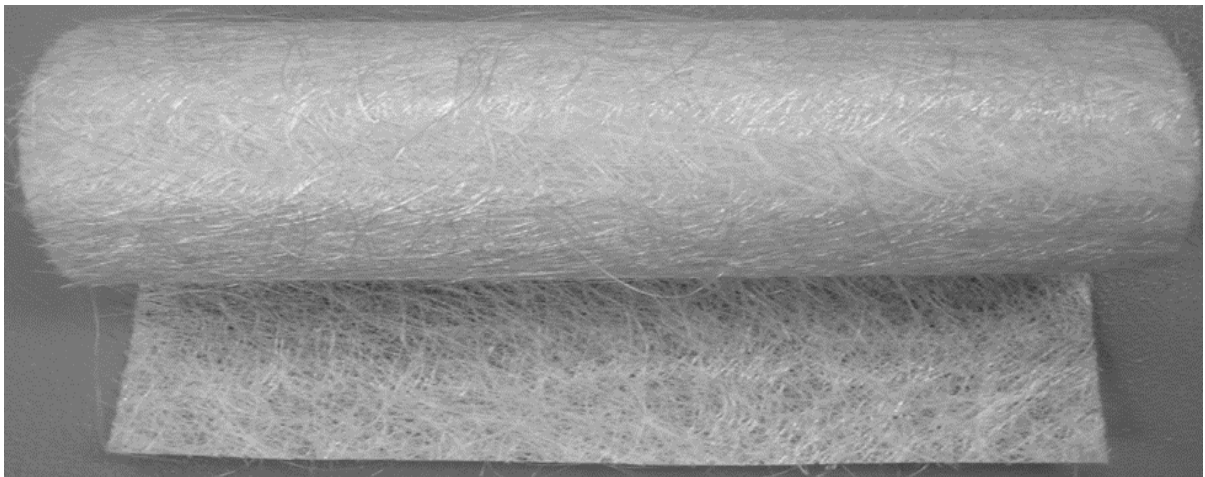


Figure 5 Chopped fibers

1.4.3 Glass fiber fabrics

To obtain wide range of properties from pultruded composite and in specific directions, fibers can be laid in specific directions (+45/-45) to longitudinal axis and at specific volume fractions. Glass fiber fabrics are generally of two types: one is woven roving fabric and other is stitched roving fabric. Woven roving has fiber orientations of zero and ninety degrees. The other type of fabric type that is used in pultrusion is a stitched fabric where the unidirectional layers of rovings in different directions are stitched together with or without a chopped mat. Popular types of stitched fabrics are biaxial and triaxial.

In this study stitched fabrics were used where unidirectional layers of +45/-45,90 degrees were stitched to a chopped mat for GSM 551 and unidirectional layers of 0 and 90 degrees were stitched to a chopped mat for GSM 936.

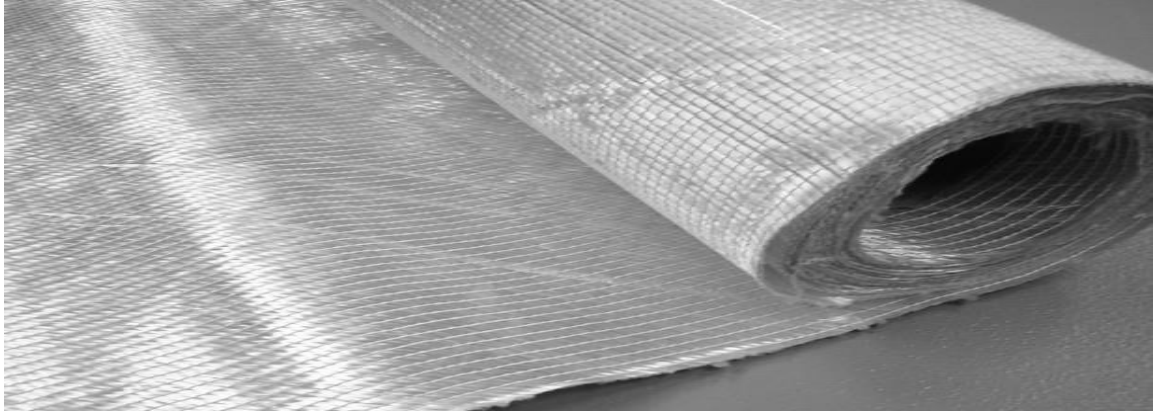


Figure 6 Stitched Glass fiber fabric

1.4.4 Matrix

Matrix used is polyester which is a thermosetting resin and is capable of being cured under proper conditions. There are wide range of polyesters depending upon the constituents like acids, glycol and monomers. If polyester is made up of acid there are generally two types: orthophthalic acids and isophthalic acids. Orthophthalic acids are inferior in terms of strength, chemical resistance and corrosion resistance when compared to isophthalic acids. Isophthalic acids offer better strength, flexibility and chemical resistance.

In this study polyester resin made up from isophthalic acid is used because of its better properties.

1.5 Pipe and Channel sections



Figure 7 Pipe used for cutting coupon specimens

GFRP pipe of 230 mm diameter and 6 mm thick (as shown in Figure 7) was used for cutting specimens for coupon testing. Pipe section was made up of GSM551 having fibers as - 45,90,45 and chop. In Pipe section rovings of 60 numbers as well as 100 numbers were used. A preformer having required number of holes was used in industry to ensure rovings are present in requisite number in the final product. In this study rovings of 4800 tex i.e. 4.8 gram/meter are used.



Figure 8 Preformer used for making pipe specimens

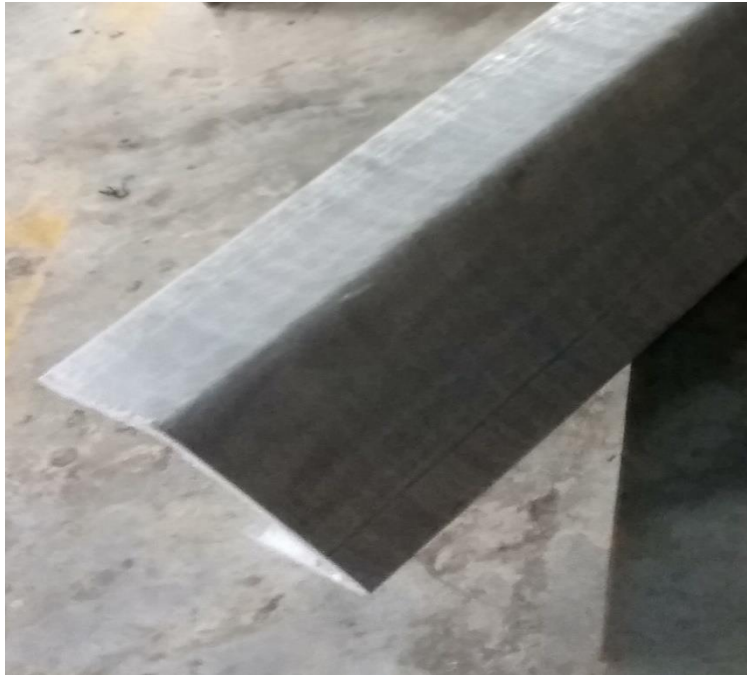


Figure 9 Channel section used for cutting coupon specimens

Coupons were cut from channel section 102 mm web, 45mm flanges and 800 mm in length. Coupon specimens were cut from web. It was of 6 mm thickness and made up of GSM936 mat and GSM 551. It had 3 GSM936 mats and 2 GSM551 mats. GSM 936 has 0,90 and chop fibers. GSM 551 has -45,90,45 and chop fibers. In Channel section rovings of 40 numbers were used. A preformer having required number of holes was used in industry to ensure rovings are present in requisite number in the final product. In this study rovings of 4800 tex i.e. 4.8 gram/meter are used.

1.6 Stacking sequence

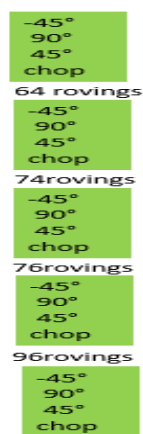


Figure 10 Stacking sequence followed for pipe section

Total five mats were used with rovings in between for specimens cut from pipe section. GSM551 mat used consisted of -45,90,45 and chop fibers. Total five mats were used with rovings in between.

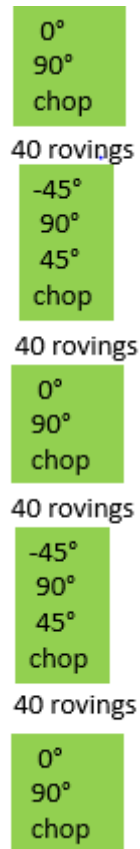


Figure 11 Stacking sequence for specimens cut from channel section

Total five mats were used with rovings in between for specimens cut from channel section. Out of the five mats used three were of GSM936 and two were of GSM551. R40 means 40 number of rovings were used. GSM 936 consisted of 0,90 and chopped fibers while GSM551 consisted of -45,90,45 and chop. While stacking the layers there were some portions that were not having reinforcements. This caused presence of material imperfection in the material. During this study it was found that coupons cut from imperfection areas had lesser strength in both tension and compression.



Figure 12 Presence of imperfection in pipe section

1.7 Volume fraction

Volume fraction for mat

For mats, volume fraction is weight of fiber per unit area of that layer divided by density of fiber and thickness of that layer. Thickness of individual ply is assumed with equal division of total thickness into number of mats and their sub layers.

$$(V_{fbL}) = (g/m^2) \times w_L \times L_L / \rho_f$$

$$V_{TL} = t_L \times w_L \times L_L$$

$$V_f = V_{fbL} / V_{TL}$$

$$V_f = (g/m^2) / \rho_f \times t_L$$

Volume fraction for roving

For roving layer, generally available information is in weight of fiber per length i.e., in TEX (mass in grams per km). Width of roving layer is assumed to be equal to adjacent mat in stacking sequence. Volume fraction for roving is calculated as:

$$V_r = (TEX \times L_L \times n) / \rho_f$$

$$V_{TL} = t_L \times w_L \times L_L$$

$$V_f = V_r / V_{TL}$$

$$V_f = (TEX \times n) / \rho_f \times t_L \times w_L$$

1.8 Problem Statement

There is a lack of study in case of use of multiaxial fibers as reinforcement. More often researchers use unidirectional fibers in their study and observe the behavior of material but

as multiaxial fibers come into picture behavior of material becomes more complex and difficult to understand.

There is lack of research on testing of electrical transmission poles (made of GFRP) under compression and flexure. Performance of these poles is very critical in bending. These poles are subjected to bending because of high wind loads, so deflection and stiffness properties of these poles are of major concern and there is a lack of research in these topics.

Due to use of unidirectional fibers such as 0 and 90 degrees, there is lack of properties in any other directions. +45/-45 oriented fibers can provide excellent shear properties but they are rarely used in the research studies.

Even in numerical studies for electrical transmission poles (made of GFRP) there is a lack of research. Electrical transmission pole can be made better in terms of strength and stiffness by changing stacking sequence, volume fraction of fibers and by inclusion of fibers in specific directions.

Behavior of unidirectional fibers under tensile and compressive stress is completely different as compared to that of multiaxial fibers. Even the type of cracks developed and failure modes are different for unidirectional and multiaxial fibers. While enough study has been done on cracks and failure modes of unidirectional fibers there is lack of study for multiaxial fibers.

1.9 Objective

Main objective of this study is characterization of material properties. Material characterization is needed for checking strength and stiffness of electrical transmission poles made up of GFRP. Material characterization will be done under tensile and compressive stress. For characterization of material properties coupons of specified dimensions and shape will be cut according to ASTM codes used for respective tests. Coupons will be cut from short hollow GFRP tubes of 230mm diameter, 300mm length and 6mm thickness. For material characterization strength and stiffness properties will be determined. Material characterization will be done for multiaxial fibers. Coupons will also be experimentally tested under bearing to check strength under bearing and for that coupons will be fabricated and tested according to relevant ASTM code.

Also objective of this study is to determine behavior of short hollow GFRP tubes of 230mm diameter, 300mm length and 6mm thickness under axial compression. As there is lack of research in behavior of multiaxial fibers under compressive stress, in this study compressive

stress and compression modulus of short hollow GFRP tubes of 230mm diameter,300mm length and 6mm thickness under axial compression will be determined.

Objective of this study includes optimization of seven –meter long GFRP poles. Stiffness values of GFRP poles will be optimized by using combinations of mats and rovings by keeping volume fraction same. Stacking sequence giving highest stiffness values will be selected and will be used in future manufacturing of GFRP poles. Shear effects will be studied by modeling 0.5 m length of GFRP pole. Behavior of different fibers under transverse load will be studied.

Objective of this study also includes development of experimental test setup for flexural test of seven-meter long GFRP pole. Pole will be tested in horizontally with fixity at one end and load or displacement applied at other end.

Objective of this study includes preparation of composite plates by hand-layup technique. Different combinations of rovings and mats will be tried keeping volume fraction same to fabricate composite plates.

Chapter 2

2.Literature Review

Behavior of GFRP at coupon and full scale level has been studied by researchers in past. Behavior of coupons under tension, compression and flexure has been extensively studied. Experimental testing of GFRP poles under flexure has also been carried out in past.

Ernesto Guades, Thiru Aravinthan, Md Mainul Islam (2014) did experimental testing to investigate mechanical properties of pultruded fiber-reinforced polymer (FRP) tube. In their experimental testing they have cut coupons from all four sides of hollow square tube (used as cross arm in electrical transmission poles. Stacking sequence for the tube was 0/+45/0/-45/0/-45/0/+45/0. They did coupon testing under tension, compression and flexure. They also performed compression and four-point bending tests on 100 mm hollow square tube. Most prevalent failure mode in their study under compression was interlaminar failure along unsupported length. All coupons under tensile stress failed by glass fiber rupture along gage length. Prevalent failure mode in flexure was fracture on tension side below point of loading, some specimens also showed inter-laminar shear fractures. In their study they performed compression and four-point bending tests on 100 mm hollow square tube. It was observed that the common type of damage during the compressive test is buckling bulge (inside and outside), delamination along the wall, glass fiber rupture, and matrix cracking.

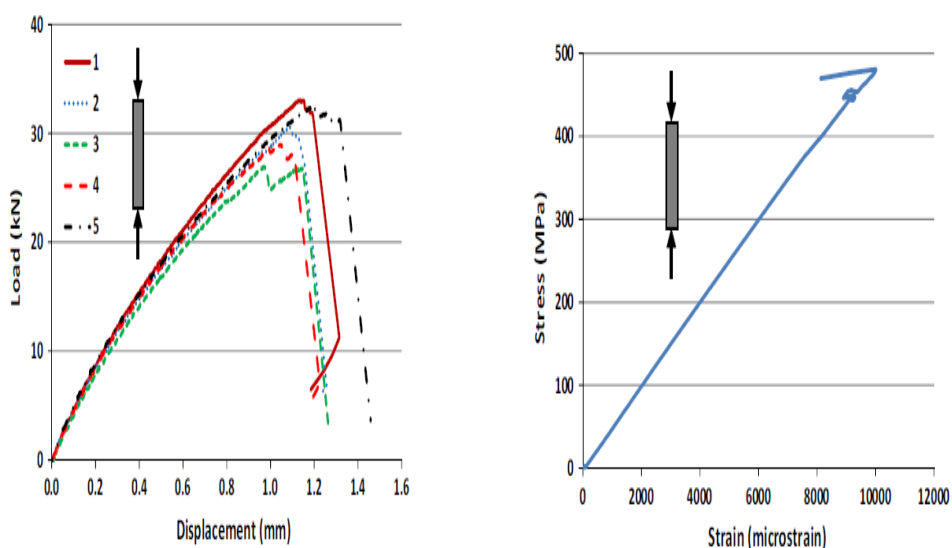


Figure 13 Load vs displacement (left) Stress vs strain graphs for coupon specimens(right) (Ernesto Guades, Thiru Aravinthan, Md Mainul Islam (2014))

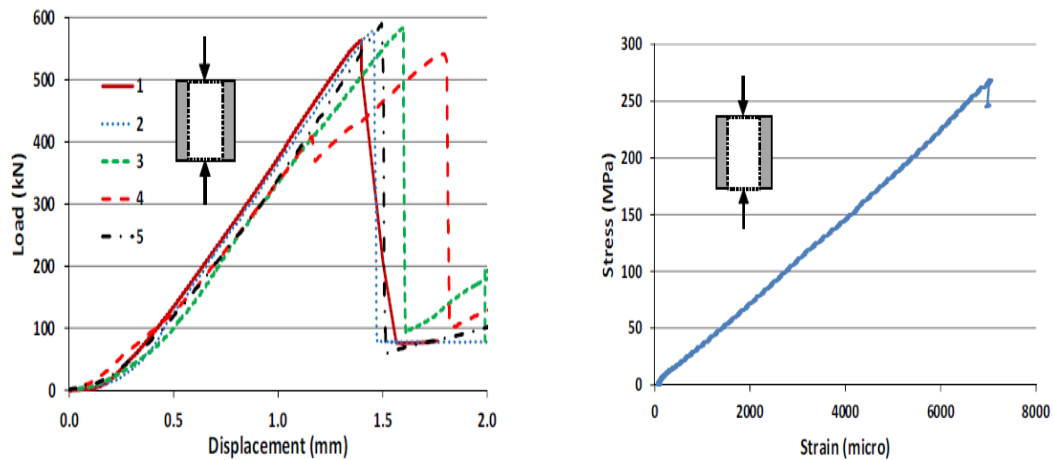


Figure 14 Load vs displacement (left) Stress vs strain graphs (right) for square hollow tube specimens (Ernesto Guades, Thiru Aravinthan, Md Mainul Islam (2014)).

Slimane Metiche and Radhouane Masmoudi (2012) did experimental testing of GFRP electric transmission poles of lengths ranging from 5.09 m to 12.09 m. Their poles had opening near base. They divided poles into different zones having according to number of layers and fiber orientation. They also focused on design approaches for design of electric transmission poles. They studied effect of location of opening (from base of pole) on cracking and failure of GFRP poles. They found that most of design guidelines ignore effect of stress concentrations and failure near opening. Further local buckling in area near to opening governs failure mode. They developed a design approach in addition to applying available design procedures (AASHTO-LTS-5-2009) to experimentally tested GFRP electrical transmission poles. They found that ultimate moment at base is inversely proportional to density of fibers. They compared deflection of pole with that of limiting deflection according to AASHTO-LTS-5-2009 and values were under maximum deflection specified. They found that when pole was tested with load combination of bending, shear and compression stress it gave worst combination case. Equations used for this combination was included from AASHTO-LTS-5-2009 provisions for aluminum poles. They recommended inclusion of this combination in AASHTO-LTS-5-2009 provisions for FRP poles.

Girum Urgessa and Sara Mohamadi (2016) performed finite element analysis of fiber reinforced GFRP poles including parametric studies on geometric characteristics, fiber

orientation, number of layers, and lamina thickness. They did finite element analysis of tapered FRP poles in ABAQUS and associated parametric studies to understand behavior of FRP poles by changing different properties. These properties include geometric characteristics, fiber orientation, taper ratio, number of layers, lamina thickness and location of transverse load. They found that maximum stress in GFRP tapered pole increases up to orientation of 45 degrees and starts decreasing as angles is increased from 45 to 60 degrees. They also found that increasing the fiber orientation increases maximum deflection of pole. Maximum deflection and maximum stress decrease with increase in number of layers and the rate of decrease reduces with increase in number of layers. They also varied individual lamina thickness without changing overall laminate thickness and studied the effect in results, they found that changing individual lamina thickness (without changing overall laminate thickness) doesn't vary results and variation is within 0.5%. They also found that using S4 elements while modeling pole in ABAQUS gave better and accurate results as compared to S8R elements.

J. F. Davalos, H. A. Salim, P. Qiao, R. Lopez-Anido and E. J. Barbero (1996) developed procedures for analysis and design of pultruded FRP beams under bending. They developed complete procedure that included calculation of volume fraction of constituents, computation of ply stiffness using calculated volume fraction and micromechanical models and computation of panel laminate engineering constants using macromechanics and ply stiffness. They compared laminate constants with that obtained from coupon tests. They studied bending response of pultruded box and H sections experimentally and analytically. They tested two box and two H sections in bending under 3 point and 4-point loading. For their numerical studies they used computer program FRP beams to model and analyze FRP shapes in bending. To verify the prediction accuracy with the FRPBEAM program, the test beams are also analyzed with the commercial finite element program ANSYS. For their analytical studies they used mechanics of laminated beams theory to obtain pultruded beam stiffness coefficients and then they used Timoshenko beam theory to get beam displacements and panel stress resultants. Finally, they used classical laminate theory to get ply stresses and strains. They got variation of 3% for E_{xx} and around 2.6 % for E_{yy} between the values that were calculated through experiments and analytically. For full scale testing of box and H beams they got difference of 5.5% for displacements and 7.9% for strains when they compared displacements and strains obtained from MLB (mechanics of laminated beams) with that of finite element analysis and experiments. Due to good

agreement with finite element analysis and experiments they recommended MLB (mechanics of laminated beams) for parametric studies and optimization of new shapes.

J.G. Teng, Y.M. Hu (2007) did study on advantages of GFRP jacketing on hollow steel tubes. They tested steel tubes without GFRP jacketing as well as with GFRP jacketing. During jacketing they varied number of plies from 1 to 3 for different specimens. They performed tensile coupon testing of steel. They also performed tensile coupon testing GFRP coupons according to ASTM D3039. For steel tube without jacketing they used four unidirectional strain gauges (8mm gauge length) and for GFRP jacketed steel tube they used four bidirectional strain gauges (20 mm gauge length). They attached strain gauges on all four sides of FRP jacketed tube at mid-depth.

They performed compression testing of all tubes in compression testing machine at a rate of 0.5mm/min. They observed that load vs axial shortening graph of bare steel had descending portion immediately after linear ascending portion but GFRP jacketed steel tubes had long and slowly ascending branch after linearly ascending region. Hence they observed increase in ductility due to GFRP jacketing. The failure mode of the bare steel tube was outward buckling around the circumference. This failure mode is known as elephant foot buckling. For steel tube jacketed with single ply failure involved outward local buckling near the ends. For GFRP jackets having two and three plies inward buckling deformations away from ends was prevalent. They found that both ultimate load as well as ultimate shortening increase with use of GFRP jacketing. They found increase in ultimate load to be around 5 to 10 % while axial shortening at peak load enhanced by around 10 times through FRP confinement. FRP confinement of circular hollow steel tubes leads to great increase in ductility with very limited increases in strength, a feature that is highly desirable in the seismic retrofit of structures. They modeled FRP jacketed steel tubes in ABAQUS and considered both geometric and material non linearity. They found that load–axial shortening curves and the failure modes from the finite element model are in close agreement with those from the experiments.

D. Polyzois, S. Ibrahim, V. Burachynsky, and S. K. Hassan did experimental testing of GFRP poles to be used in transmission and distribution lines. They performed full scale tests on tapered GFRP poles with hollow circular cross section subjected to cantilever bending. They performed bending tests on 12 full scale GFRP poles of 6.25 m up to failure. They tested GFRP pole vertically and casted square reinforced concrete base of 800mm width and

1000 mm high with tapered circular hole in middle to hold the specimens vertically. They applied load horizontally 600 mm below the pole and at increment of 0.25mm/sec. Linear measurement transducers were used to measure deflection of pole as well as change in the diameter. Along with longitudinal layers circumferential layers were provided (except 2 specimens). They found that poles having 6 longitudinal layers and 2 circumferential layers performed better than poles having all layers as longitudinal. Almost all poles failed by local buckling on compression side at a height which varied from 200 mm to 800 mm above the concrete base. GFRP poles were modeled in ANSYS. Eight-node quadrilateral layered shell element was used to model GFRP poles. The portion of the specimen, embedded inside the concrete base, was also included in the model. They performed geometric nonlinear analysis considering ovalisation of pole diameter and large deflection happening in top of pole. They determined average ratio of the experimental-to-theoretical ultimate load to be approximately 0.99 with a standard deviation of 12%.

P. Sangeetha, R. Sumathi (2010) performed axial compression tests on circular concrete columns of 150mm diameter and 300 mm length wrapped with GFRP. In their study they varied wrapping materials which includes GFRP Materials Surface Mat(SM), Chopped Strand Mat (CSM), Woven Roving Mat(WRM), number of plies and period of curing. They prepared a total of 42 columns out of which 21 were cured for 7 days and 21 were cured for 28 days. They did not provide any wrapping for 6 cylinders. They also varied number of plies from 1 to 3. All the columns were tested in compression testing machine of 50 KN capacity and ultimate load was found out. They found that when columns were jacketed by Woven Roving Mat results were better than any other type of fiber. They found that percentage increase in compressive strength was 28.97% for Woven Roving Mat, 21.46% for Chopped Strand Mat and 3.6% for Surface Mat with one ply as compared to concrete columns without any jacketing. They also found that percentage increase in Compressive Strength for column wrapped with Woven Roving Mat for Single Ply and Triple Plies is 29 and 168% respectively. Hence they found that confinement of concrete columns with GFRP has increased strength and ductility.

Rami Haj-Ali and Hakan Kilic (2002) performed experimental coupon testing under tension, compression and shear using off axis coupons cut with different roving reinforcement orientations. Their composite was made by pultrusion process and was made of E glass, vinyl ester resin. They identified overall linear elastic properties along with nonlinear stress-strain behavior under in plane multiaxial tension and compression loading.

They performed their coupon testing with off axis angles of 0,15,30,45,60 and 90 degrees. They found that compression modulus was larger than tension modulus. This is because of presence of voids and defects in matrix that tend to open up during tension loading. They also found that nonlinear response for 0 and 15 degrees loading starts at higher level of strain but for angles greater than 15 degrees nonlinear response starts at lower strain. They also did parametric finite element study. During modeling they applied grip pressure on top and bottom grips to simulate displacement controlled test procedure by axially and rigidly sliding end surfaces of grips in a uniform manner. They applied displacement in loading direction. They found percent difference between axial strain and uniform strain and concluded that strain data readings of experimental coupon testing were reliable enough. To determine shear response, they did V notch shear tests. They also determined shear response occurring due to off axis coupon tests (under compression and tension) from off axis angles of 30 and 45 degrees. They found that shear response due to compression test was similar to that with V notch test while in tension response was different that can be attributed to presence of voids and micro cracks in matrix. They also proposed 3D nonlinear micromodels for roving and continuous filament mat. They found good agreement for all off axis coupon tests when compared with 3D micromodel results.

Togay Ozbakkaloglu, Deric J. Oehlers (2008) studied effect of CFRP confinement on concrete cylinders of 150 X 300 mm cross section and 600 mm height. They casted 10 cylinders, 3 without any CFRP reinforcement and rest with CFRP reinforcement. Three plies were used for CFRP reinforcement. They recommended new techniques of reinforcement such as GFRP confinement tube with internal panel and FRP tube with internal crossies. They performed tensile coupon testing of CFRP according to ASTM D3039 with 10 mm uniaxial strain gauge on both side of coupon. They found tensile strength of coupon less than given by manufacturer, which they said happened because of misalignment of the fibers with respect to the action line of applied loading. Columns were tested under axial compression using 5000KN UTM (universal testing machine). They used LVDTs to measure axial deformation and strain gauges to measure axial and circumferential strain. They found that all of confined columns failed by rupture of FRP tube which occurred on upper half of column. They suggested that this failure occurred because of shrinkage of concrete in that area. They found that maximum strains recorded at damaged portions of tube were lower than failure tension strains of coupons. They found that internal reinforcement to tube in form of interior panel provided better confinement as compared to tube with crossies as reinforcement. FRP tube with internal panel as reinforcement had

ultimate axial strain 50% higher than FRP tube without reinforcement. They found that confinement of rectangular columns with FRP tubes lead to substantial improvement in the ductility of the columns.

Fabio Minghini, Nerio tullini, Ferdinando laudiero performed three point and four-point bending tests on pultruded FRP profiles. To eliminate possible error in beam rigidities during shear and flexural tests, they prepared a new test configuration and compared it with that of existing schemes of three and four-point bending tests. They also performed parametric studies by varying span length and relative position of applied loads. They analyzed influence of load and deflection measurement errors and proposed proper confidence intervals for calculated rigidities. They found that with proposed four-point bending test when load is applied to end sections gives shear modulus having low scatter.

Ferdinando laudiero, Fabio minghini, Nicola ponara, Nerio tullini studied buckling mode interaction in wide-flange pultruded fiber-reinforced plastic (PFRP) columns under pure compression. They analyzed sensitivity to flatness and angularity as reported by manufacturers. In their numerical results they found imperfection amplitude has crucial role. They found that stocky members exhibit a stable post buckling behavior that is affected by material strength. They also performed incremental finite element analysis to check the response of imperfect pultruded fiber reinforced plastic under bending. They found that for low amplitude imperfection buckling-mode interaction does not influence the beam response significantly. In their numerical models they included geometric imperfection in form of straightness("S"), flatness ("F") and angularity ("A"). They used Tsai-wu failure criteria to determine onset of failure in web and flanges and proposed quadratic failure criteria for web-flange junction. They found angularity imperfection was ineffective for both stocky as well as slender columns. They found that limiting imperfection amplitude alter failure mode already given in literature. They also found that for intermediate length profiles with more realistic imperfection amplitudes, the drawbacks due to the buckling-mode interaction are moderate. They also proposed expression for rotational spring stiffness of web –flange junction and it yields accurate predictions of the local buckling moment.

Chapter 3

3.Experimental Program

3.1 General

Coupons were tested in tension, compression and bearing

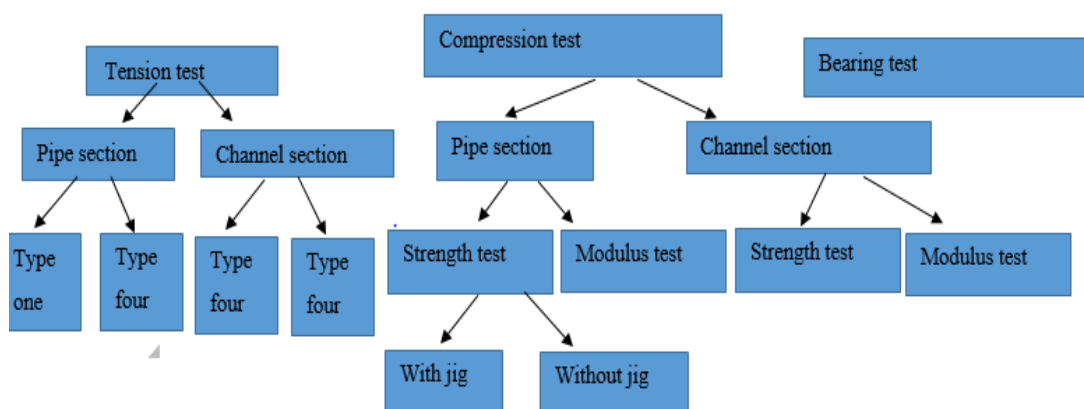


Figure 15Flow chat explaining experimental program

3.2. Tensile coupon testing

ASTM D 638 was followed to do the tensile coupon testing of the specimens. This test method covers the determination of the tensile properties of unreinforced and reinforced plastics in the form of standard dumbbell-shaped test specimens. This test method is applicable for testing materials of any thickness up to 14 mm (0.55 in.). For performing experimental testing according to ASTM D 638 a testing machine having constant rate of crosshead movement and having a stationary member holding one grip and a movable member holding another grip is needed. Grips for holding the test specimen between the fixed member and the movable member of the testing machine can be either the fixed or self-aligning type Fixed grips are rigidly attached to the fixed and movable members of the testing machine. Extreme care is taken to ensure that the test specimen is inserted and clamped so that the long axis of the test specimen coincides with the direction of pull through the center line of the grip assembly.

3.2.1. Dimensions of specimens according to ASTM D 638

There are various types of specimens depending on thickness of specimen. Type I specimen is the preferred specimen and shall be used where sufficient material having a thickness of 7 mm (0.28 in.) or less is available. Type II specimen is recommended when a material does not break in the narrow section with the preferred Type I specimen. Type III specimen must be used for all materials with a thickness of greater than 7 mm (0.28 in.) but not more than 14 mm (0.55 in.). Type IV specimen is generally used when thickness is 4mm or less and when direct comparisons are required between materials in different rigidity cases (that is, nonrigid and semi rigid). Type V specimen shall be used where only limited material having a thickness of 4 mm (0.16 in.) or less is available for evaluation, or where a large number of specimens are to be exposed in a limited space (thermal and environmental stability tests, etc.).

Since specimens tested were having thickness greater than 4 mm and less than 7mm they fall in TYPE 1 category.

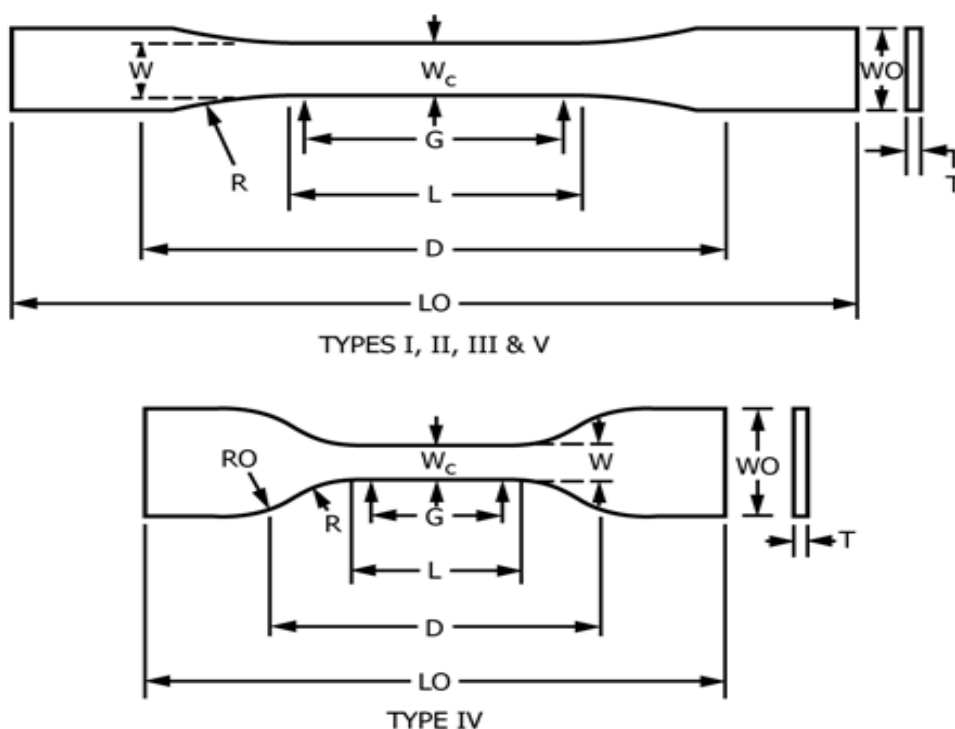


Figure 16 Different types of specimen according to ASTM D 638

Dimensions (see drawings)	Specimen Dimensions for Thickness, T , mm (In.) ^A					Tolerances
	7 (0.28) or under		Over 7 to 14 (0.28 to 0.55), Incl	4 (0.16) or under		
	Type I	Type II	Type III	Type IV ^B	Type V ^{C,D}	
W —Width of narrow section ^{E,F}	13 (0.50)	6 (0.25)	19 (0.75)	6 (0.25)	3.18 (0.125)	± 0.5 (± 0.02) ^{B,C}
L —Length of narrow section	57 (2.25)	57 (2.25)	57 (2.25)	33 (1.30)	9.53 (0.375)	± 0.5 (± 0.02) ^G
W_0 —Width overall, min ^G	19 (0.75)	19 (0.75)	29 (1.13)	19 (0.75)	...	+ 6.4 (+ 0.25)
W_0 —Width overall, min ^G	9.53 (0.375)	+ 3.18 (+ 0.125)
L_0 —Length overall, min ^H	165 (6.5)	183 (7.2)	246 (9.7)	115 (4.5)	63.5 (2.5)	no max (no max)
G —Gage length ^I	50 (2.00)	50 (2.00)	50 (2.00)	...	7.62 (0.300)	± 0.25 (± 0.010) ^G
G —Gage length ^I	25 (1.00)	...	± 0.13 (± 0.005)
D —Distance between grips	115 (4.5)	135 (5.3)	115 (4.5)	65 (2.5) ^I	25.4 (1.0)	± 5 (± 0.2)
R —Radius of fillet	76 (3.00)	76 (3.00)	76 (3.00)	14 (0.56)	12.7 (0.5)	± 1 (± 0.04) ^G
RO —Outer radius (Type IV)	25 (1.00)	...	± 1 (± 0.04)

Figure 17 Standard specimen dimensions according to ASTM D638

3.2.2 Dimensions of tested specimens (TYPE ONE)

Specimen were fabricated according to dimensions in ASTM D 638 and according to type one specimen. Specimens were cut from pipe (230 mm dia, 300 mm long and 6mm thick) and channel sections (102mm web x 45mm flanges x 6mm thick).

Specimen	Gauge portion			Whole specimen		
	Length (mm)	Width (mm)	Thickness (mm)	Length (mm)	Width (mm)	Thickness (mm)
P2	50	14.41	6.03	165	19.53	6.44
P3	50	12.88	5.89	165	19.93	6.2
P5	50	14.05	6.16	165	20.13	6.33
P6	50	13.64	6.19	165	19.73	6.22
P11	50	12.75	6	165	20	7.1
P13	50	13.7	6.04	165	19.75	6.28
P15	50	13.22	6.1	165	19.41	6.38

Table 4 Dimensions of specimens cut from pipe section (type one)

Specimen	Gauge portion			Whole specimen		
	Length (mm)	Width (mm)	Thickness (mm)	Length (mm)	Width (mm)	Thickness (mm)
C3	50	12.65	6.07	165	19.28	6.13
C4	50	13.81	6.17	165	18.82	6.33
C5	50	12.64	6.12	165	19.59	6.16
C6	50	13.12	6.1	165	19.5	6.14
C9	50	13.51	6.16	165	19.64	6.14

Table 5 Dimensions of specimens cut from channel section (type one)

In channel sections coupon specimens were cut from web

3.2.3 Speed of testing

Speed of testing shall be the relative rate of motion of the grips or test fixtures during the test. As the tested specimens were Type I the rate of loading was selected as 5mm/min.

Classification ^{af}	Specimen Type	Speed of Testing, mm/min (in./min)	Nominal Strain ^c Rate at Start of Test, mm/mm·min (in./in.-min)
Rigid and Semirigid	I, II, III rods and tubes	5 (0.2) ± 25 %	0.1
		50 (2) ± 10 %	1
		500 (20) ± 10 %	10
	IV	5 (0.2) ± 25 %	0.15
		50 (2) ± 10 %	1.5
		500 (20) ± 10 %	15
V	1 (0.05) ± 25 %	0.1	
	10 (0.5) ± 25 %	1	
	100 (5) ± 25 %	10	
Nonrigid	III	50 (2) ± 10 %	1
		500 (20) ± 10 %	10
		500 (20) ± 10 %	15
IV	50 (2) ± 10 %	1.5	
	500 (20) ± 10 %	15	
	500 (20) ± 10 %	15	

Figure 18 Standard speeds for different types of specimens ASTM D 638

3.2.4 Procedure

Width and thickness of each specimen was measured with Vernier caliper. A properly calibrated fatigue testing machine of 500 KN capacity is used. Specimens were placed in the grips of the testing machine, taking care to align the long axis of the specimen and the grips with an imaginary line joining the points of attachment of the grips to the machine. Grips are tightened evenly and firmly to the degree necessary to prevent slippage of the specimen during the test, but not to the point where the specimen would be crushed. Speed of testing was set at the proper rate. Load-extension curve of the specimen was recorded. For strain

measurement a clip on extensometer was used. Gauge length of extensometer was 50 mm. Strain was determined by dividing displacement obtained from the extensometer by its gauge length. Tensile strength was calculated by dividing the maximum load sustained by the specimen in Newton by the average original cross-sectional area in the gage length segment of the specimen in square millimeters. Result is expressed in Mpa as tensile strength at break. Stress vs strain graph and load vs deflection graphs of specimens were plotted.

3.2.5 Fixture



Figure 19 Fixture used for tension coupon testing

Grips of 500KN FTM (Fatigue testing machine) served as a fixture for the coupon specimens tested in tension. One of the grips was connected to movable member while another was connected to stationary member. Specimen was properly centered between the grips and tensile load was applied.

3.2.6 Dimensions of tested specimens (TYPE FOUR)

Specimen were fabricated according to dimensions in ASTM D 638 and according to type four specimen. Specimens were cut from pipe (230 mm dia, 300 mm long and 6mm thick) and channel sections (102mm web x 45mm flanges x 6mm thick). These specimens were prepared for determining tension strength properties of the material.

Specimen	Gauge portion			Whole specimen		
	Length (mm)	Width (mm)	Thickness (mm)	Length (mm)	Width (mm)	Thickness (mm)
PF1	28.9	7.2	5.2	115.8	27.2	5.3
PF2	25.8	7.7	5.8	116	26.8	6
PF3	27.4	6	5.3	116	26	5.5
PF4	28.8	8.2	5.3	115.6	28.1	5.1
PF5	29.9	6.9	5.4	117.4	27.2	5.4
PF6	28.9	6	5.2	116.5	28.4	5.0
PF7	31.6	6.3	5.2	116.4	26.8	5.7
PF8	31	8.1	5.8	115.2	28.5	6.1
PF9	32.7	6.8	5.4	116.6	28	5.8
PF10	30.36	8.43	5.6	117.3	29.6	5.7

Table 6 Dimensions of TYPE four specimens cut from pipe section

Specimen	Gauge portion			Whole specimen		
	Length (mm)	Width (mm)	Thickness (mm)	Length (mm)	Width (mm)	Thickness (mm)
C1	32.2	7.3	6.5	115.9	28	7
C2	27.9	7.8	6.7	117.5	27	6.7
C3	26.4	7.7	6.1	116	27.5	6.2
C4	37.9	8.1	6.8	118.2	27.5	7.1
C5	33.9	7.5	6.7	115.3	27.6	6.8
C6	29	8	6	117.5	27.5	6.1
C7	30.2	7.7	6	117.3	27.8	6.1
C8	32.4	6.7	6.8	117.05	27.2	6.5
C9	29.3	7.8	6.6	114.1	27.2	7
C10	30.8	7.1	6	115.5	27.3	6.1
C11	30	7.2	6	115.9	27.2	6.2

Table 7 Dimensions of TYPE four specimens cut from channel section

3.2.7 Tension testing of type four specimen

Speed of tension coupon testing for type four specimen was maintained same as that of type one and maintained as 5 mm/min. Type four specimens were testing in order to determine

only maximum tensile stress properties. Fixture adopted for type four specimens was similar to type one but for type four specimens experimental testing was done in 30 KN UTM (Universal testing machine) with one of the grips was connected to movable member while another was connected to stationary member.

Procedure adopted for experimental testing of Type four specimens was same as that adapted for Type one. Load was until failure of specimen to record maximum tensile stress.

3.3 Compression testing

ASTM D 695 code was followed to do the compressive coupon testing of the specimens. This test method covers the determination of the mechanical properties of unreinforced and reinforced rigid plastics, including high-modulus composites, when loaded in compression at relatively low uniform rates of straining or loading. Test specimens of standard shape are employed. This procedure is applicable for a composite modulus up to and including 41,370 Mpa. This test method is used to produce compressive property data for specifications of plastic materials. These property data are useful for material characterization as well as for research and development.

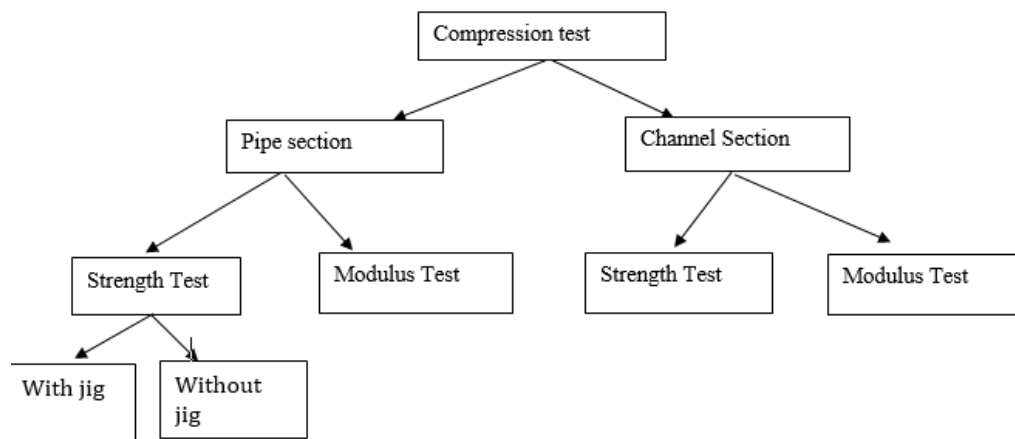


Figure 20 Flow chart showing experimental testing for compression test

3.3.1 Specimen Preparation

Specimens were cut from gauge length of coupons used for tension testing. Coupons were cut according to standard dimensions given in ASTM D 695 from both pipe and channel coupon specimens. Specimens used were of different dimensions according to property determined. For strength determination specimens were like cube having equal length and

width and for modulus determination specimens were cuboidal with length almost double of width.

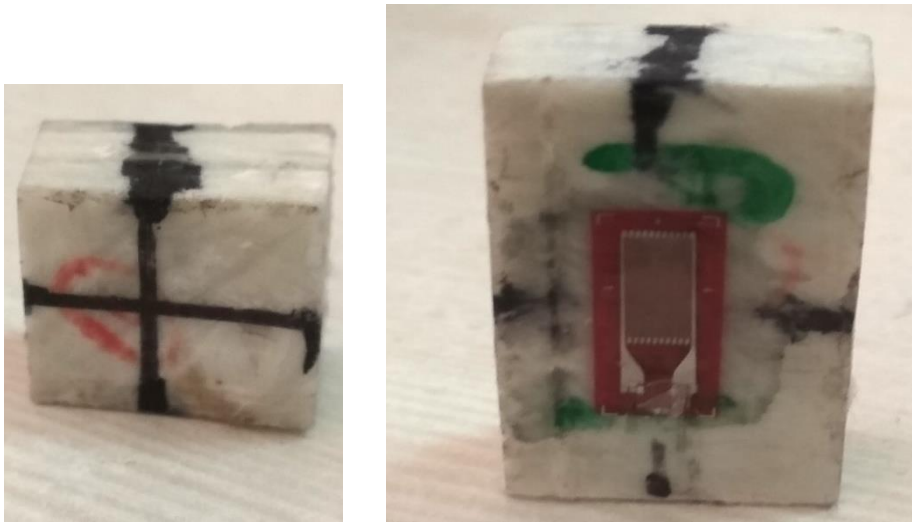


Figure 21 Specimen prepared for strength test(left), Specimen prepared for modulus test (right)

3.3.2 Dimensions of specimens according to ASTM D 695

According to ASTM D 695 for specimens having thickness in between 3.2mm to 6.4 mm specimen fabricated for strength measurement shall consist of a prism having cross section of 12.7mm by thickness of specimens and should have length of 12.7 mm. Code also recommends to shorten length if buckling is observed. For modulus measurement code recommends specimen dimensions such that slenderness ratio should be in the range of 11 to 16. which comes down to a dimension of 12.7mm by thickness of specimens and a length of 25.4mm. Code recommends use of following formula for slenderness ratio calculation.

$$\lambda = L_c / r$$

$$r = 0.289 t_c$$

3.3.3 Dimensions of specimens used for compression testing

Specimens were prepared according to ASTM D 695 Provisions. For strength test specimens of 12.7mmx12.7mmx6mm were prepared and for modulus test specimens of 25.4mm x12.7mmx6mm were prepared.

Table 3.5 Dimensions of specimens used for strength test

Specimen	Length(mm)	Width(mm)	Thickness(mm)
P-10	12.85	12.56	6.26
P-14	12.77	11.63	5.93
P-12	14.17	12.83	6.22

P-4	12.84	12.59	6.11
P-8	12.87	12.7	5.92

Table 3.6 Dimensions of specimens used for modulus test

Specimen	Length(mm)	Width(mm)	Thickness(mm)	Radius of gyration	Slenderness ratio
PL-12	25.22	12.53	5.97	1.725	14.62
PL-10	25.98	12.8	5.95	1.719	15.11
PL-14	25.48	11.4	6.03	1.742	14.62
PL-4	25.81	12.84	5.98	1.728	14.93
PL-8	25.18	12.94	6.11	1.766	14.26

ASTM D 695 recommends slenderness ratio to be in the range of 11 to 16 for specimens prepared for modulus measurement. In this study slenderness ratio is maintained between 11 to 16.

3.3.4 Speed of testing

Speed of test takes into account relative motion of grips or test fixtures during the test. Speed of test was maintained in accordance to ASTM D 695. Speed of 1.3 mm/min was used.

3.3.5 Procedure

Width and thickness of specimens were measured for each of the specimens using Vernier calipers. Length of specimens was also measured and slenderness ratio was calculated for each of specimen and it was made sure that it lies within prescribed limits. Specimens were properly aligned and centered on 100mm diameter compression platens and it was made sure that ends of specimens are flat and parallel and they are properly aligned with compression platens. Specimens were tested in 100 KN FTM (Fatigue testing machine) in which load was applied through top platen. 6 mm uniaxial strain gauges were pasted on the specimens to measure strain.

Test was conducted with speed of 1.3mm/min. Maximum load carried by specimens was recorded. Maximum load carried by the specimens was divided by width and thickness of specimens to get Maximum compressive stress. Maximum compressive strain was recorded

by strain gauge. Stress vs strain graph and load vs deflection graphs of specimens were plotted.

3.3.6 Fixture



Figure 22Compression platens

100 mm diameter compression platens were used for placing and centering of specimen. Load was transferred to specimens through compression platens. Surface of specimens were made flat and parallel and properly aligned and parallel with compression platens. Bottom platen was stationary while load was applied through top platen. Platens had inscribed circles for centering and placing the specimens.

3.4 Bearing Test

Bearing test was done to find out maximum bearing stress carried by the specimen. ASTM D 953 codal provisions were used to perform the test. This test method is used to produce bearing property data for specifications of plastic materials. These property data are useful for material characterization as well as for research and development. Bearing test can be performed under tension loading as well as under compression loading. In this study bearing test under tension loading was performed.

3.4.1 Dimensions of specimens according to ASTM D 953

ASTM D 953 requires specimen with hole to be fabricated for bearing strength test. It recommends that thicker specimens with larger bearing hole are expected to give more accurate and precise results, but it's better to use thinner specimens with smaller bearing hole for brittle plastics so that they are less likely to fail prematurely.

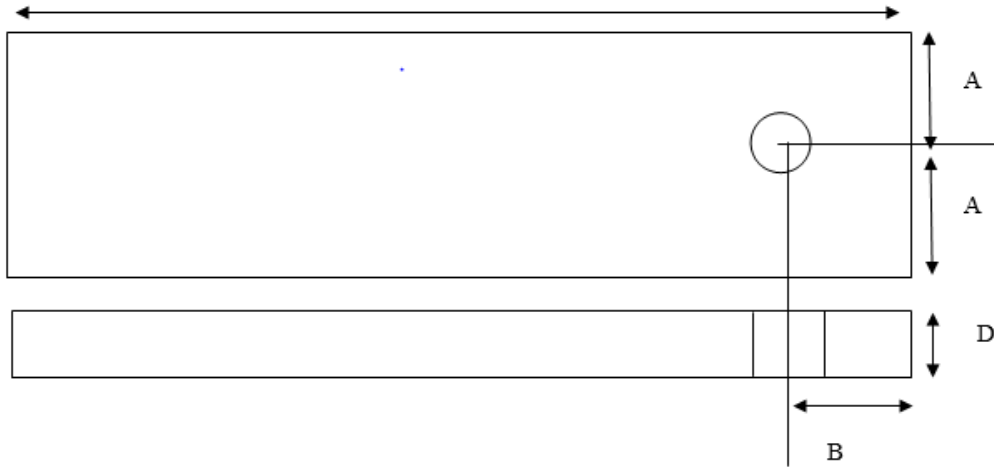


Figure 23 Dimensions of specimen for bearing strength test according to ASTM D 953

Type	A(mm)	B(mm)	C(mm)	D(mm)	Hole diameter(mm)
I	11.913±0.127	19.05±0.127	120.6	3.2	3.2±0.025
II	11.913±0.127	19.05±0.127	120.6	6.4	6.375±0.025

Table 8 Dimensions of specimen for bearing strength test (ASTM D 953)

where C: length of the specimen in (mm)

A: distance from the center of the bearing hole to the edge of the specimen perpendicular to the direction of the principal stress.

B: distance from the center of the bearing hole to the edge of the specimen in the direction of the principal stress.

D: bearing hole diameter.

3.4.2 Dimensions of specimens used for bearing strength test

Specimens were fabricated according to dimensions given in ASTM D 953.

Specimen	C(mm)	2A(mm)	B(mm)	Thickness(mm)	D(mm)
B1	122	25.4	18.8	4	4
B2	120.79	22.21	18.81	4.03	4.03
B3	122	22.77	19.01	4.03	4.03

B4	121.08	22.85	18.8	4.05	4.05
B5	120.1	22.23	18.62	4	4
B6	120.6	21.56	18.8	3.43	3.73
B7	120.95	23.1	18.24	3.46	3.97
B8	120.07	20.74	18.49	3.87	3.87
HRB1	123.3	25.7	18.79	3.81	3.88
HRB2	123.53	24.97	18.72	3.69	3.92
HRB3	123.3	24.9	19.05	3.67	3.84
HRB4	123.17	25	18.73	3.97	3.96
HRB5	123.51	24.66	19.05	4.02	3.95
HRB6	123.84	25.19	18.76	4.1	3.73
HRB7	122.28	25.92	18.84	4.03	3.7
HRB8	123.32	24.99	19.02	4.0	3.83

Table 9 Dimensions of specimens used for bearing strength test

3.4.3 Speed of testing

Speed of test takes into account relative motion of grips or test fixtures during the test. Speed of test was maintained in accordance to ASTM D 953. Specimens were tested in 30KN UTM (universal testing machine) with speed of 1.3mm/min.

3.4.3 Fixture

A three-plate tension fixture of hardened steel consisting of hardened spacer plate, side plate and test specimen was adopted. Hardened steel pin was inserted in the reamed hole. Bearing strength test was performed under tension loading.

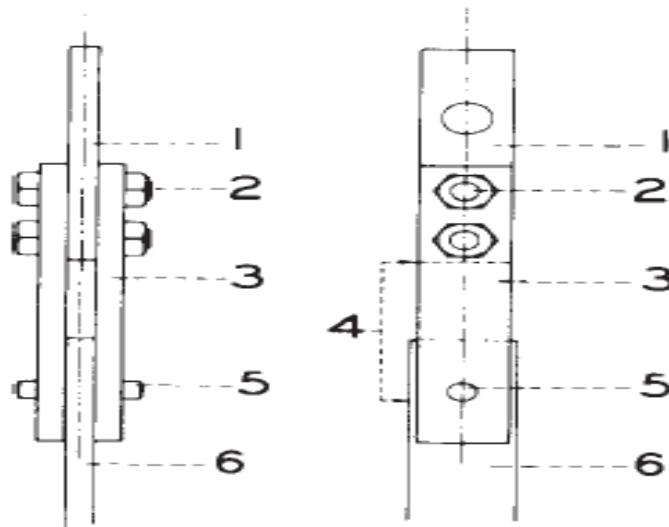


Figure 24Side view(left) and Front view (right) of tension fixture

- 1: Hardened spacer plate
- 2: 6.3 mm steel bolts in reamed holes
- 3: Hardened side plate
- 4: Extensometer span
- 5: Hardened steel pin in reamed hole

Type	Bearing hole diameter (mm)	Bearing pin diameter (mm)	Thickness of spacer plate (mm)
I	3.175±0.025	3.15	3.2
II	6.35±0.025	6.325	6.3

Table 10Dimensions of Fixture used for bearing strength test (tension loading)

3.4.4 Procedure

Dimensions of each specimen was measured with Vernier caliper. Special care was taken to measure diameter and thickness of specimen. The specimen to be tested was mounted in the tension loading fixture. Long axis of the specimen was aligned with the center line of the testing fixture. Specimen was loaded with the prescribed rate of crosshead travel i.e. 1.3 mm/min. Only maximum bearing stress was determined by this test. Test is continued until the maximum load is sustained. Load –deflection curve for each specimen was plotted. Maximum bearing stress is calculated by dividing the maximum load by the product of the bearing hole diameter and the specimen thickness. Stress vs strain graph for each of the specimen was plotted. Maximum bearing stress taken by specimen is calculated.

3.5 Compression test on short hollow tubes

3.5.1 General

Testing of short hollow cylindrical tubes of 230 mm diameter, 6 mm thickness and 300 mm length is done. Objective of the test is to find out compressive strength, modulus of elasticity and failure loads of specimens and compare it with that of coupon specimens. Load is applied axially and failure load and strength are found out. A fixture is manufactured consisting of steel plates with roller on top of it to provide hinge-hinge boundary conditions on both the ends. Strain gauges are located on predefined location to measure strains. Rate of loading is maintained same as coupon testing of 1.3 mm/min. Experiment is carried on till failure of specimen and compressive strength, modulus of elasticity and failure loads are recorded.

3.5.2 Equipment used

For testing 5000 KN CTM (compression testing machine) was used. Machine consists of two platens of 300 mm diameter in which bottom platen is movable while top platen is static. Centre of platens was marked and specimen's Centre was made to coincide with platen Centre. Fixture consisting of steel plates and roller was placed below platens of machine.

3.5.3 Speed of test

Speed of test is considered as the relative motion between compression platens. Speed of testing was maintained same as that of coupon test of 1.3 mm/min.

3.5.4 Fixture

A fixture is manufactured consisting of steel plates with roller on top of it to provide hinge-hinge boundary conditions on both the ends.

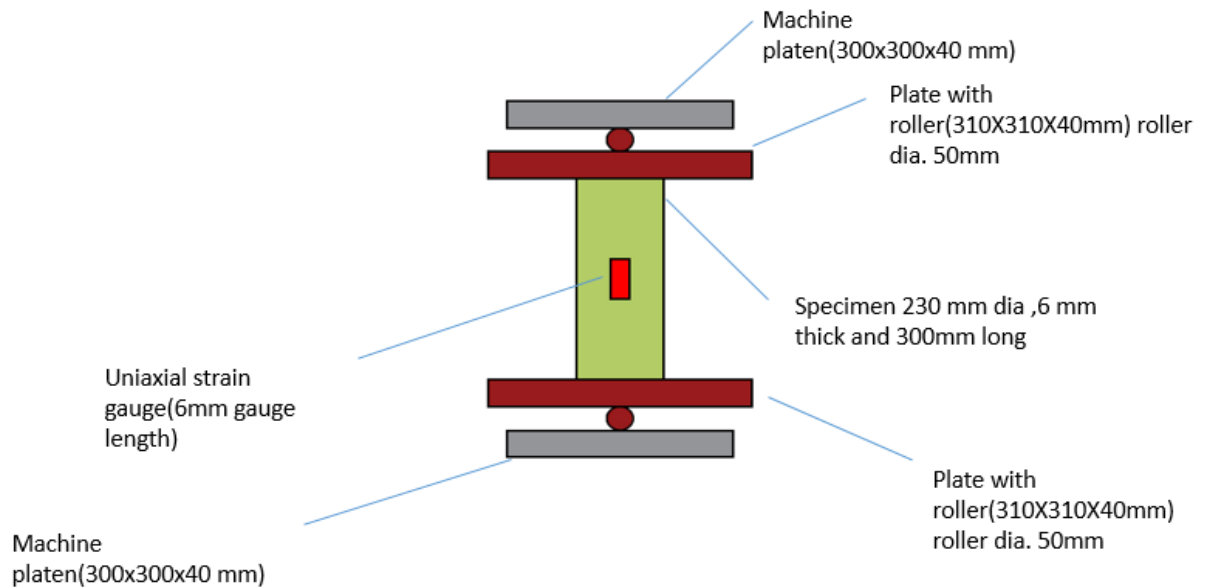


Figure 25 Fixture for compression test of short hollow GFRP tubes

Fixture is placed directly between the platens without any connection or support to ensure hinge-hinge boundary conditions. Plate in fixture is selected such that it has adequate thickness to counter the compressive load applied by machine platens and to ensure that no crushing of fixture plates take place. Mild steel plate of 40 mm thickness was placed on both sides of specimen.

3.5.5 Dimensions of specimens

Dimensions of each of the specimen was maintained same with 230 mm diameter, 300 mm length and 6 mm thickness. Slenderness ratio of tube can be calculated as

$$\lambda_{\text{tube}} = L_{\text{tube}} / r_{\text{tube}}$$

$$r_{\text{tube}} = \sqrt{I_{\text{tube}} / A_{\text{tube}}}$$

3.5.6 Orientation of strain gauges

Strain gauges were placed all over the circumference of the specimen at diametrically opposite points. It was ensured that strain gauges are placed in the imperfection located area to record the failure strain.

3.5.6.1 Orientation of strain gauge for specimen one

A total of 3 specimens were tested under axial compression. Strain gauges were positioned at diametrically opposite points.

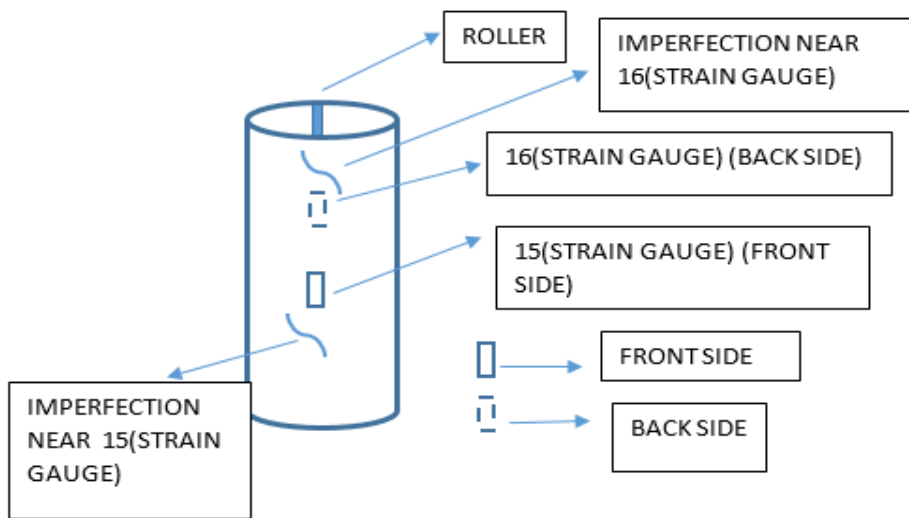


Figure 26 Orientation of strain gauges for specimen one

As it can be seen in Figure 26 strain gauge 15 and 16 are provided on diametrically opposite sides. Both the strain gauges were placed near imperfection area to record failure strain. Both the strain gauges were provided along the direction of roller.

3.5.6.2 Orientation of strain gauge for specimen two

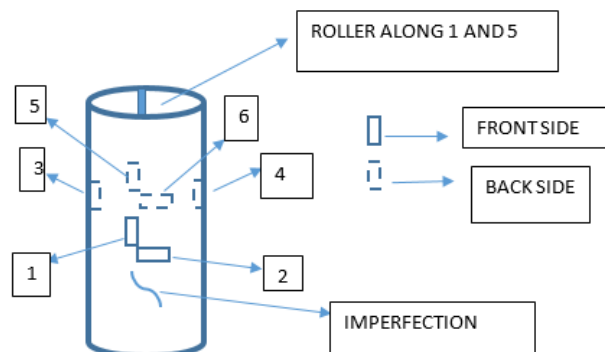


Figure 27 Orientation of strain gauge for specimen two

As it can be seen in above Figure 27 that 1 and 5 strain gauges are placed along the roller and 2 and 6 are placed perpendicular to 1 and 5 respectively. 3 and 4 are placed perpendicular to roller along the sides of the tube. Imperfection was present near 1 and 2 strain gauge. Strain gauges were positioned in this manner to record both longitudinal as well as circumferential strain.

3.5.6.3 Orientation of strain gauge for specimen three

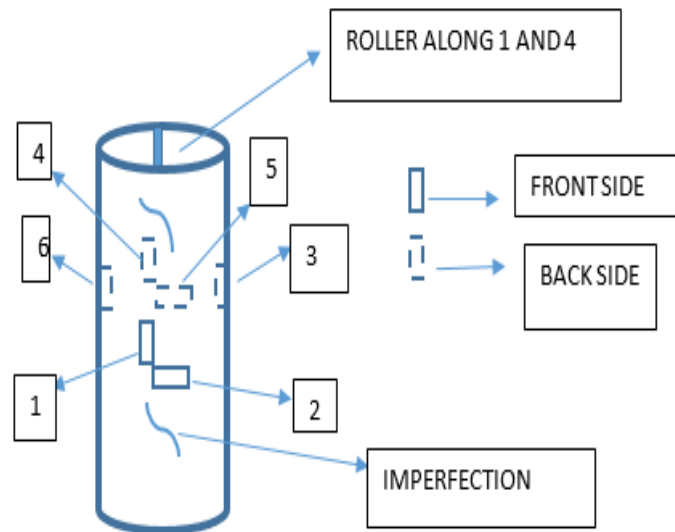


Figure 28 Orientation of strain gauges for specimen three

Strain gauges were provided at diametrically opposite points. Strain gauge 1 and 4 are provided along the roller. Strain gauges 2 and 5 are provided perpendicular to strain gauge 1 and 4 respectively. Strain gauges 3 and 6 are provided perpendicular to roller along the sides of tube. Imperfection was present near 1 and 2 strain gauge as well as around 4 and 5 strain gauge.

3.5.7 Procedure

Diameter, thickness and length of hollow circular tube were measured. Thickness was measured with Vernier caliper to have pin point accuracy. Uniaxial axial strain gauges of 6 mm gauge length were pasted to predefined positions that varied from specimen to specimen. Centre of specimens were marked and were made to align with the Centre of fixture and machine platen. AN 5000 KN CTM (compression testing machine) was used for test and speed of loading was maintained same as coupon test of 1.3 mm/min. LVDT of 50

mm gauge length was placed on bottom platen to measure displacement of specimen. Specimen was loaded till failure and load vs displacement and stress vs strain curves of specimen were plotted.

3.6 Compression test with jig

3.6.1 General

Compression test was performed with jig according to provisions of ASTM D 695. It was performed with jig to provide lateral support to provide any possible delamination occurring in specimens. All loading conditions and fixtures were maintained same as that for compression test without jig.

3.6.2 Speed of test

Speed of test was maintained according to provisions of ASTM D 695. Speed of test was maintained as 1.3 mm/min.

3.6.3 Dimensions of specimens

Specimens were dimensioned as according to provisions of ASTM D695. Specimens to be tested with jig have longer length as compared to specimens without jig.

Specimen	Width	Thickness	Length(overall)	Width(overall)
1	12.48	6.21	78.27	18.83
2	12.83	5.95	79.08	18.44
3	13.65	6.19	78.30	19.44
4	14.51	6.09	79.42	19.48
5	13.22	6.12	78.02	18.62
7	13.39	6.15	79.73	19.13

Table 11 Dimensions of coupons used for compression testing with jig

3.6.4 Fixture

Specimen was centered between compression platens of 100 mm diameter. Care was taken to align jig at the center of platen. Inscribed circles in the compression platen were used to center the specimen.



Figure 29 Fixture for compression test of coupons with jig

3.6.5 Procedure

Width and thickness of specimens were measured for each of the specimens using Vernier calipers. Length of specimens was also measured. Specimens were properly aligned and centered on 100mm diameter compression platens. Specimens were inserted in jig and were finger tightened and were made properly aligned and centered with respect to the compression platens. Specimens were tested in 100 KN FTM (Fatigue testing machine) in which load was applied through top platen

Test was conducted with speed of 1.3mm/min. Maximum load carried by specimens was recorded. Maximum load carried by the specimens was divided by width and thickness of specimens to get Maximum compressive stress. Stress vs strain graphs of specimens were plotted.

3.7 Preparation of plates by hand layup technique

3.7.1 General

A set of four composite plates were prepared by hand layup technique. Dimensions of these plates were 300mm X 300mm X 6 mm. Volume fraction was maintained same for all 4 composite plates. Out of four composite plates, one was without rovings and was made with 10 mats. For remaining composite plates rovings as well as mats were varied in number. For

second plate a total of 339 rovings were used along with 2 mats one on top and bottom of rovings. For third plate a total of 255 rovings were used along with 4 mats on top and bottom of rovings. For fourth plate a total of 170 rovings were used along with 6 mats on top and bottom of rovings. Mat used in hand layup was GSM 688 having only 90 and 0 degree fibers.

3.7.2 Volume fraction calculation

For calculation of volume fraction g/m^2 of mat was multiplied with length(300mm) and width(300mm) of the plate to determine weight of mat. Weight of all 10 mats was divided by density of glass fibers to determine total volume of mats. For rovings tex(gram/km) was multiplied with length of plate to determine weight of single roving. Then weight of mats was replaced by weight of rovings by subtracting weight of mats used from the total weight of all mats. Total weight of rovings was then divided by weight of single roving to get the number of rovings used. 15 segments were made in steel rod for wrapping rovings in them. These segments were 20 mm in length and were made in 300 mm length of steel rod. Total number of rovings were then divided by number of segments to determine number of rovings in each segment.

By performing above calculations volume fraction came out to be 43.46% and was maintained in all composite plates.

3.7.3 Stacking sequence

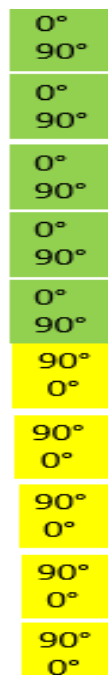


Figure 30 Stacking sequence followed for composite plate 1

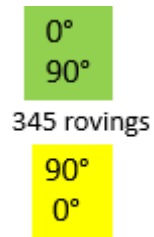


Figure 31 Stacking sequence followed for composite plate 2

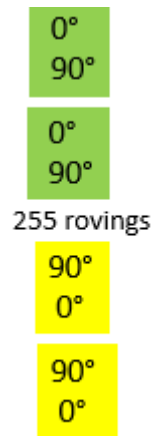


Figure 32 Stacking sequence followed for composite plate 3

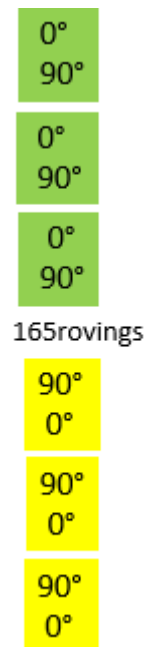


Figure 33 Stacking sequence followed for composite plate 4

Mats of 0 and 90 degrees were arranged in such a manner that laminate becomes symmetric. Mats of 90 and 0 degrees were stacked in such way that stacking sequence becomes symmetric.



Figure 34Placing of mat in plastic film

Mats were placed in plastic film and were tensioned slightly before application of resin. Resin was applied on both sides of mat. Mats were placed in such order that zero degree comes at top of laminate.



Figure 35Application of resin in mats

Resin was applied in appropriate amount such that fiber mats are not left dry. Amount of resin was taken more than required amount as in last some amount of resin was wasted while making the surface flat and while removing air voids.

Rovings were tied on steel bar. Segments were marked on steel bar; total 15 segments were marked on 300 mm length of steel bar. For composite plate two twenty-three rovings were provided in each segment. For composite plate three 17 rovings were provided in each segment. For composite plate four 11 rovings were provided in each segment.



Figure 36Tensioning of rovings done with help of steel rods

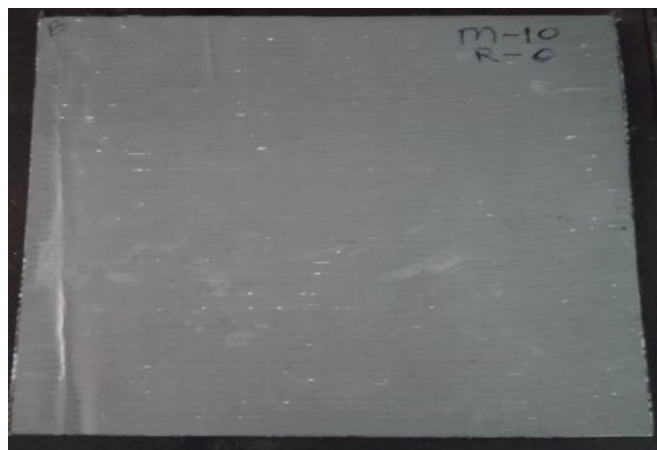


Figure 37Composite plate with no rovings and with 10 mat

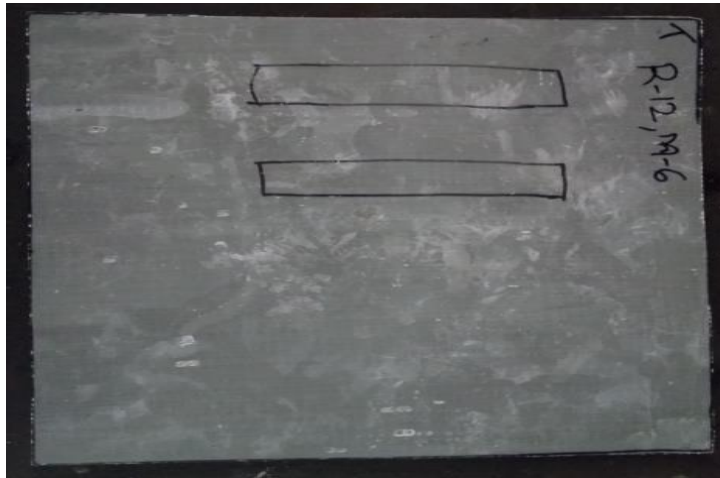


Figure 38 Composite plate with 165 rovings and 6 mats

Orientation of zero degree to cut coupons from composite plates was marked in plates. Dogbone specimens of TYPE 1 according to ASTM D 638 will be cut from composite plates.

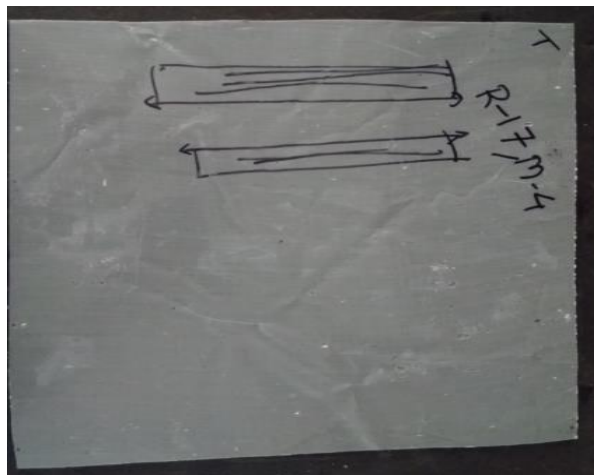


Figure 39 Composite plate with 255 rovings and 4 mats

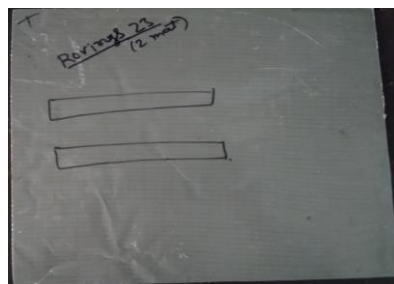


Figure 40 Composite plate with 345 rovings and 2 mats

Chapter 4

4. Numerical studies

4.1 Modeling of H beams (validation study)

Numerical validation of two H beams is performed. Beams are modeled in Abaqus. Beams are stacked using composite layup in Abaqus. Beams are modeled using S4 shell element. Mid-span deflection of the two beams for a specified load is calculated. Mid span deflections obtained for two H beams are validated with the midspan deflections obtained experimentally.

4.1.1 H beam 1

4.1.1.1 Material properties of H beam1

Material properties for H beam1 (6 x 6 x 1/4) were taken from Barbero et.al. These properties consist of longitudinal and transverse young modulus, shear modulus, poisson's ratio and thickness of individual layer. These properties are entered in the material property section in Abaqus.

Layer	E1 (10 ⁶ psi)	E2 (10 ⁶ psi)	G12 (10 ⁶ psi)	v	t (in)
1.5oz csm	1.716	1.716	0.605	0.419	0.025
2oz csm	1.861	1.861	0.655	0.421	0.03
22rovings	4.047	0.909	0.351	0.294	0.05
28 rovings	5.016	1.104	0.428	0.289	0.05
25 rovings	4.532	0.999	0.387	0.292	0.05
Matrix	0.49	0.49	0.198	0.24	0.045

Table 12 Material properties for H beam1 (Barbero et.al)

4.1.1.2 Stacking sequence of H beam 1

Stacking sequence for the pultruded H beam 1 consists of 7 layers in the top flange, 7 layers in the web and 7 layers in the bottom flange.

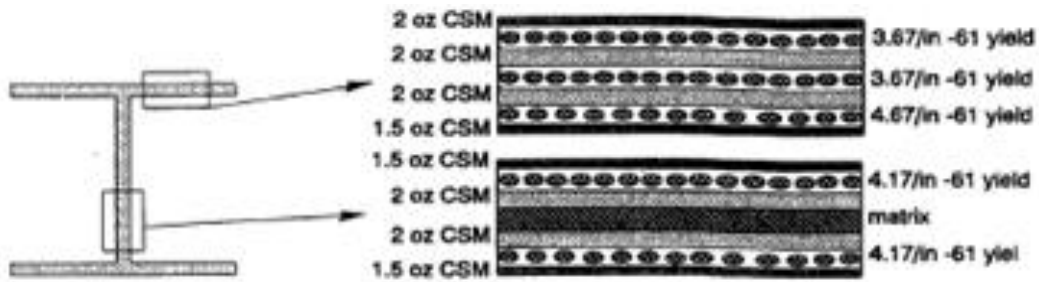


Figure 41 Stacking sequence of H beam 1 (Barbero et.al)

The above mentioned layup of the beam was given in Abaqus using the composite layup option. In the composite layup option region and material for the corresponding ply is selected and the corresponding thickness is given. Layup CSYS coordinate system is selected and the rotation angle is given. 3 integration points are provided, which means integration is done at bottom surface, middle surface and top surface of the ply.

		Ply Name	Region	Material	Thickness	CSYS	Rotation Angle	Integration Points
1	✓	Ply-1	(Picked)	two_oz_CSM	0.03	<Layup>	0	3
2	✓	Ply-2	(Picked)	roving_22	0.05	<Layup>	0	3
3	✓	Ply-3	(Picked)	two_oz_CSM	0.03	<Layup>	0	3
4	✓	Ply-4	(Picked)	roving_22	0.05	<Layup>	0	3
5	✓	Ply-5	(Picked)	two_oz_CSM	0.03	<Layup>	0	3
6	✓	Ply-6	(Picked)	roving_28	0.05	<Layup>	0	3
7	✓	Ply-7	(Picked)	onehalf_oz_CSM	0.025	<Layup>	0	3

Figure 42 Stacking sequence of H beam 1 used in abaqus (composite layup)

4.1.1.3 Load and boundary conditions for H beam 1

Load is applied as distributed load at center with a magnitude of 1000lb. H Beam 1 is given simply supported boundary conditions restraining the translation in x, y and z directions.

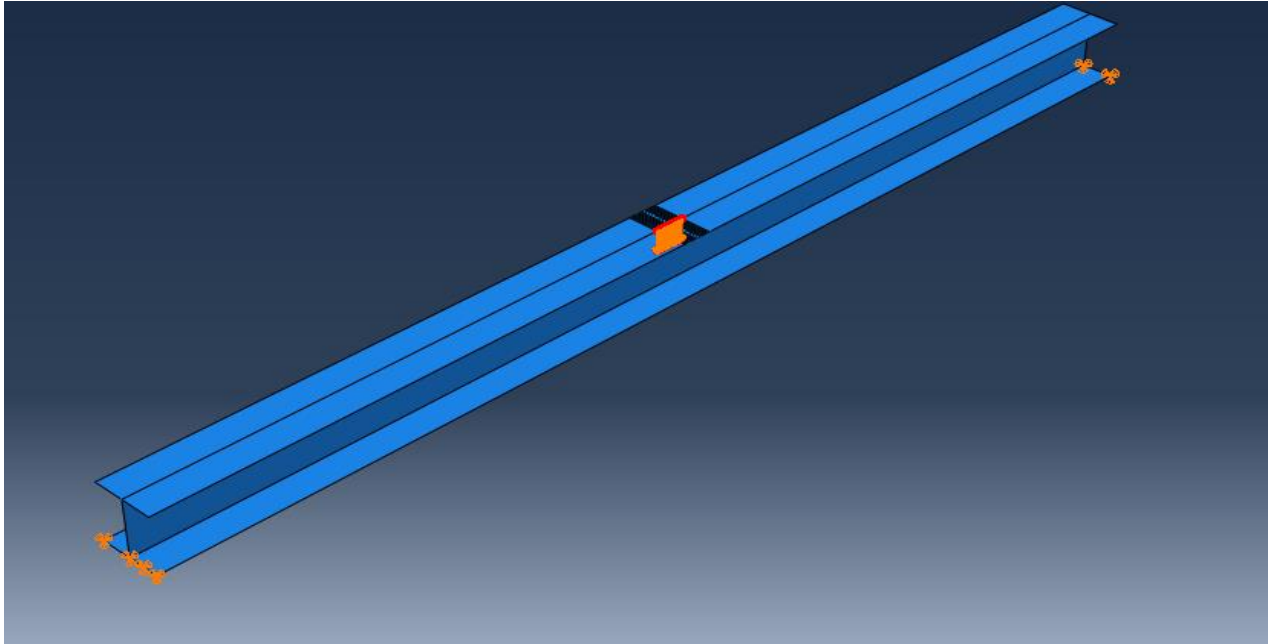


Figure 43 Load and boundary conditions used for H beam 1

4.1.2 H beam 2

4.1.2.1 Material properties of H beam2

Material properties for H beam2 (4 x 4 x 1/4) were taken from Barbero et.al. These properties consist of longitudinal and transverse young modulus, shear modulus, poisson's ratio and thickness of individual layer. These properties are entered in the material property section in Abaqus.

Table 12 Material properties of Hbeam2 (Barbero et.al)

Layer	E1 (10 ⁶ psi)	E2 (10 ⁶ psi)	G12 (10 ⁶ psi)	v	t (in)
1.5oz csm	1.716	1.716	0.605	0.419	0.025

2oz csm	1.861	1.861	0.655	0.421	0.03
30rovings	4.320	0.959	0.371	0.293	0.05
28 rovings	4.065	0.912	0.353	0.294	0.05
Matrix	0.49	0.419	0.198	0.24	0.045

4.1.2.2 Stacking sequence of H beam 2

Stacking sequence for the pultruded H beam 2 consists of 7 layers in the top flange, 7 layers in the web and 7 layers in the bottom flange.

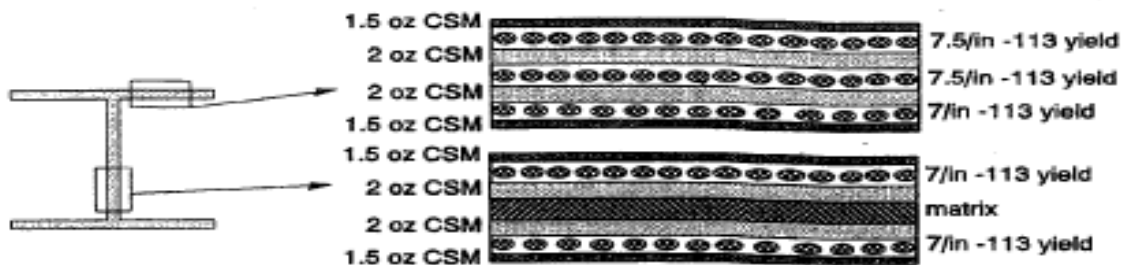


Figure 44 Stacking sequence of H beam 2 (Barbero et.al)

The above mentioned layup of the beam was given in Abaqus using the composite layup option. In the composite layup option region and material for the corresponding ply is selected and the corresponding thickness is given. Layup CSYS coordinate system is selected and the rotation angle is given. 3 integration points are provided, which means integration is done at bottom surface, middle surface and top surface of the ply.

	Ply Name	Region	Material	Thickness	CSYS	Rotation Angle	Integration Points
1 ✓	1.5 OZ CSM	(Picked)	ONE AND HALF CSM	0.025	<Layup>	0	3
2 ✓	30 ROVING	(Picked)	THIRTY ROVINGS	0.05	<Layup>	0	3
3 ✓	2 OZ CSM	(Picked)	TWO OZ CSM	0.03	<Layup>	0	3
4 ✓	30 ROVING2	(Picked)	THIRTY ROVINGS	0.05	<Layup>	0	3
5 ✓	2 OZ CSM 2	(Picked)	TWO OZ CSM	0.03	<Layup>	0	3
6 ✓	28 ROVING	(Picked)	NTY EIGHT ROV	0.05	<Layup>	0	3
7 ✓	1.5 OZ CSM 2	(Picked)	ONE AND HALF CSM	0.025	<Layup>	0	3

Figure 45 Stacking sequence of H beam 2 used in abaqus (composite layup)

4.1.1.3 Load and boundary conditions for H beam 2

Load is applied as distributed load at the center with a magnitude of 1000lb. Beam 2 is given simply supported boundary conditions restraining the translation in x, y and z directions.

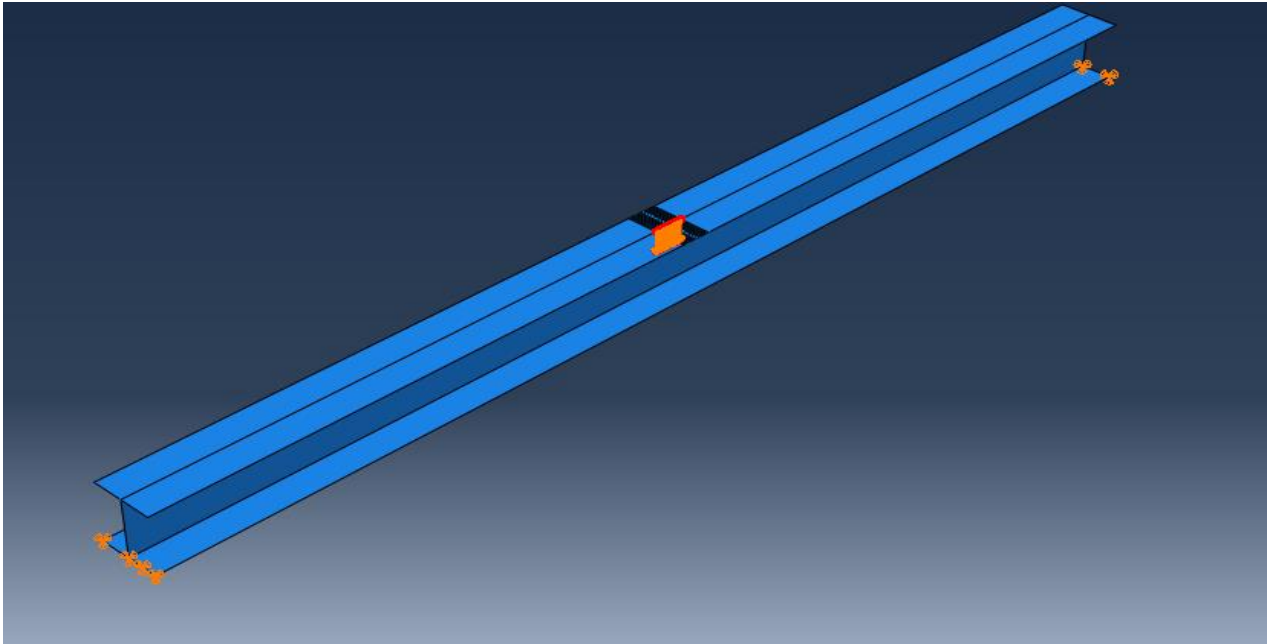


Figure 46 Load and boundary conditions used for H beam2

4.2 Optimization studies for seven-meter pole

Seven-meter-long GFRP pole was modeled in abaqus. Shell element was used to model GFRP pole because of the layered nature of material. First of all, pole was modeled with original stacking sequence and with the number of rovings present initially between the mats. A section of pole was selected and number of rovings and mats were counted in that section and modeled. There were discontinuities present between the mats.



Figure 47Preformer used for manufacturing GFRP pole

As it can be seen in above Figure 47 there are discontinuities present between the mats so at maximum there can be only five mats present along a section. There were two rovings coming out of hole, Total number of rovings were counted. There were a total of 328 holes and a total of 656 rovings.

4.2.1 Modeling of seven-meter-long pole with original stacking sequence

Seven-meter-long pole with stacking sequence used in industry was modeled first to know the stiffness. For that a displacement of 1050 mm was applied at one end and the other end was fixed. Displacement was applied at 300 mm from free end.

MAT 1

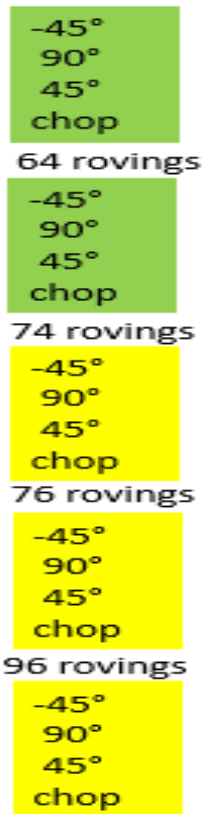


Figure 48 Original stacking sequence used for pipe section in industry

Volume fraction of pole was calculated by using gram per square meter of mats used and number of rovings used. Total width of mats used was determined and multiplied with unit length to get area. This area was then multiplied with gram per square meter to get total weight of mats which was then divided by density of glass fiber to get total volume of mats. Total number of rovings were multiplied with tex (4.8gram/meter) by taking unit length to get total weight of rovings which was then divided by density of glass fiber to get total volume of rovings. Total volume of mats and rovings were added to get overall volume which was then divided by volume of hollow cylindrical pole to get overall volume fraction.

Vf(total) (%)	Vf rovings (%)	Vf mat (%)	Vf 90 (%)	Vf 45 (%)	Vf -45 (%)	Vf Chop (%)	Rov ings(secti on)	Total (roving s)
45.7	28.7	17	8.87	3.13	3.13	1.88	310	656

Table 13 showing overall volume fraction and for individual glass fibers

As it can be seen in Figure 48 for modeling at a section total 5 mats and a total of 310 rovings distributed among all the mats were used.

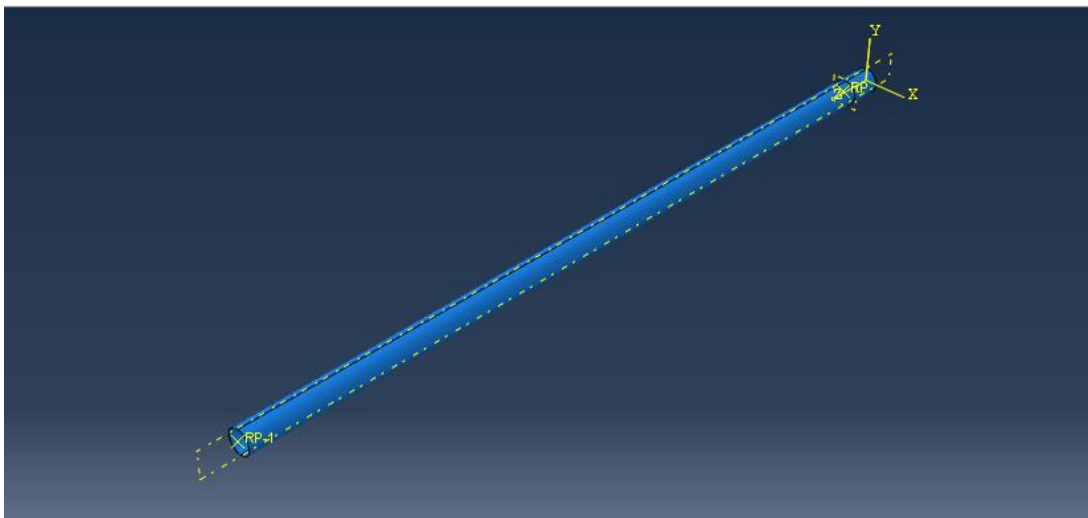


Figure 49 Seven-meter-long pole modeled in abaqus

Local coordinates were assigned using discrete orientation in abaqus. Normal axis was defined as surface with axis 3 as the direction. Primary axis direction was given as first direction by using edge partitioned along length of pole.

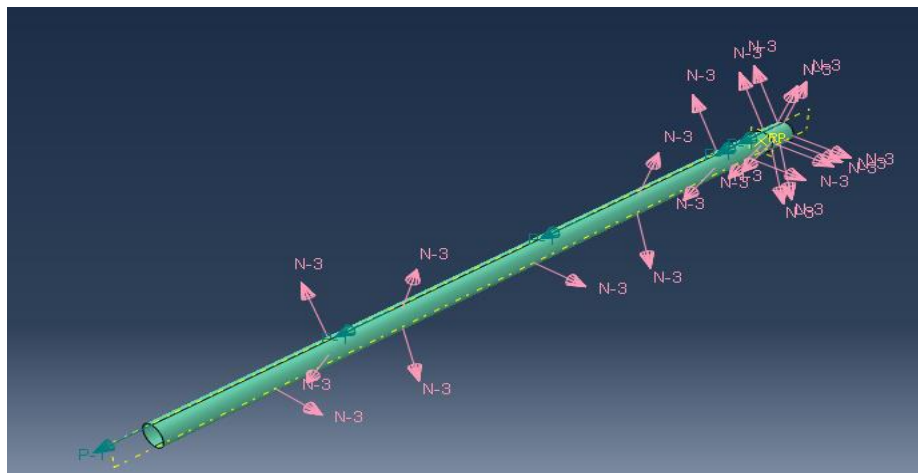


Figure 50 Assigning local coordinates to pole

Composite layup was used in abaqus to assign ply orientation, integration points along with CSYS used. Material as well as thickness of each of ply used was also entered in composite layup.

Edit Composite Layup

Name: CompositeLayup-1

Element type: Conventional Shell Description: -

Layup Orientation

Definition: Discrete

Normal axis: Surface -- Surf-4

Primary axis: Edge -- Set-30

Normal direction: Axis 1 Axis 2 Axis 3

Additional rotation: None Angle: 0 Distribution:

Section integration: During analysis Before analysis

Thickness integration rule: Simpson Gauss

Plies Offset Shell Parameters Display

Make calculated sections symmetric

		Ply Name	Region	Material	Thickness	CSYS	Rotation Angle	Integration Points
1	✓	Ply-1	(Picked)	chop	0.166667	<Layup>	0	3
2	✓	Ply-2	(Picked)	fortyfive	0.166667	<Layup>	45	3
3	✓	Ply-3	(Picked)	ninety	0.166667	<Layup>	90	3
4	✓	Ply-4	(Picked)	fortyfive	0.166667	<Layup>	-45	3
5	✓	Ply-5	(Picked)	r96(340)	0.666667	<Layup>	0	3
6	✓	Ply-6	(Picked)	chop	0.166667	<Layup>	0	3
7	✓	Ply-7	(Picked)	fortyfive	0.166667	<Layup>	45	3
8	✓	ply-8	(Picked)	ninety	0.166667	<Layup>	90	3
9	✓	ply-9	(Picked)	fortyfive	0.166667	<Layup>	-45	3
10	✓	ply-10	(Picked)	r76(340)	0.666667	<Layup>	0	3

Figure 51 Composite layup used for pole

A displacement of 1050 mm was applied at 300 mm from the free end. For that pole was partitioned at 300 mm from free end and a reference point was created. A displacement of 1050 mm was applied at the reference point using rigid body constraint. Other end of pole was fixed.

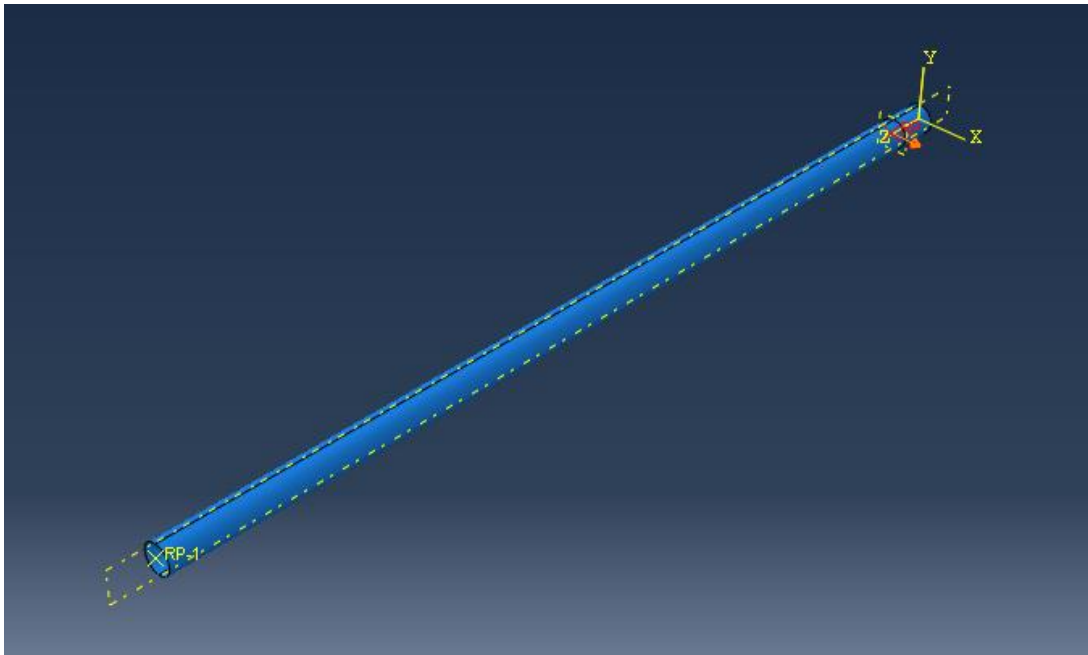


Figure 52 Displacement of 1050mm applied at one end of pole

For mesh quad shaped element was used and structured technique was used. S4 element was used. A global mesh size of 33mm was used.

4.2.2 Using different stacking sequences to optimize pole stiffness

5 mats of 90-0 configuration with symmetric configuration with rovings in between was used to see possible optimization in pole stiffness.

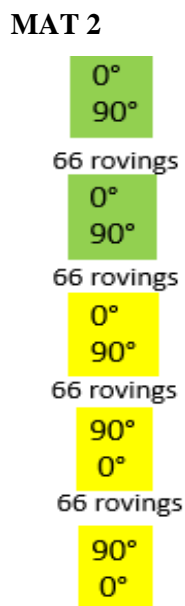


Figure 53 90-0 mat used with rovings in between

Vf(total) (%)	Vf rovings(%)	Vf mat (%)	Vf 90 (%)	Vf 0 (%)			Rovings (section)	Total (rovings)
45.7	24.5	21.2	10.7	10.5			264	559

Table 14 showing overall volume fraction and for individual glass fibers

Overall volume fraction of 45.7 was maintained by changing volume fraction of rovings, mats and number of rovings at a section. Stiffness of pole was determined for 90-0 configuration with same model and configuration as used for modeling pole with original stacking sequence.

MAT 3

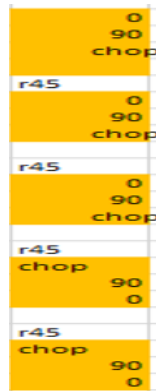


Figure 54 0-90-chop mat used with rovings in between

Vf(total) (%)	Vf rovings(%)	Vf mat (%)	Vf 90 (%)	Vf 0 (%)	Vf chop (%)		Rovings (section)	Total (rovings)
45.7	16.8	28.9	9	10.5	9.4		180	383

Table 15 showing overall volume fraction and for individual glass fibers

4.3.3 Removing mats and adding more rovings to increase pole stiffness

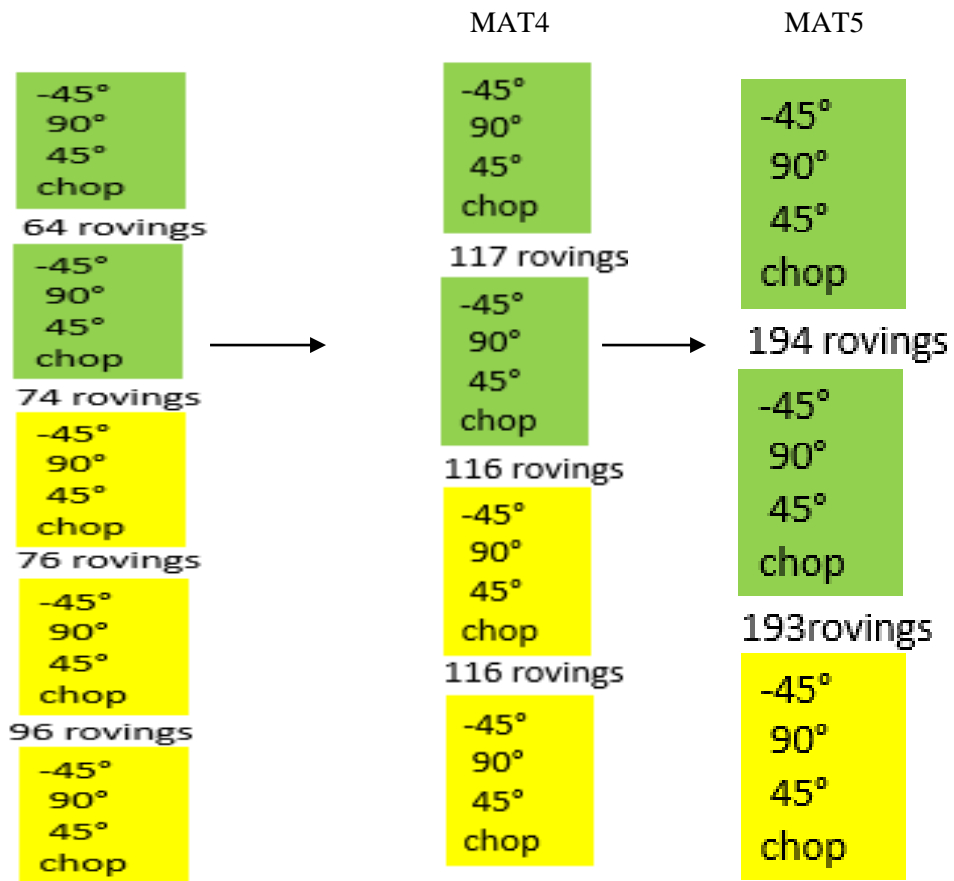


Figure 55 Mats removed and rovings increased (for original stacking sequence)

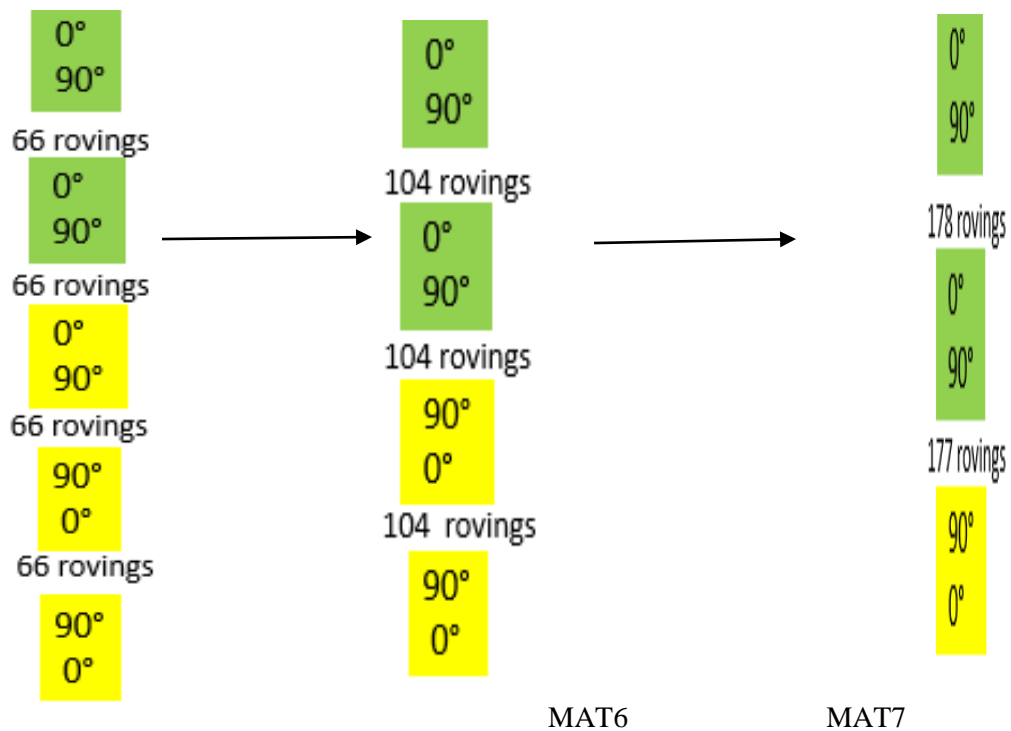


Figure 56 Mats removed and rovings increased (for MAT 2)

4.4 Modeling of 500 mm short pole (to study shear effects)

A short GFRP pole of 500 mm length was modeled in abaqus to study shear effects. All the modeling configurations, stacking sequence as well as local coordinates were kept same as that of 7-meter-long pole. Load obtained from analysis of meter long pole was taken and same load was applied for 500 mm short pole to obtain the deformation. Applied load was divided by obtained deformation and stiffness was determined. Stacking sequence giving best stiffness value was considered.

4.4.1 Modeling of 500 mm short pole with original stacking sequence (MAT 1)

A 500 mm long short pole was modeled with MAT 1 stacking sequence.

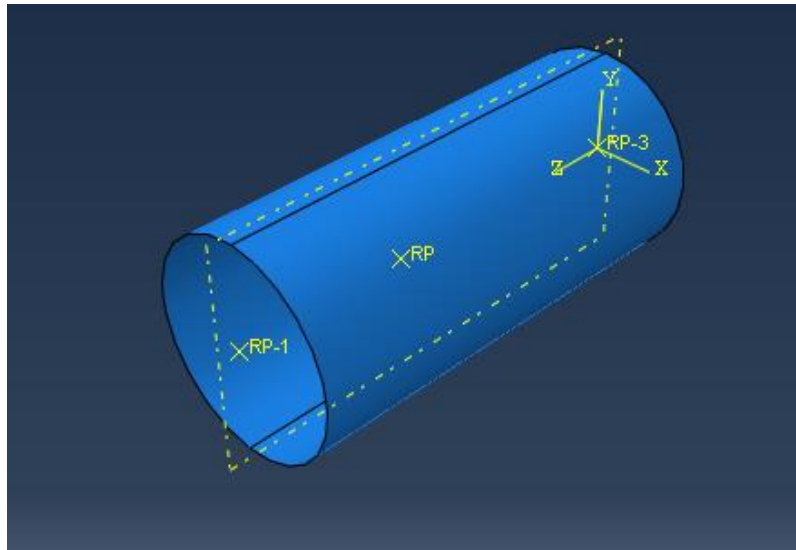


Figure 57 500 mm long short pole modeled in abaqus

Load obtained from analysis of 7-meter-long pole (7.592 KN) was taken and same load was applied for 500 mm short pole to obtain the deformation. Other end of short pole was fixed.

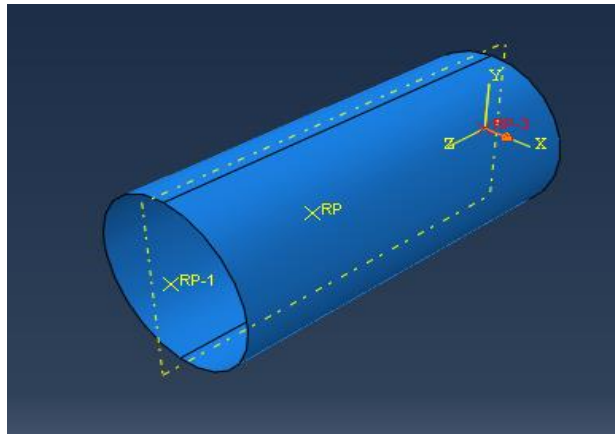


Figure 58 Load applied to 500 mm short pole.

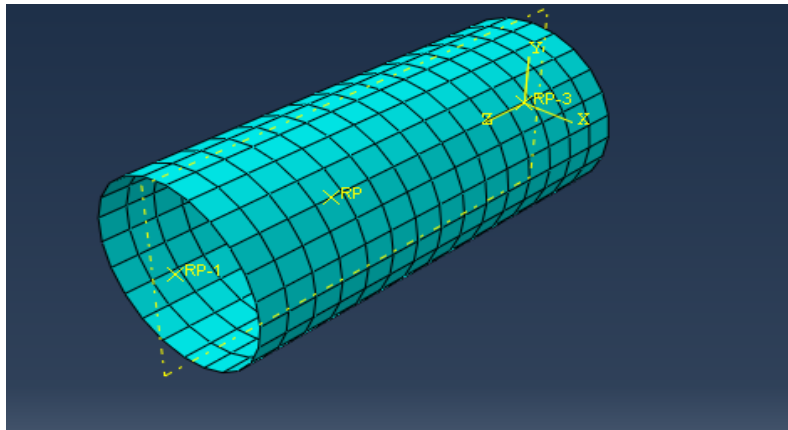


Figure 59 Mesh for 500 mm short pole

A mesh size of 33 mm was selected. For mesh quad shaped element was used and structured technique was used. S4 element was used.

Deformation was determined in loading direction that is in U1 direction. Applied load was divided by obtained deformation and stiffness was calculated.

4.5 Analysis of support plates proposed for experimental set up

Experimental set up was proposed for testing of seven-meter pole under bending. In setup total four steel plates were used. Two steel plates used at bottom were attached to strong floor. Two steel plates were placed above GFRP pole and threaded bolts were used to connect top and bottom plates.

4.5.1 Analysis of top plate

A 380.5mm by 300mm steel plate was modeled in abaqus to understand the behavior of plate under flexural load. Steel plate was modeled with solid elements.

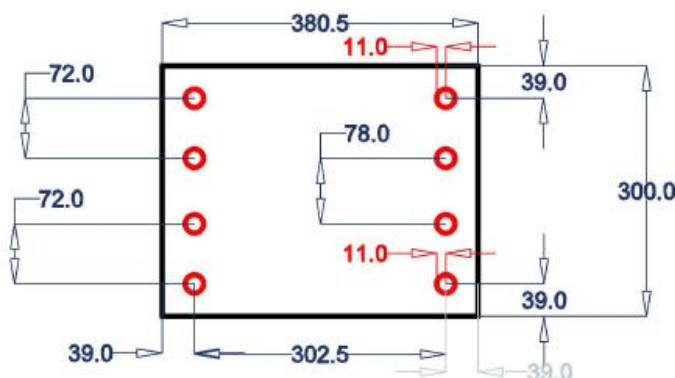


Figure 60 Dimensions of plate used at top of GFRP pole

Thickness of the plate used at top of GFRP pole was 60 mm.

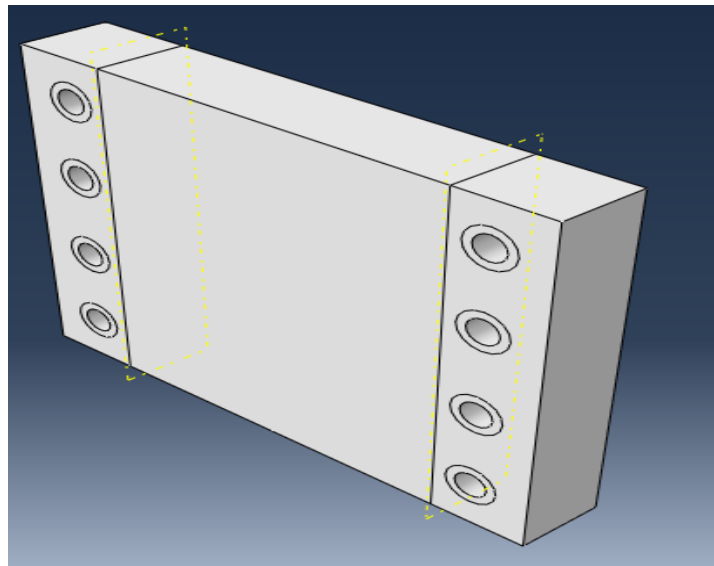


Figure 61 Solid part created for top plate

Plate was partitioned in the central area to apply pressure load. Plate was modeled according to dimensions shown in figure 60. Cut extrude of 22mm diameter was made through solid plate and partition was done to simulate washer around that hole. Diameter of washer considered as 35 mm was given to these holes by using partitioning with sweep edges.

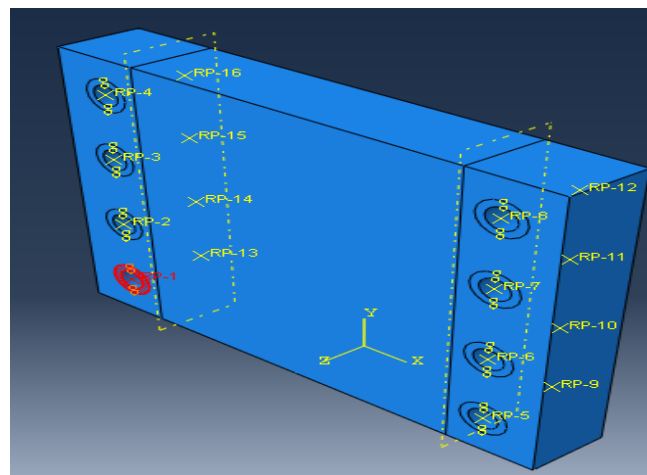


Figure 62 Rigid body constraint used to tie bolt with washer

Inscribed area between bolt hole and washer was tied to a reference point. This was repeated for each of the holes and a total of 16 representative points were created, one for each hole.

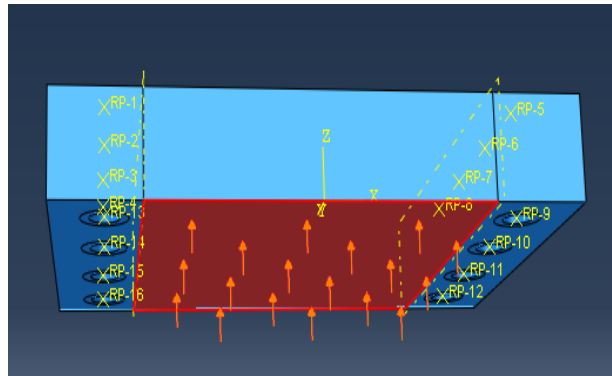


Figure 63 Pressure load applied to top plate

A pressure load of 0.8326 N/mm^2 was applied at bottom of top plate. Maximum load acting on seven-meter-long GFRP pole was determined and factored and then it was divided by an area of $250\text{mm} \times 300 \text{ mm}$ in which pressure load was applied. Maximum factored load on GFRP pole was 62.445 KN.

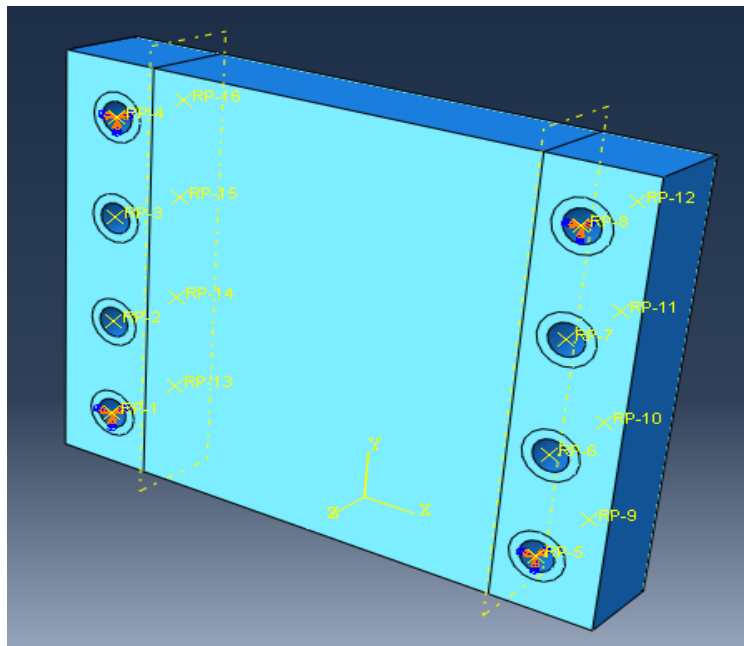


Figure 64 Fixed boundary conditions given to corner holes

Threaded rods were passing through corner holes and a fix-fix boundary condition was given to these holes

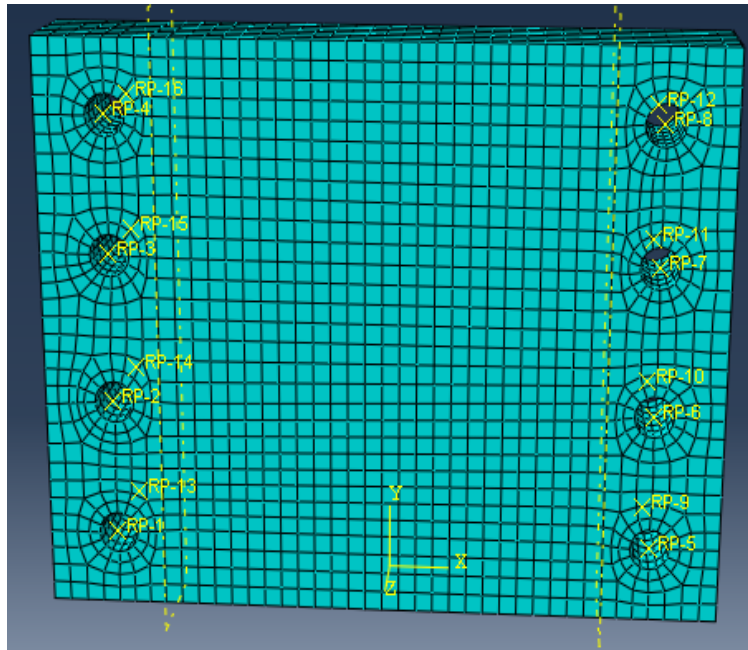


Figure 65 Mesh created for top plate

Local seeds were provided for each of hole with 16 number of elements around each hole. Global seeds were provided with a size of 10 mm. C3D8R solid element was used. Hexagonal element shape was adopted and sweep technique was used for meshing.

4.5.2 Analysis of bottom plate

A 700 mm by 700 mm steel plate was modeled in abaqus to understand the behavior of plate under flexural load. Steel plate was modeled with solid elements.

Thickness of plate used was determined by trial and error basis. When for a given constant yield stress under varying plastic strain there was no plastic strain developing in final results, it was concluded that there is no bending in plates.

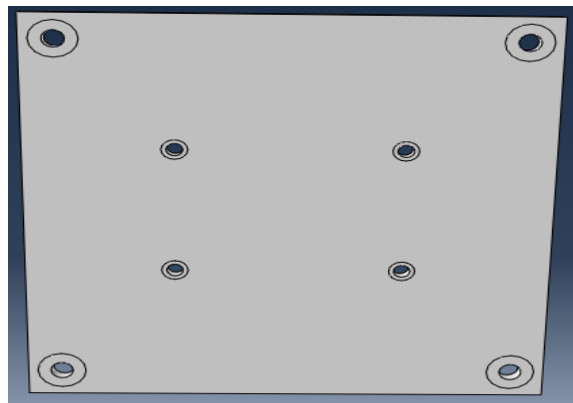


Figure 66 Solid part created for bottom plate

Corner holes were made as 30mm diameter holes. Holes present in lab were having 27 mm diameter bolts and hence 3 mm clearance was taken for hole. Washer used in lab were 65 mm outer diameter. Hence in part module cut extrude of 30 mm diameter was made and 65 mm washer was modeled using partitioning by sweep edges. In center of plate four holes were provided of 22 mm diameter and were cut made using cut extrude and a washer of 35 mm was given to these holes using partitioning by sweep edges.

As done in top plate, all the holes were tied to washers by using rigid body constraint and area surrounding hole and washer was tied to reference point.

Maximum factored load on GFRP pole was 62.445 KN and was divided between all central 22 mm diameter holes, which gave a load of 15.611 KN applied on each of hole. Load was applied to reference point which was tied to area between bolt and washer.

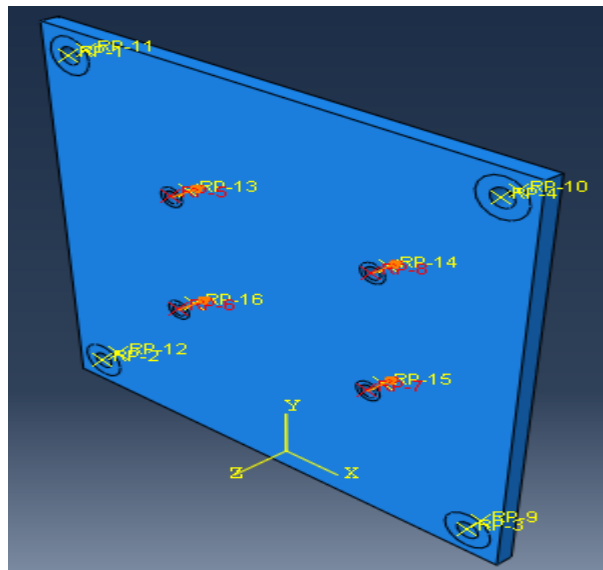


Figure 67 Loading applied to bottom plate

Corner holes of bottom plate were given fix-fix boundary conditions. They were fixed to strong floor. Reference point tied to inscribed area between bolt and washer was given fix-fix boundary condition.

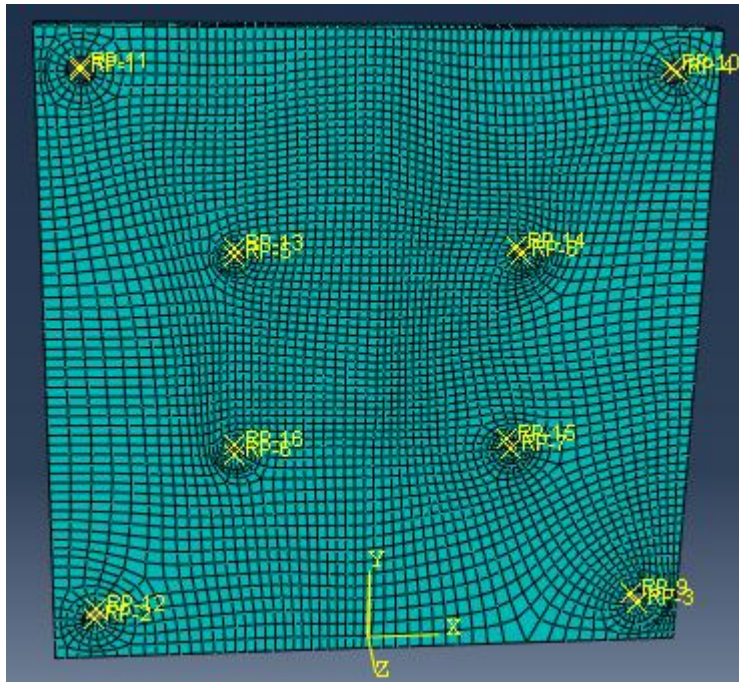


Figure 68 Mesh created for bottom plate

Local seeds were provided for each of hole with 16 number of elements around each hole. Global seeds were provided with a size of 12 mm. C3D8R solid element was used. Hexagonal element shape was adopted and sweep technique was used for meshing.

4.6 Modeling of tension coupon specimen

Coupons were modeled according to (Type 4) dimensions given in ASTM D 638. Coupons were modeled in Abaqus.

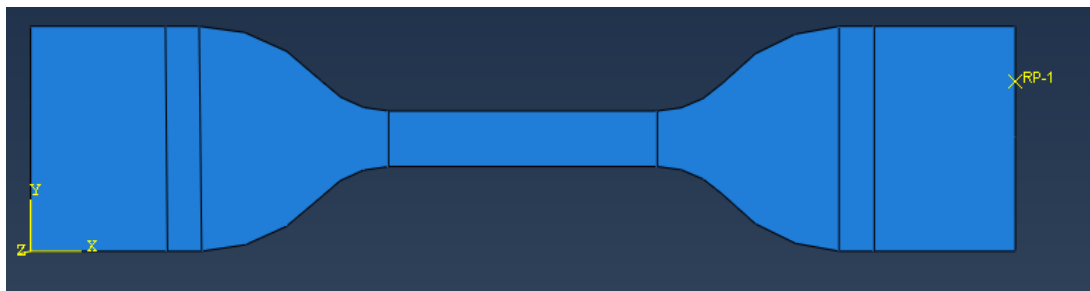


Figure 69 Tension coupon created in Abaqus

Coupons were fixed at one end and at the other end load was applied as displacement of 4.219 mm.

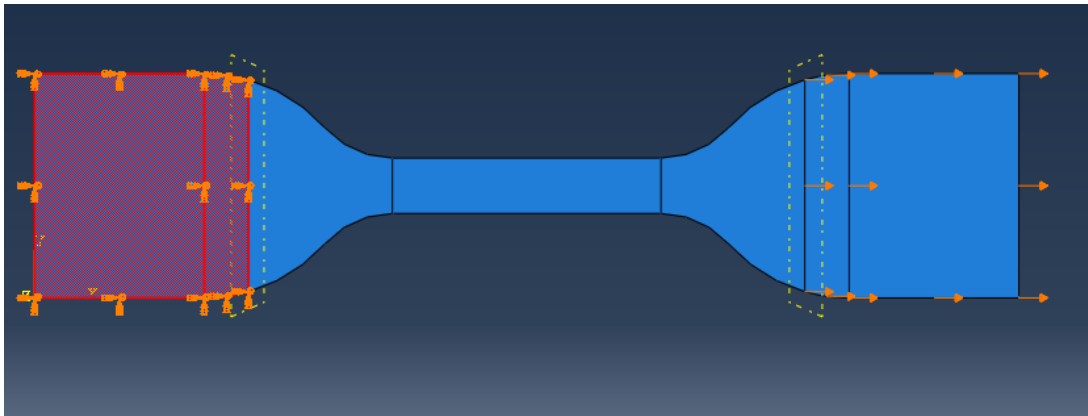


Figure 70 Load and boundary conditions applied to coupon specimen

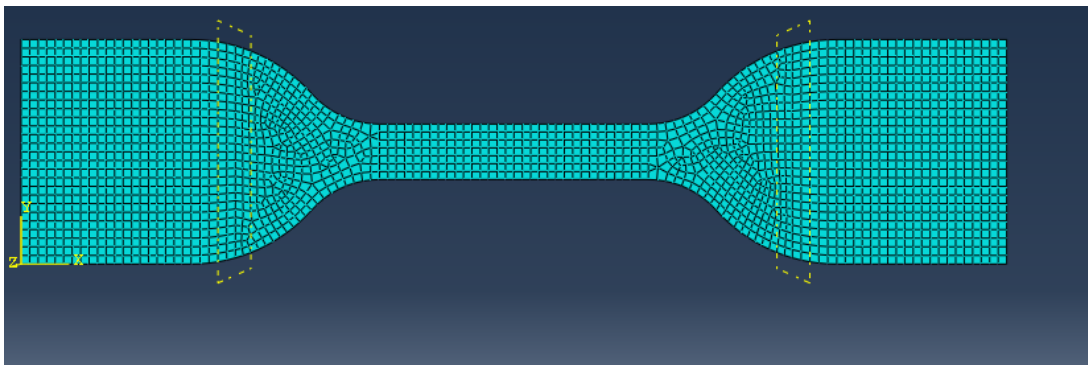


Figure 71 Mesh for coupon specimen

A mesh size of 1mm was used. S4 element was used for modeling coupon specimen.

		Ply Name	Region	Material	Thickness	CSYS	Rotation Angle	Integration Points
1	✓	Ply-1	(Picked)	fortyfive	0.1667	<Layup>	-45	3
2	✓	Ply-2	(Picked)	ninety	0.1667	<Layup>	90	3
3	✓	Ply-3	(Picked)	fortyfive	0.1667	<Layup>	45	3
4	✓	Ply-4	(Picked)	chop	0.1667	<Layup>	0	3
5	✓	Ply-5	(Picked)	rovinghundred	0.6667	<Layup>	0	3
6	✓	Ply-6	(Picked)	fortyfive	0.1667	<Layup>	-45	3
7	✓	Ply-7	(Picked)	ninety	0.1667	<Layup>	90	3
8	✓	Ply-8	(Picked)	fortyfive	0.1667	<Layup>	45	3
9	✓	Ply-9	(Picked)	chop	0.1667	<Layup>	0	3
10	✓	Ply-10	(Picked)	rovinghundred	0.6667	<Layup>	0	3

Figure 72 Composite layup used for modeling coupon specimen

4.6 Modeling of coupon specimen under compression

Coupon specimens of dimensions 12.7mm x 12.7 mm x 6 mm were modeled in abaqus.

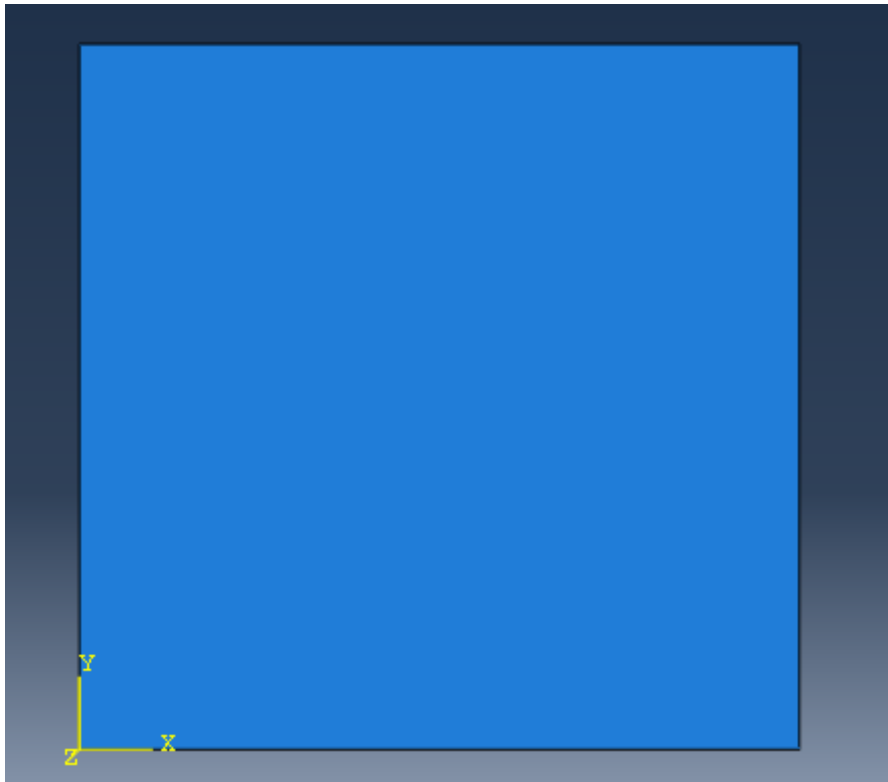


Figure 73 Coupon(strength) specimen modeled in abaqus

One end of coupon specimen was fixed and at other end load was applied as boundary condition. A displacement of 0.5872 mm was applied at the other end.

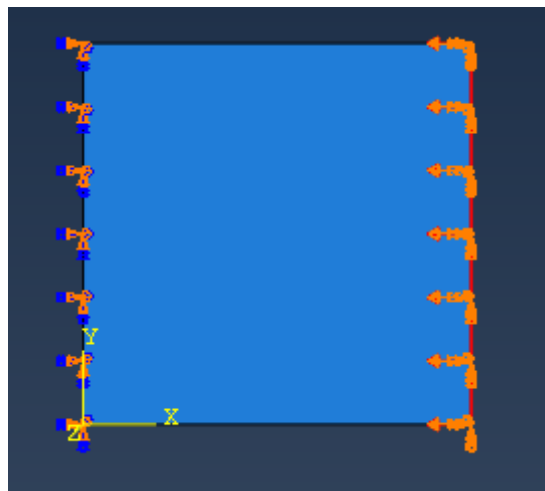


Figure 74 Load and boundary conditions of coupon (strength) specimens

Mesh of coupon specimen was created. Mesh size of 0.65 mm was chosen. S4 R element was chosen for mesh.

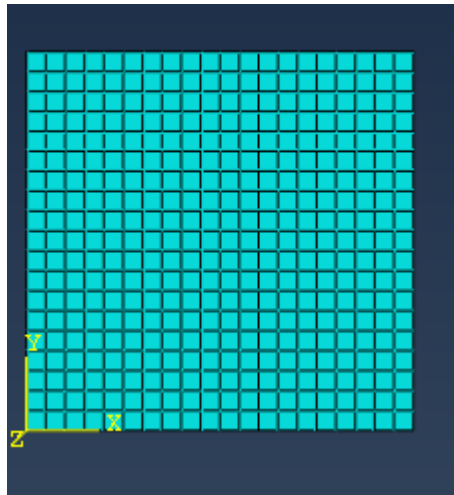


Figure 75 Mesh created for coupon (strength)specimen

4.7 Modeling of coupon specimen under compression (for stiffness determination)

Coupon specimens of dimensions 25.4 mm x12.7 mm x 6 mm were modeled in abaqus.

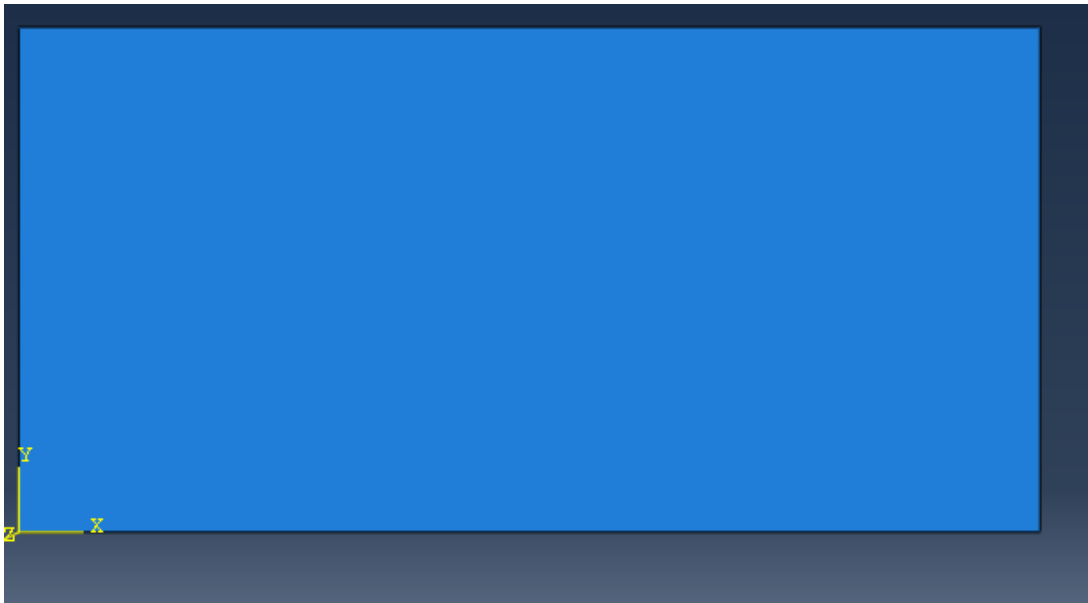


Figure 76 Coupon(stiffness) specimen modeled in abaqus

One end of coupon specimen was fixed and at other end load was applied as boundary condition. A displacement of 0.5872 mm was applied at the other end.

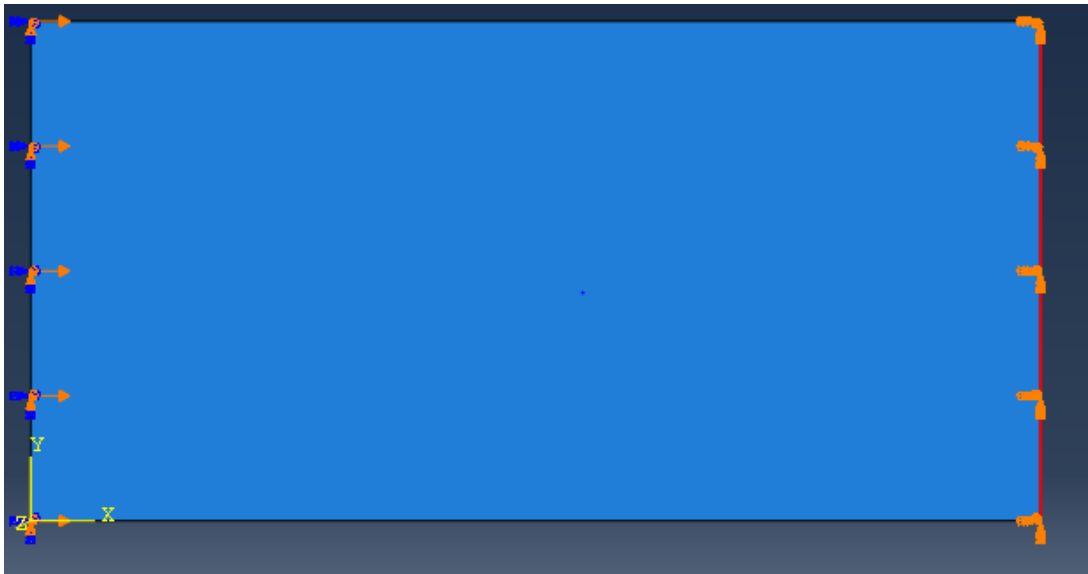


Figure 77Coupon(stiffness) specimen modeled in abaqus

Mesh of coupon specimen was created.Mesh size of 1.3 mm was chosen.S4R element was chosen for mesh.

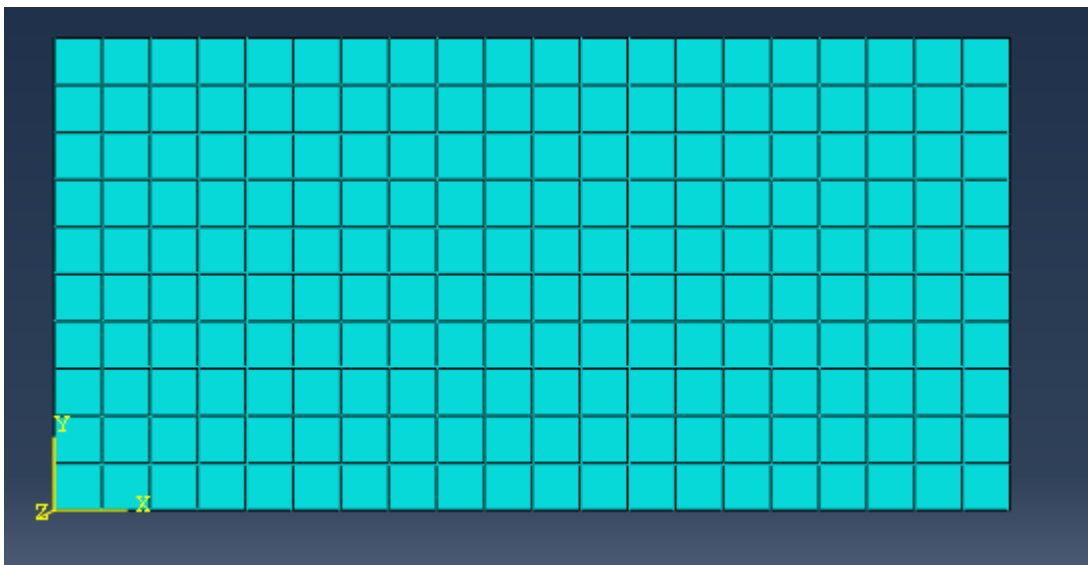


Figure 78Mesh of coupon (stiffness) specimen in abaqus

CHAPTER 5

5.RESULTS AND DISCUSSION

5.1 Corrections in graph and toe compensation

5.1.1 Toe compensation done in tensile testing of coupons

ASTM D 638 recommends for toe compensation for those specimens which have a pronounced toe region.

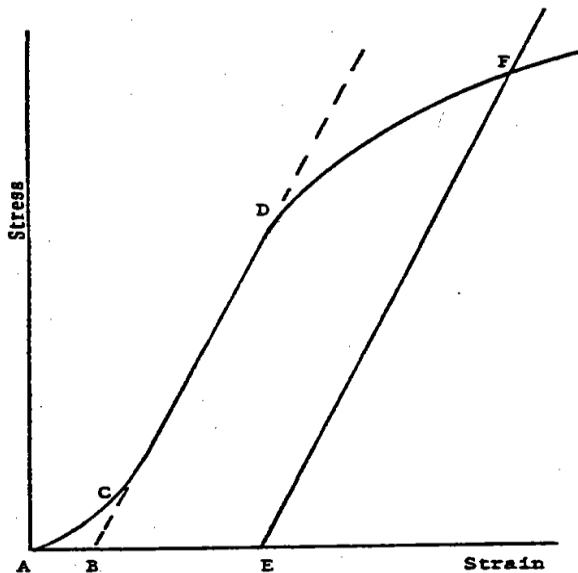


Figure 79 Toe compensation recommended by ASTM D 638

Toe region is caused due to take up of slack and seating of specimen. This region does not represent property of material. During start of experimental testing some slack is there when specimen is adjusted into machine. ASTM D 638 recommends to extend the major linear portion of the graph to intersect strain axis and the point where it intersects strain axis should be treated as corrected zero strain point and all the strain measurements should now be made with reference to that point. ASTM D 638 recommends to measure young's modulus by dividing the stress at any point along the line CD (or its extension) by the strain at the same point (measured from Point B, defined as zero-strain).

So following guidelines of ASTM D 638 toe compensation was done in specimens tested under tensile loading.

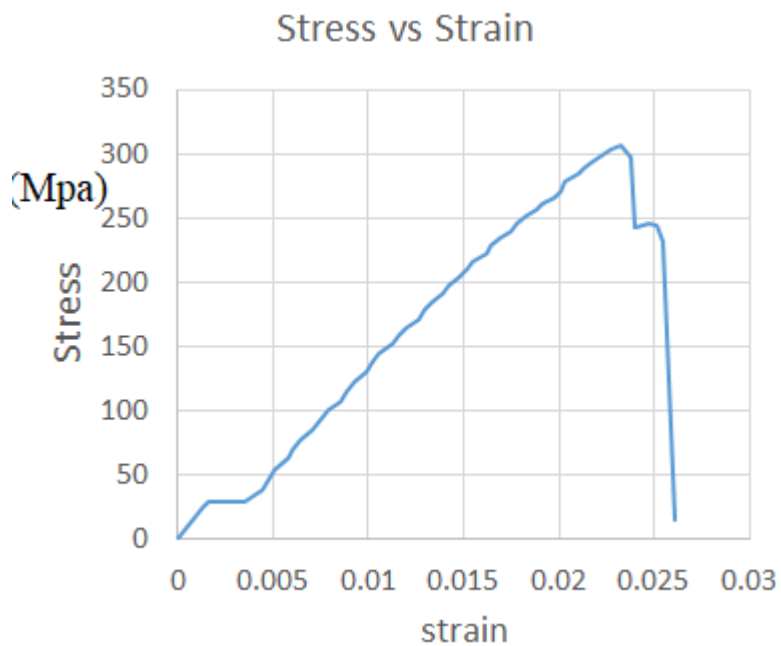


Figure 80 Stress vs strain graph having toe region

As seen in above figure 80 there is presence of toe region at start of curve. This region does not represent material property. Hence this region should be removed and toe compensation should be done so that curve starts from zero stress axis and has a corrected strain point.

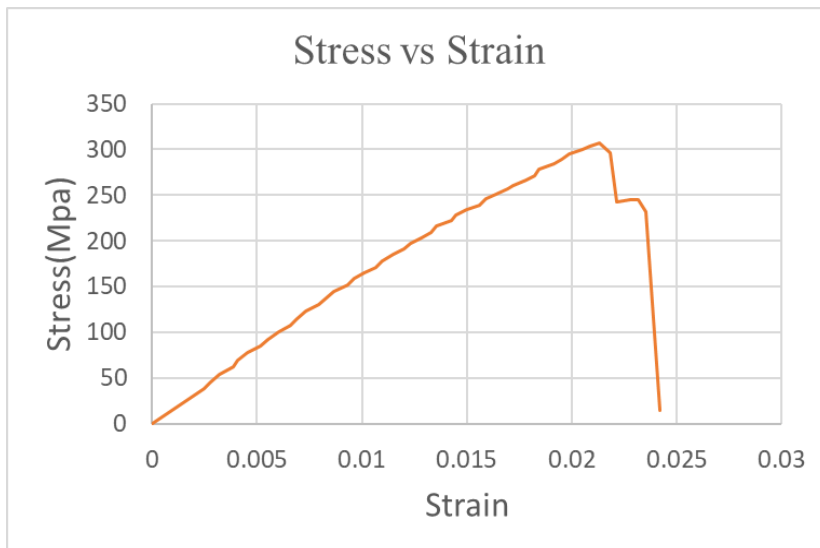


Figure 81 Stress vs strain graph after toe compensation

Region having toe effect was determined and coordinates of the point at the end of toe region was determined. Point at end of toe region was made to start from origin. Hence

curve was shifted to left side. While shifting the curve left it was made sure that difference of strain values in original stress-strain curve (with toe region) remains same even in corrected stress-strain curve. It is clearly visible now that toe region has been removed as this region does not give true representation of material property. This toe region comes when strain values recorded from machine are plotted with the stress values, as they is some slack during seating and alignment of specimen in machine.

5.1.2 Stiffness correction done during tensile testing

As already mentioned due to slack effect strain values given by machine were not accurate. While calculating modulus of elasticity from machine strain and stress values it can to be much less than modulus of elasticity calculated from machine stress and extensometer strain. Main reason behind this difference is overestimation of strain values given by machine. Values of strain given by machine are higher because of slack caused during seating and alignment of specimen. Hence there was a need for correction on stiffness values.

For stiffness correction, modulus of elasticity from machine was determined for a particular stress from stress vs strain graph corrected with toe compensation. Modulus of elasticity was also determined for the same stress value from extensometer. Modulus of elasticity obtained from machine was divided by modulus of elasticity obtained from extensometer. This ratio of modulus of elasticity was then multiplied with strain values obtained from machine to get corrected strain values. Hence stress vs strain curve obtained from machine now has same modulus of elasticity as that obtained from extensometer and stiffness correction is done.

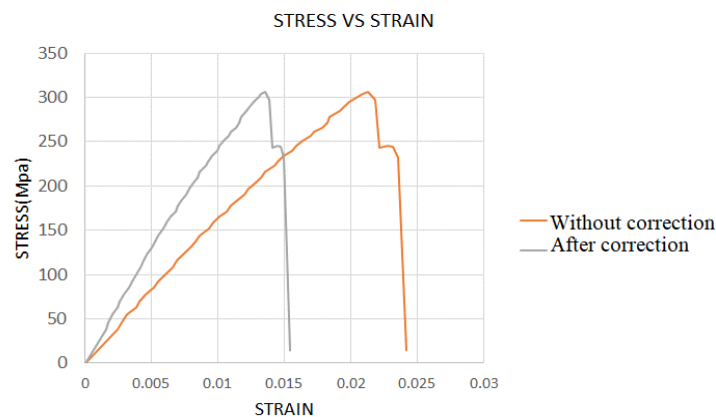


Figure 82 Stress vs strain curve without and after stiffness correction

As seen in Figure 82 strain values from machine are now corrected and modulus of elasticity can now be accurately determined from machine stress –strain data. This correction was mainly done to determine corrected ultimate failure strain.

5.1.3 Negative strain correction in compression(strength)test

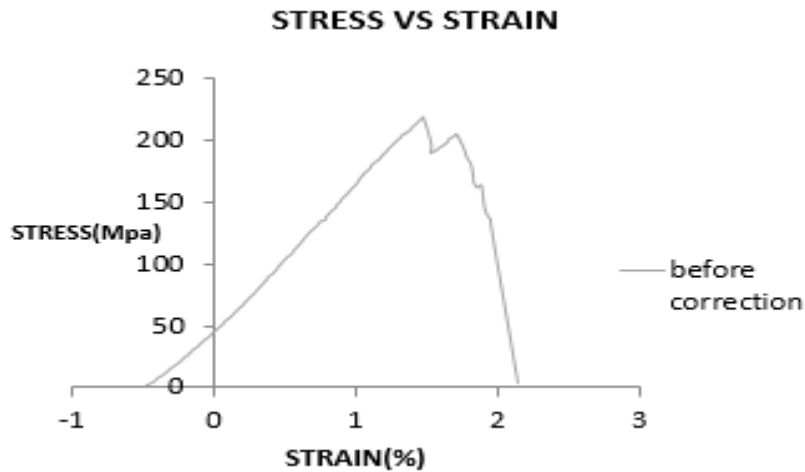


Figure 83 Stress vs strain curve during compression strength test (before correction)

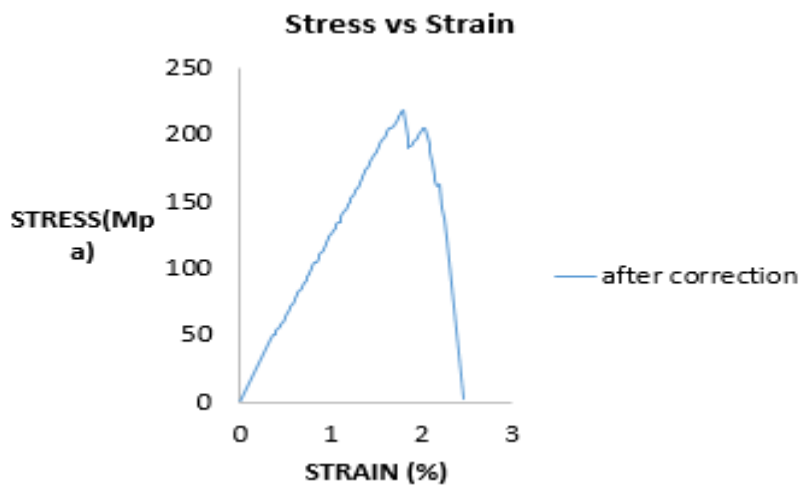


Figure 84 Stress vs strain curve during compression strength test (after correction)

In Figure 83 strain (from machine) is starting from a negative value in the negative x axis. To correct this as shown in the figure 84, magnitude of negative strain was determined and

the same magnitude was added to other strain values, hence curve was shifted to right side. This negative strain is caused due to presence of slack during aligning and seating of specimen. Strain recorded here was directly from machine.

5.1.4 Strain correction in compression (modulus) test

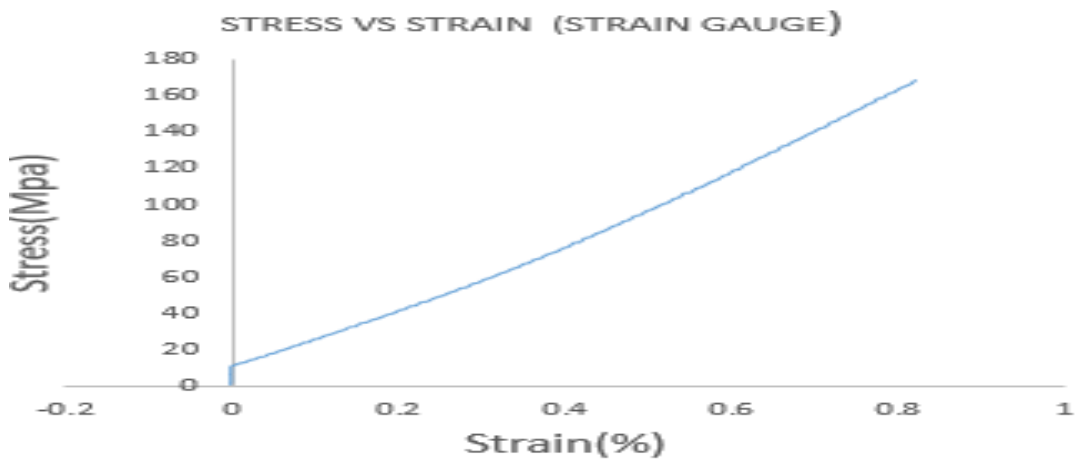


Figure 85 Stress vs strain curve during compression modulus test (before correction)

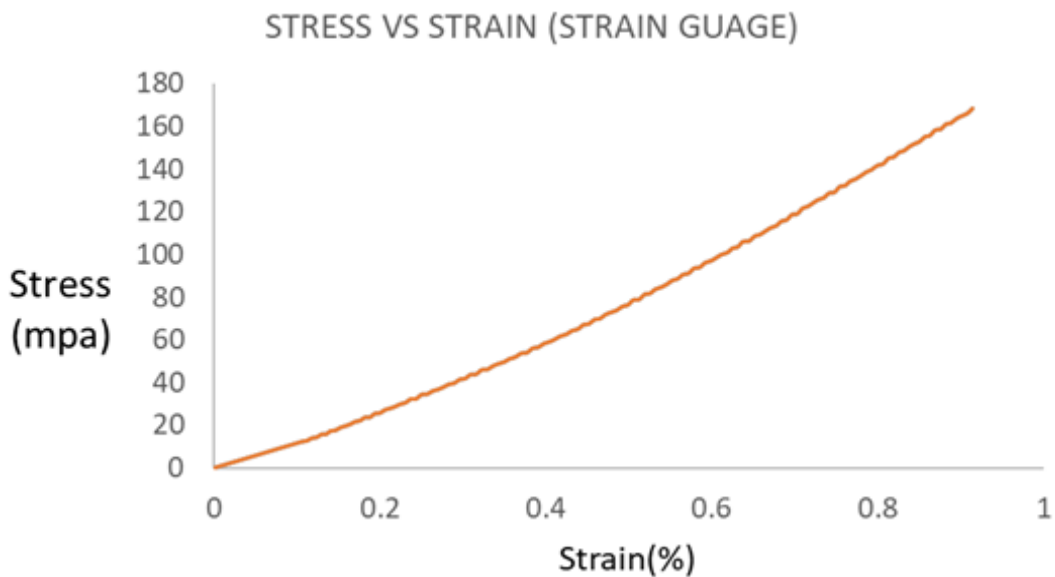


Figure 86 Stress vs strain curve during compression modulus test(after correction)

As seen in Figure 85 stress vs strain curve is not starting from origin, but it has some intercept in stress axis. Coordinates of point at end of intercept was determined and curve was extended till it touches zero stress axis. Point where curve intersects zero stress axis were found out and the corresponding strain values of point are added to other strain values

such that curve was shifted to right side. Now curve is starting from origin and strain correction is done. Strain recorded here was from strain gauge.

5.1.5 Stiffness correction in compression (modulus test)

Due to take up of slack and relative movement of the components of the machine, strain values given by the machine is of higher magnitude as compared to the values given by the strain gauge, as a result modulus of elasticity given by machine is of lower magnitude as compared to the modulus of elasticity given by the strain gauge. Hence correction factor is calculated based on the ratio of modulus of elasticity given by machine and strain gauge and the same correction factor is multiplied to the strain values given by machine to reduce its magnitude. For calculation of correction factor a particular stress range was selected and modulus of elasticity was computed in that particular stress range for both strain gauge as well as for machine. Then ratio of modulus of elasticity of machine was taken with respect to strain gauge and was termed as a correction factor. This correction was done mainly to accurately measure corrected failure strain value.

After correction stress strain curve given by machine and strain are coinciding and now it is possible to accurately measure failure strain.

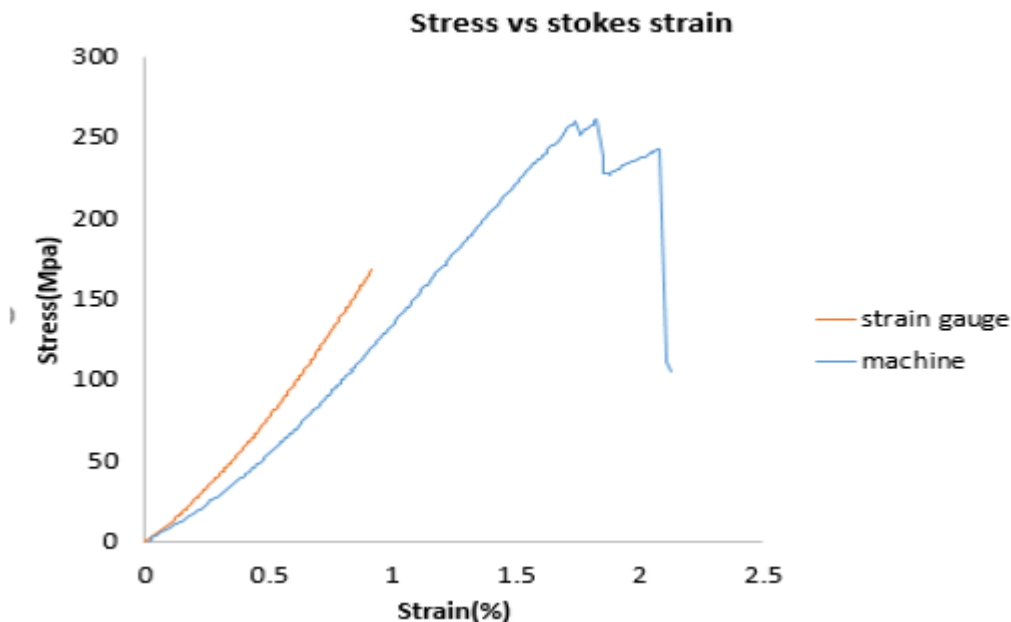


Figure 87 Stress vs strain curve for machine and strain gauge (before correction)

We can see here that stress-strain curve obtained from machine and strain gauge vary considerably before correction. This is because of overestimation of compressive strain recorded by machine. Hence modulus of elasticity recorded by machine is considerably

lower. This overestimation of strain by machine is because of slack caused during alignment and seating of specimen in machine during experimental testing.

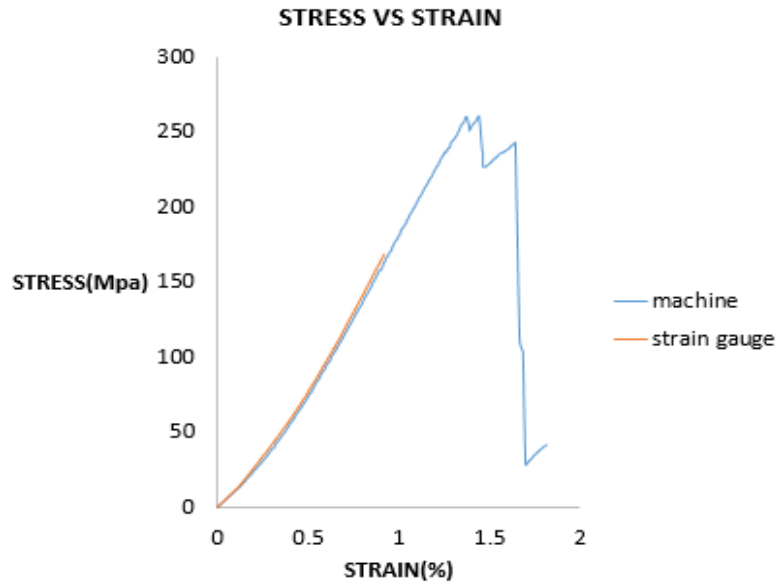


Figure 88 Stress vs strain curve for machine and strain gauge (after correction)

Now we can see here that stress -strain curve obtained from machine and strain gauge match after correction. Now it is possible to accurately measure failure strain.

5.1.6 Strain correction in compression test of short hollow circular tube

For axial compression testing of short hollow circular tube, similar strain correction was done as adopted in strain correction for compression modulus test

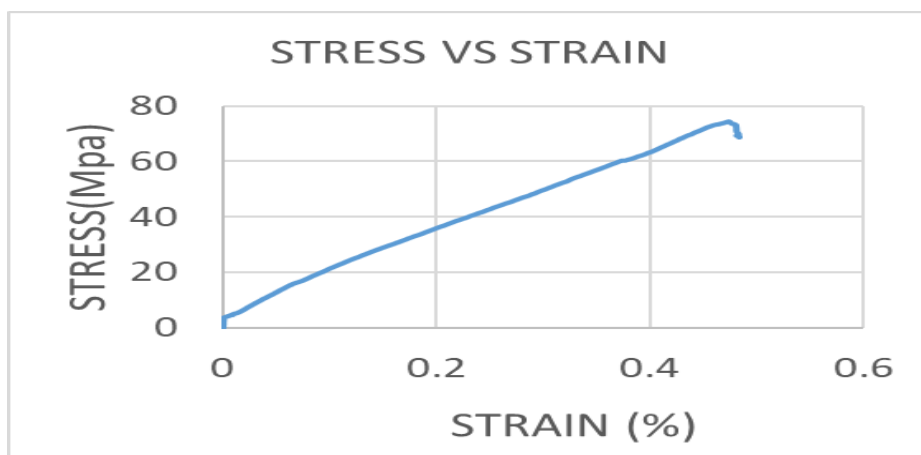


Figure 89 Stress vs strain curve for short hollow tube under axial compression (without correction)

It can be seen that in Figure 89 stress vs strain curve is not starting from origin, but it has some intercept in stress axis. Coordinates of point at end of intercept was determined and curve was extended till it touches zero stress axis. Point where curve intersects zero stress axis were found out and the corresponding strain values of point are added to other strain values such that curve was shifted to right side. Strain recorded here was from strain gauge.

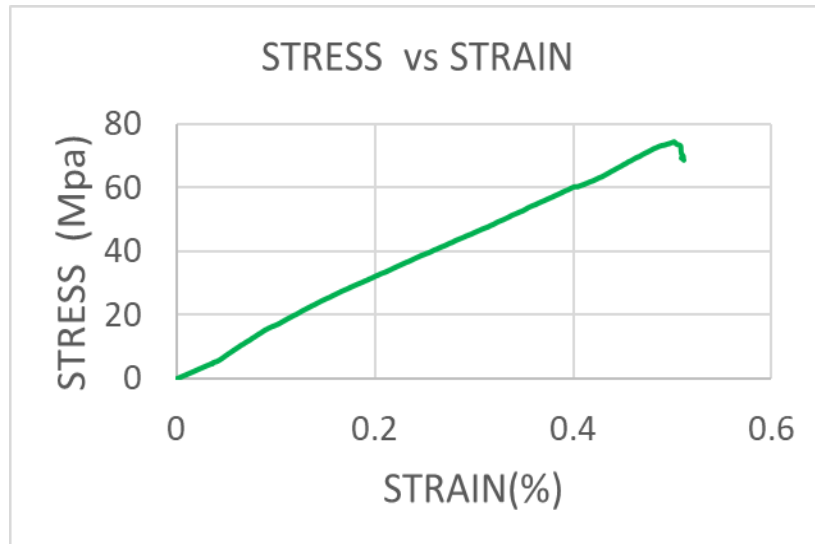


Figure 90 Stress vs strain curve for short hollow tube under axial compression (with correction)

Now after correction we can see that stress vs strain curve is starting from origin and intercept is removed.

5.1.7 Correction for displacement during compression test of short hollow circular tube

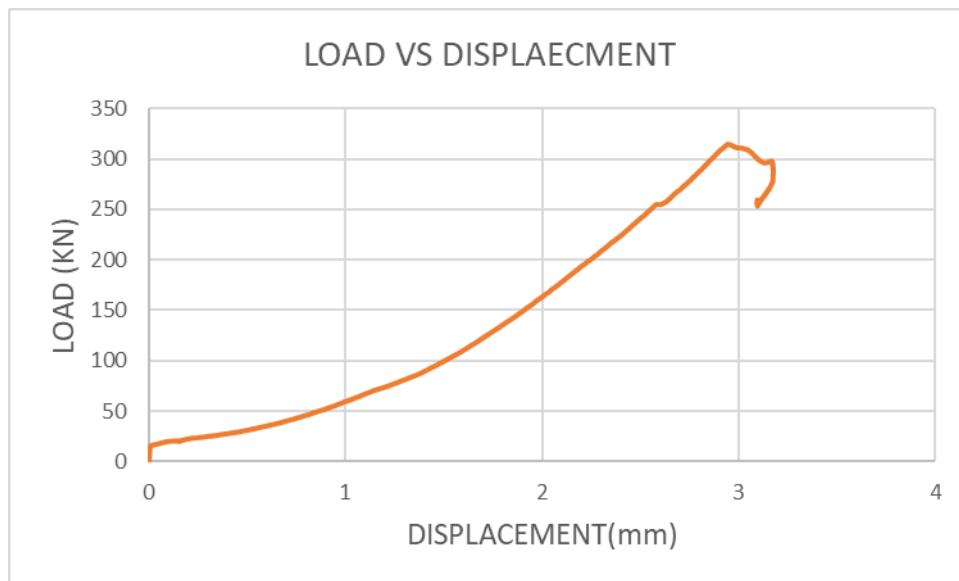


Figure 91 Load vs displacement for short hollow tube under axial compression (without correction)

As seen in the Figure 91 displacement values (given by machine) are starting from a negative value on x axis. For correction curve is extended backwards and the coordinates of the point where it intersects negative x axis are found out. Same coordinates of displacement are added to positive displacements and curve is shifted to right side. Displacement recorded during the test was from LVDT (Linear variable displacement transducer) of 50 mm gauge length.

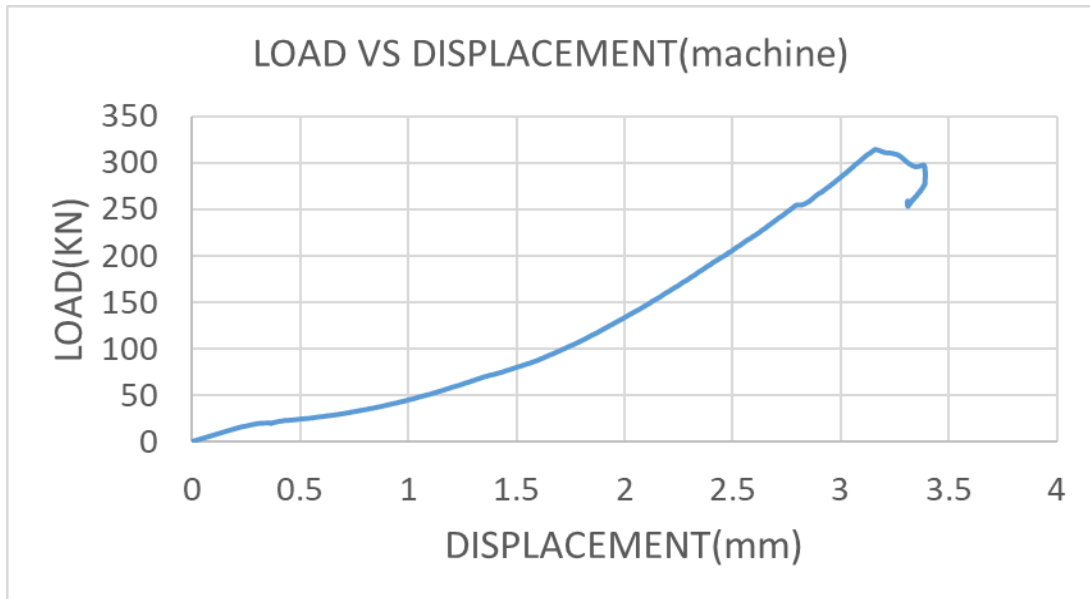


Figure 92 Load vs displacement for short hollow tube under axial compression (with correction)

As seen in Figure 92 now the load –displacement curve is now starting from origin and displacement correction is done.

5.2 Results of tensile coupon testing

Tension coupon testing was performed on dogbone specimen cut from pipe and channel section. Tension coupon testing was done for both type one and type four type specimens of ASTM D 638. Specimens were cut from pipe (230 mm dia, 300 mm long and 6mm thick) and channel sections (102mm web x 45mm flanges x 6mm thick). Specimens were cut from web for channel section.

5.2.1 Results for tension test of channel section specimens (Type one)
STRESS VS STRAIN

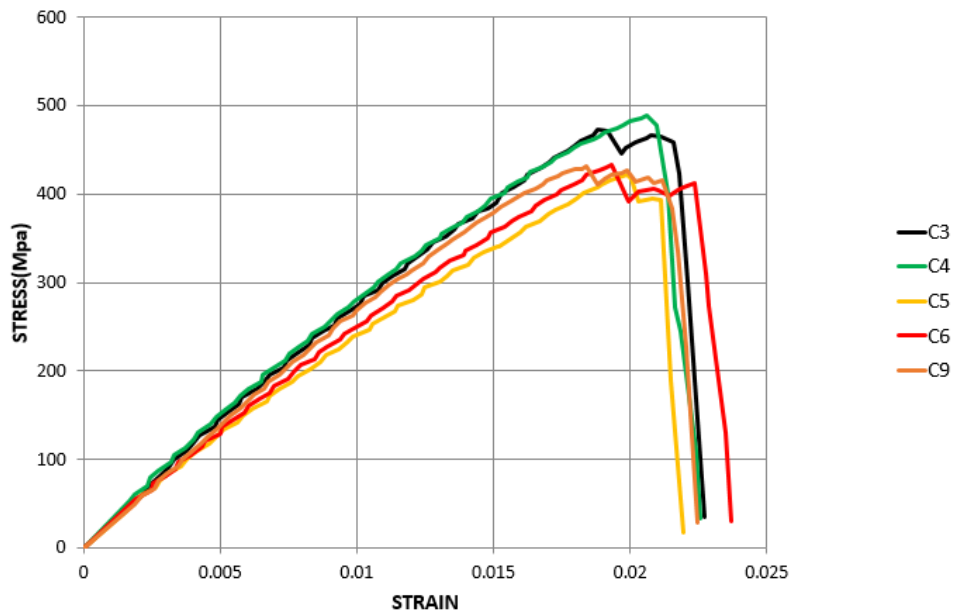


Figure 93 Stress vs strain graph for channel section specimens (Type one)

As seen in Figure 93 C4 specimen took maximum stress of 489.08Mpa which is highest among all the specimens.C5 took minimum stress of just 421.38 Mpa and average stress taken by all specimens came out to be 449.68 Mpa.

Youngs modulus was also determined in the test.C3 showed maximum youngs modulus of 29.78 Gpa. While minimum youngs modulus turned out to be 26.98 Gpa. Average youngs modulus was found out to be 28.29 Gpa.

Failure mode was also determined during experimental testing.C3 failed by a shear rupture crack and delamination.C5 and C9 failed by delamination.C4 and C6 failed by shear rupture crack and delamination.



Figure 94 Shear rupture and delamination failure in channel section specimens (type one)



Figure 95 Shear plane rupture occurring in channel section specimens (type one)

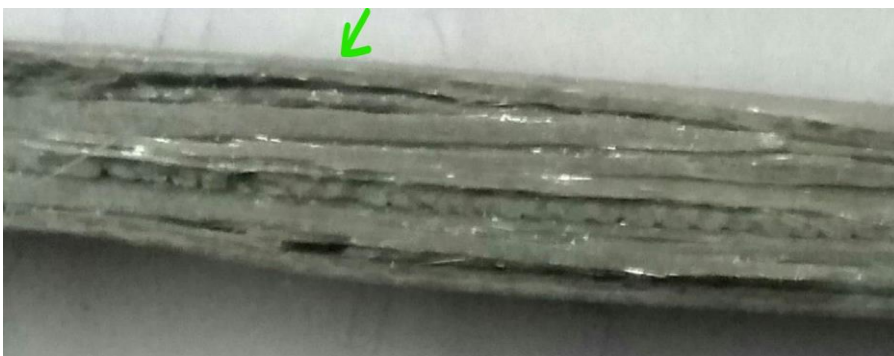


Figure 96 Delamination occurring in channel section specimens (type one)

4.2.2 Results for tension test of channel section (Type 4)

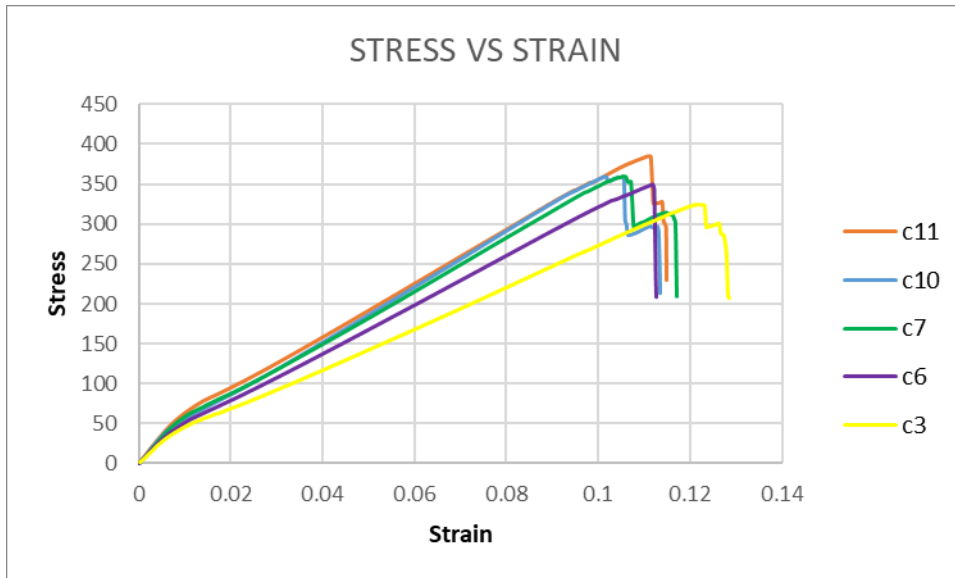


Figure 97 Stress vs strain graph for channel section specimens (type four)

As seen in Figure 97 C11 took highest maximum stress of 384.76 Mpa. C7 took maximum stress of 360.01 Mpa while C10 failed at maximum stress of 359.02 Mpa. C6 failed at maximum stress of 349.94 Mpa and C3 failed at maximum stress of 325.08 Mpa. For type four specimens only stress values were determined and modulus determination was not done.

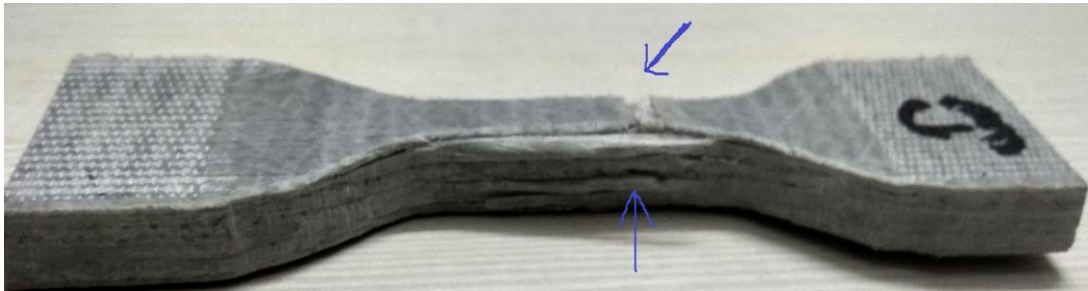


Figure 98 Shear plane fracture and delamination in channel section specimens (type four)

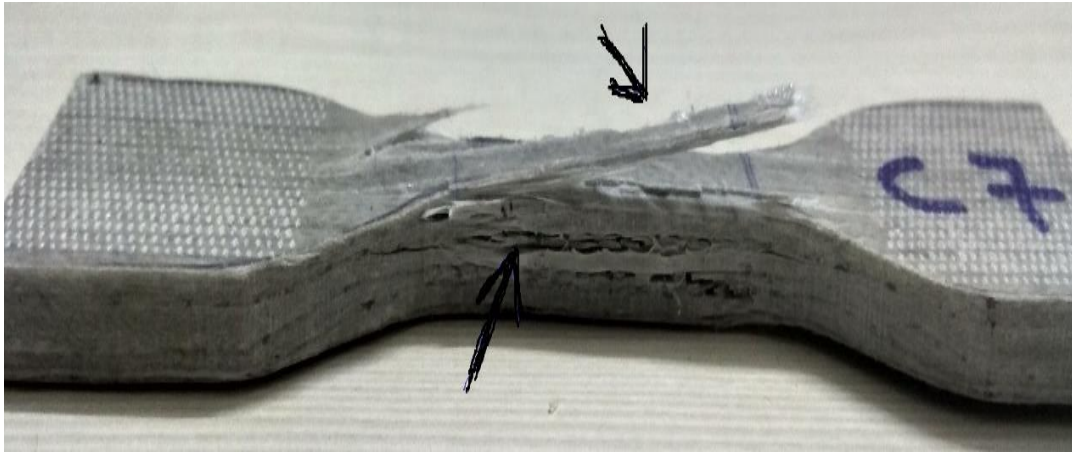


Figure 99 Delamination and debonding in channel section specimens (type four)



Figure 100 Delamination in channel section specimens (type four)

As we can see in above figures delamination, shear plane fracture, debonding failure modes occurred in specimens from channel section of type four. Apart from these failure modes a combination of delamination and shear plane fracture or combination of delamination and debonding were also observed. All specimens failed in gauge length portion.

5.2.3 Results for tension test of pipe section specimens (type one)

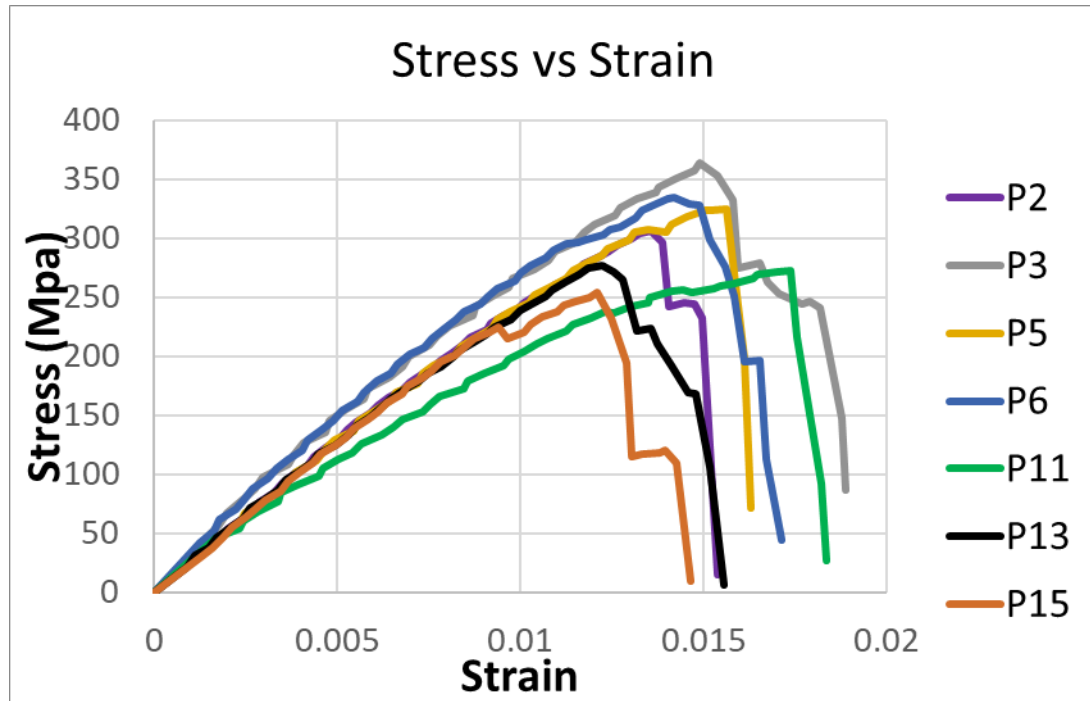


Figure 101 Stress vs strain graph for pipe section specimens (Type one)

As seen in Figure 101 P3 specimen took maximum stress of 363.97 Mpa which is highest among all the specimens. P11 took minimum stress of just 254.14 Mpa and average stress taken by all specimens came out to be 304.73 Mpa.

Youngs modulus was also determined in the test. P3 showed maximum youngs modulus of 31.55 Gpa. While minimum youngs modulus turned out to be 22.2 Gpa. Average youngs modulus was found out to be 27.09 Gpa.

5.2.4 Results for tension test of pipe section specimens (type four)

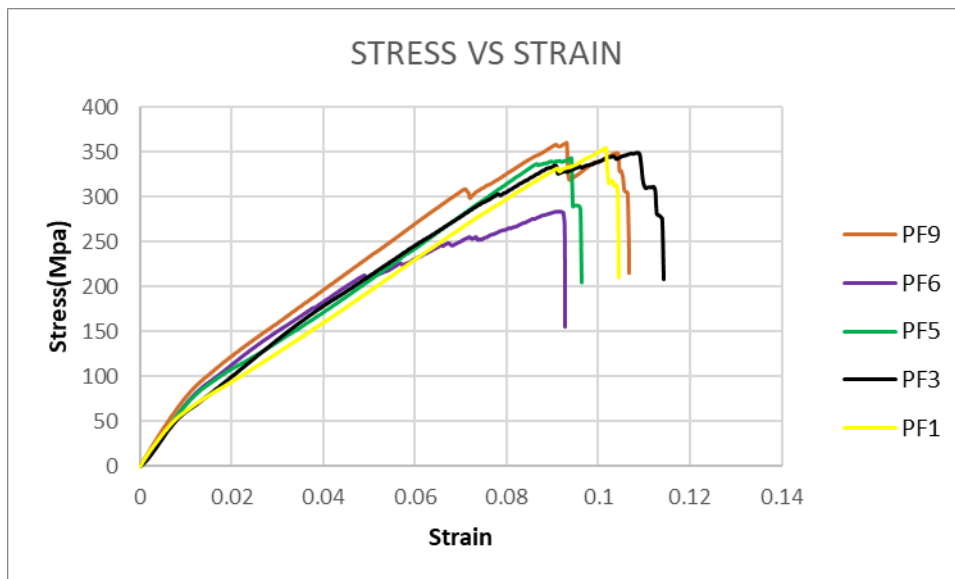


Figure 102 Stress vs strain graph for pipe section specimens (Type four)

As seen in Figure 102 PF9 took highest maximum stress of 360.82 Mpa. PF1 took maximum stress of 355.01 Mpa while PF3 failed at maximum stress of 349.24 Mpa. PF5 failed at maximum stress of 343 Mpa and PF6 failed at maximum stress of 284.39 Mpa. For type four specimens only stress values were determined and modulus determination was not done.



Figure 103 Shear plane rupture and delamination for pipe section specimens (type four)



Figure 104 Shear plane rupture for pipe section specimens (type four)



Figure 105 Delamination in pipe section specimens (type four)

As we can see in above figures delamination, shear plane fracture, debonding failure modes occurred in specimens from pipe section of type four. Apart from these failure modes a combination of delamination and shear plane fracture or combination of delamination and debonding were also observed. All specimens failed in gauge length portion.

5.3 Results of compression coupon testing

5.3.1 Results of compression strength test of channel section specimens

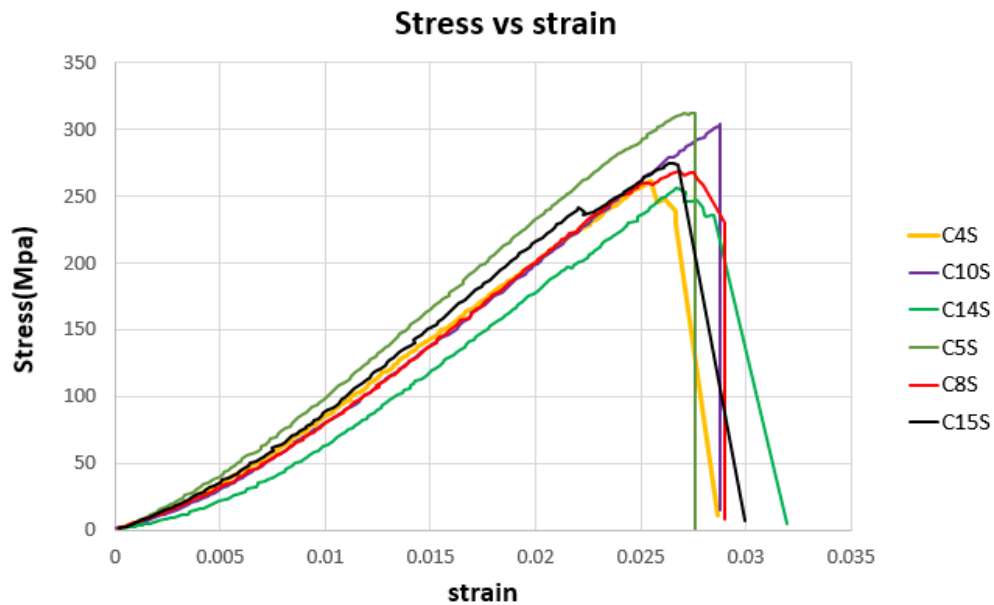


Figure 106 Stress vs strain graph of compression strength test of channel section specimens

As seen in Figure 106 C5s specimen took maximum stress of 312.91 Mpa which is highest among all the specimens. C9s took minimum stress of just 220.91 Mpa and average stress

taken by all specimens came out to be 263.22 Mpa. This test was performed just to know strength of coupon specimens in compression.



Figure 107 Delamination in compression strength test for channel section specimens



Figure 108 Rupture occurring in compression strength test for channel section specimens

Rupture and delamination occurred in most of the specimens, Brooming was also observed in one specimen. This test was performed without any lateral confinement to specimens. Hence there was possibility of delamination happening in specimens. And most of the specimens failed by delamination failure mode, some of them failed by rupture also. Brooming happened in some of the specimens. Brooming is possible because of improper

surfaces of specimen, because of which it was not properly leveled in machine. Hence load was not applied properly to specimen that caused them to broom at ends. This error should be avoided and specimen surfaces should be made flat and parallel while machining and should be properly aligned between machine platens.

5.3.2 Results of compression modulus test of channel section specimens

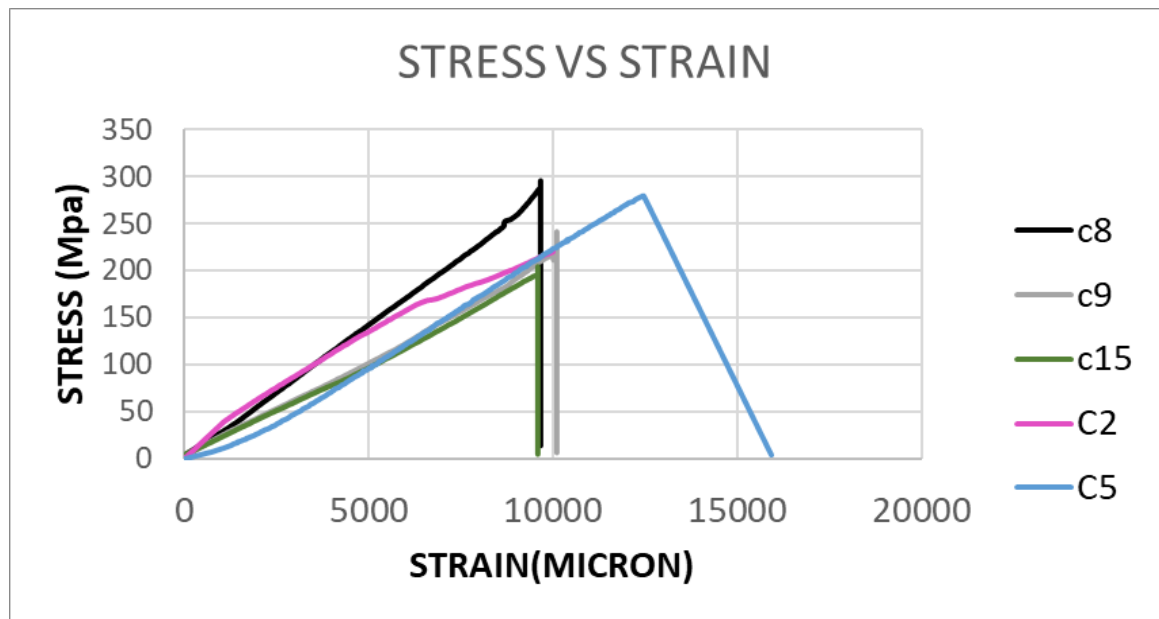


Figure 109 Stress vs strain graph for compression modulus test of channel section specimens

Young's modulus was also determined in the test. C2 showed maximum young's modulus of 24.27 Gpa. While C5 showed minimum young's modulus of 21.65 Gpa. Average young's modulus was found out to be 23.37 Gpa. Strain gauge was used to measure strain. Strain gauges stopped working after a particular strain limit.



Figure 110 Delamination observed during compression modulus test of channel section specimens

Delamination and rupture are most common failure modes that were seen during compression modulus test. Almost all specimens failed by delamination. Delamination occurred because there was lack of confinement for the specimens in lateral direction. Hence specimens started delaminating



Figure 111 Rupture observed during compression modulus test of channel section specimens

5.3.3 Results of compression strength test of pipe section specimens

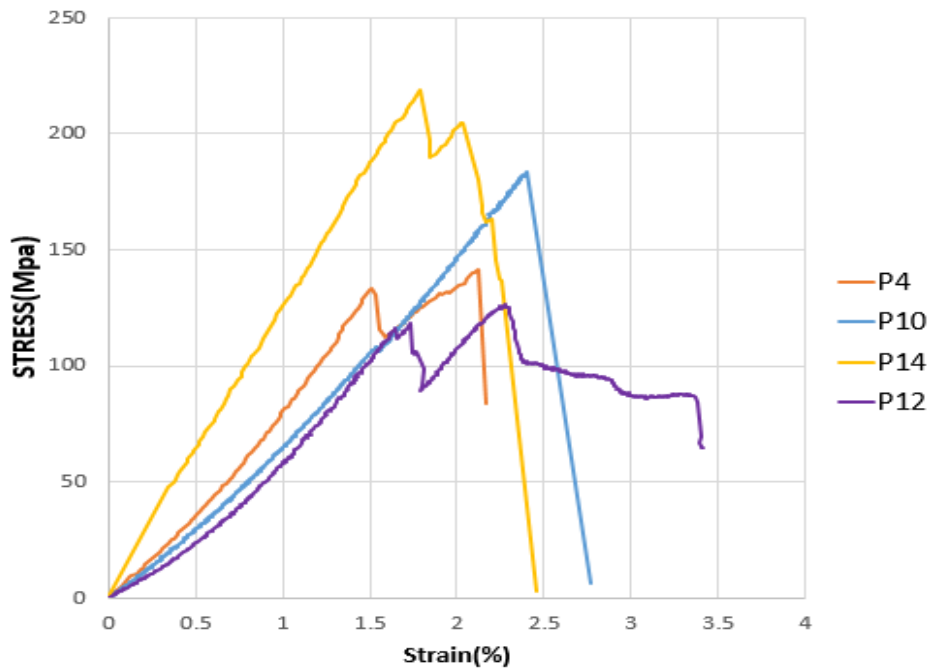


Figure 112 Stress vs strain graph for compression strength test of pipe section specimens

P14 showed highest maximum stress of 218.694 Mpa with failure load of 15.082 KN. P12 showed lowest maximum stress of 126.266 Mpa with failure load of 10.076 KN. Average strength and load for the test was found out to be 167.552 Mpa and 12.62 KN. There was standard deviation of 41.91 Mpa in maximum stress values.

Variation in maximum stress is because specimens were not confined during the test that caused delamination to occur in specimens. ASTM D 695 recommends use of jig to prevent delamination. Jig will be used in compression strength tests (explained later) to prevent delamination.



Figure 113 Delamination occurred during compression strength test of pipe section specimens

5.3.4 Results of compression modulus test of pipe section specimens

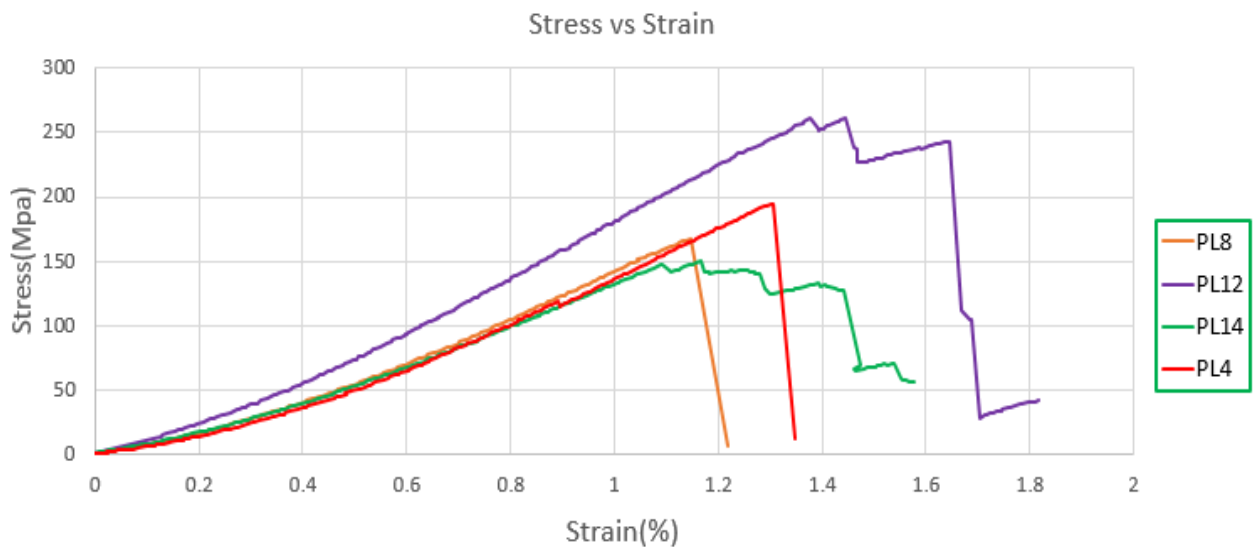


Figure 114 Stress vs strain graph for compression modulus test of pipe section specimens

PL4 showed maximum modulus of elasticity of 17.98 Gpa and PL14 showed minimum modulus of elasticity of 15.85 Gpa. Average modulus of elasticity was found out to be 17.15 Gpa, which is quite acceptable considering modulus of glass fibers is around 80Gpa and specimen is having fibers in four directions (0/+45/-45/90).Standard deviation of 0.94Gpa was observed which is quite acceptable.



Figure 115 Delamination in compression strength test of pipe section specimens

Similar to specimens that were cut from channel section, specimens from pipe section also delaminated. Delamination occurred because there was lack of confinement for the specimens in lateral direction. Hence there is a need for lateral confinement to be given to specimens.

5.4 Bearing strength test results

5.4.1 Bearing strength test results for HRB series

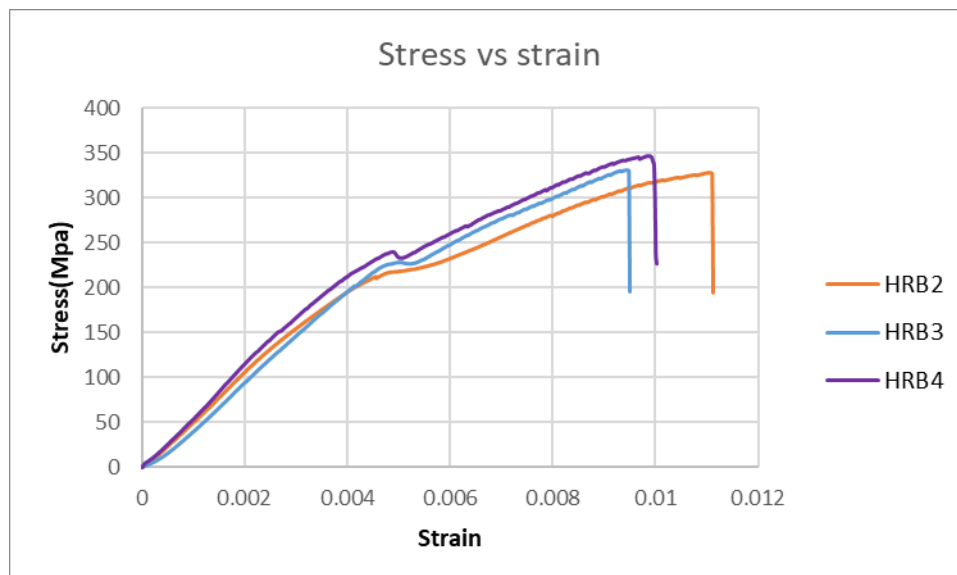


Figure 116 Stress-strain graph for bearing strength test(HRB series)

HRB4 failed at highest maximum stress of 347.45 Mpa while HRB3 failed at maximum stress of 331Mpa.HRB2 failed at lowest maximum stress of 328.47 Mpa.HRB4 failed by shear out failure.HRB2 failed by bearing failure.HRB3 also failed by shear out failure. Average maximum stress came out to be 335.64 Mpa.



Figure 117 Shear out failure observed in HRB3



Figure 118 Bearing failure observed in HRB2

5.4.2 Bearing strength test results for B series

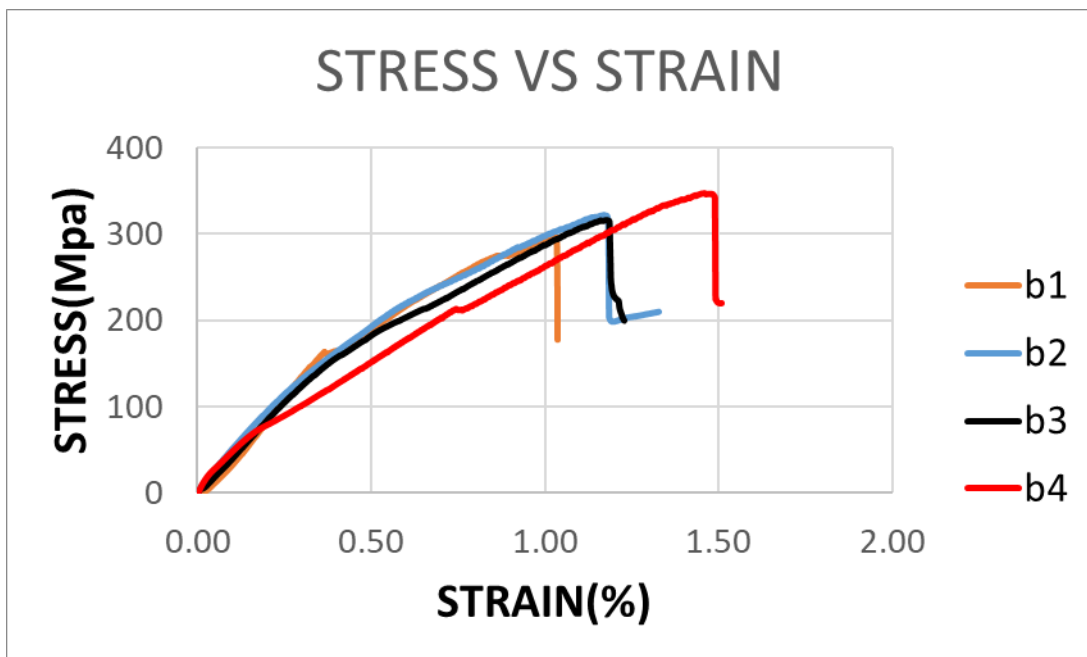


Figure 119 Stress vs strain graph for bearing strength test (B series))

b4 failed at highest maximum stress of 347.22 Mpa while b2 failed at maximum stress of 322.08Mpa. b3 failed at lowest maximum stress of 315.9 Mpa.b1 failed at lowest maximum stress of 296.27 Mpa. Average maximum stress came out to be 320.37 Mpa.

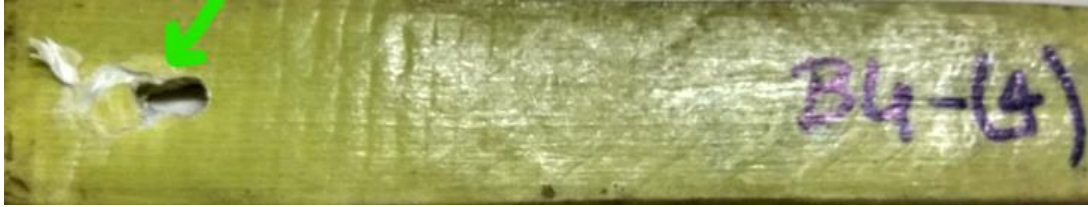


Figure 120 Shear out failure observed in b4



Figure 121 Bearing failure observed in b1

b2, b3 and b4 failed by shear out failure while b1 failed by bearing failure mode

5.5 Axial compression test on short hollow circular tubes

5.5.1 Axial compression test on specimen1

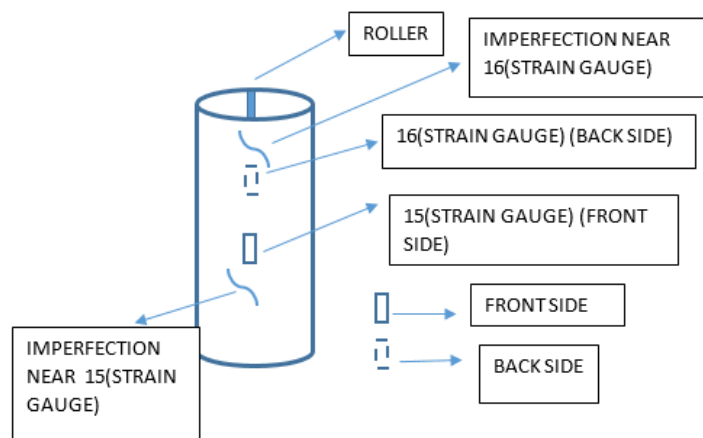


Figure 122 Orientation of strain gauges on specimen 1

Strain gauges were positioned at diametrically opposite points. Imperfection area was present near both the strain gauges. Both strain gauges were pasted along the direction of roller.

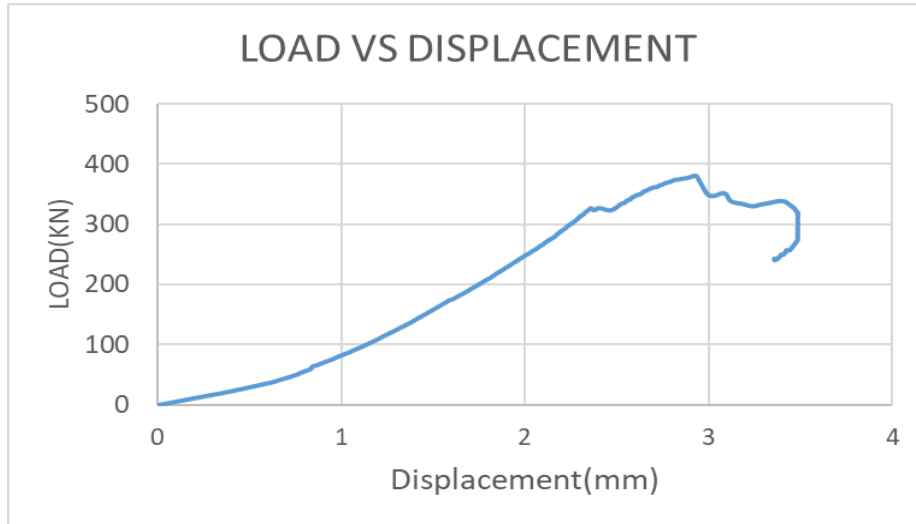


Figure 123 Load vs displacement graph for specimen1

Failure load of 379.95 KN was observed and failure stress of 89.99Mpa was observed. Experiment was performed in displacement control mode with a rate of 1.3 mm/min.

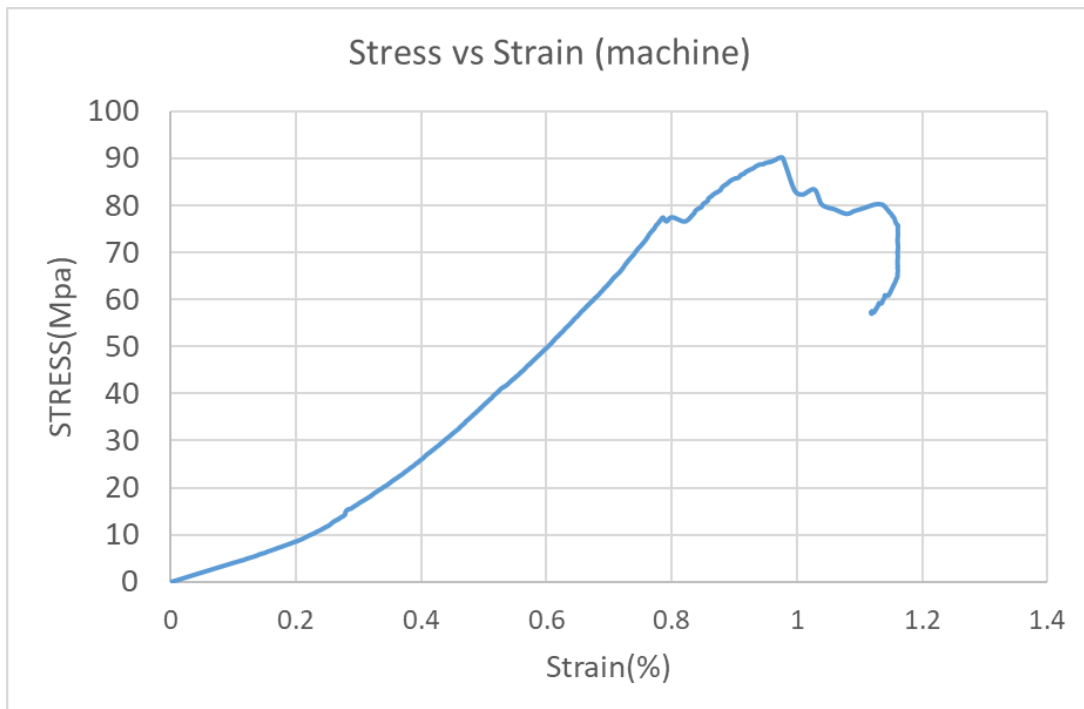


Figure 124 Stress vs strain graph for specimen1

Stress vs strain graph for specimen1 was also plotted.Stress was calculated by dividing the maximum load taken by specimen by cross sectional area of specimen.Strain was measured using strain gauges arranged according to orientation shown in Figure 122.

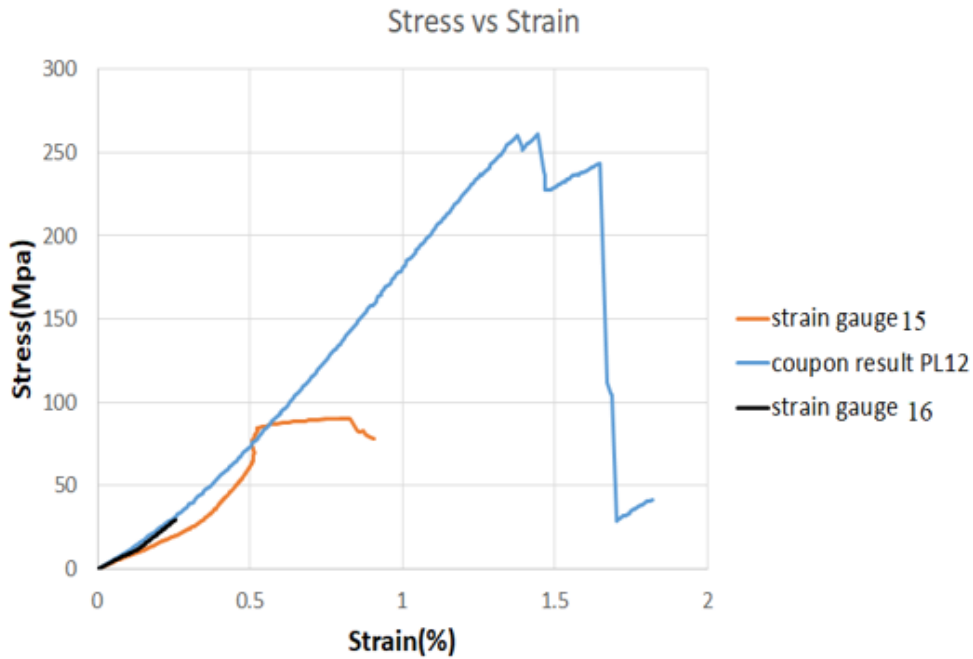


Figure 125 Comparison with coupon specimen PL12

As seen in above Figure 125 stiffness of strain gauge 16 in which failure occurred coincided with that of coupon specimen while that of strain gauge 15 was below stress strain curve of coupon specimen. Failure occurred along both strain gauges and strain gauge 16 stopped during failure.



Figure 126 Failure mode in specimen 1(front side)



Figure 127 Failure mode in specimen 1(back side)

As it can be seen in Figure 126 and 127 there was delamination and rupture throughout length of specimen. This was more prominent in areas having material imperfection and hence it triggered failure in specimen. Because of this specimen failed before reaching their true ultimate strength. This is a major concern and hence manufacturing will be taken proper care of in future.

5.5.2 Axial compression test on specimen2

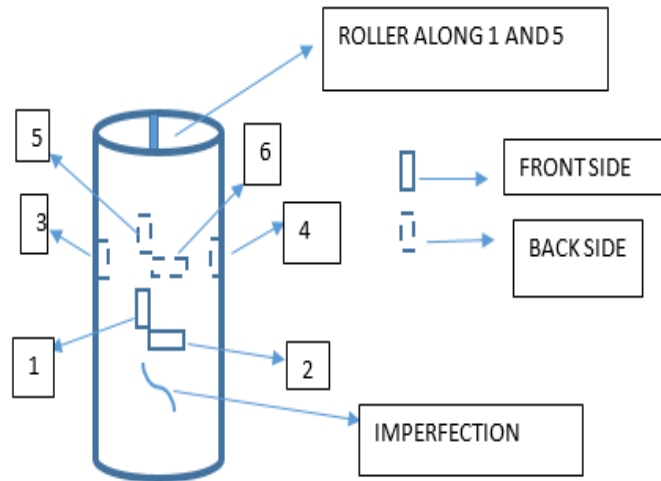


Figure 128 Orientation of strain gauges on specimen 2

Strain gauges were positioned at diametrically opposite points 1 and 5. At 1, a perpendicular strain gauge 2 was also provided to measure lateral strain. Similarly, at 5, 6 was provided. Roller is provided along the straight line between strain gauge 1 and 5. 3 and 4 strain gauges were provided perpendicular to direction of roller (along sides). 3 and 4 are diametrically opposite. Imperfection was present only in 1st and 2nd strain gauge area.

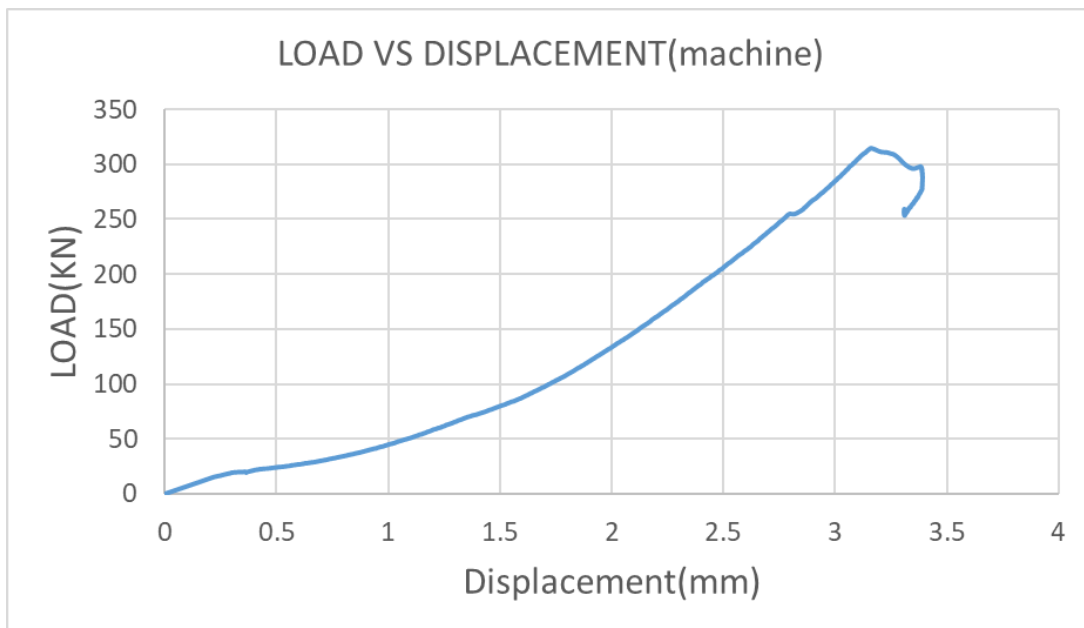


Figure 129 Load vs displacement graph for specimen 2

Failure load of 314.2 KN was observed and failure stress of 74.42Mpa was observed. Experiment was performed in displacement control mode with a rate of 1.3 mm/min.

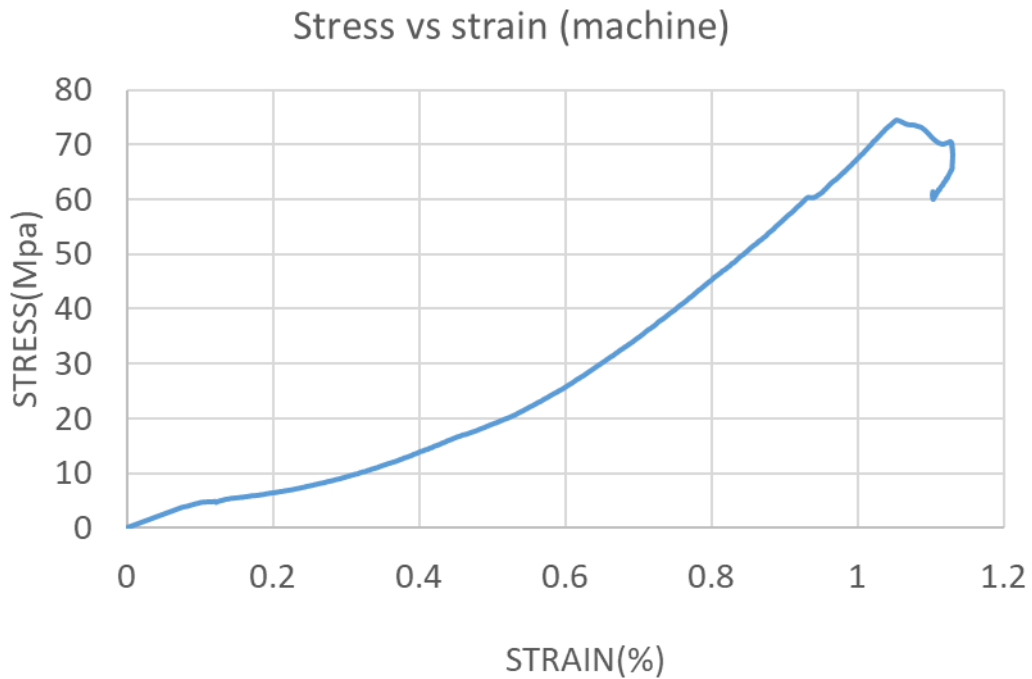


Figure 130 Stress vs strain graph for specimen2

Figure 130 Stress vs strain graph for specimen2 was also plotted. Stress was calculated by dividing the maximum load taken by specimen by cross sectional area of specimen. Strain was measured using strain gauges arranged according to orientation shown in Figure 128.

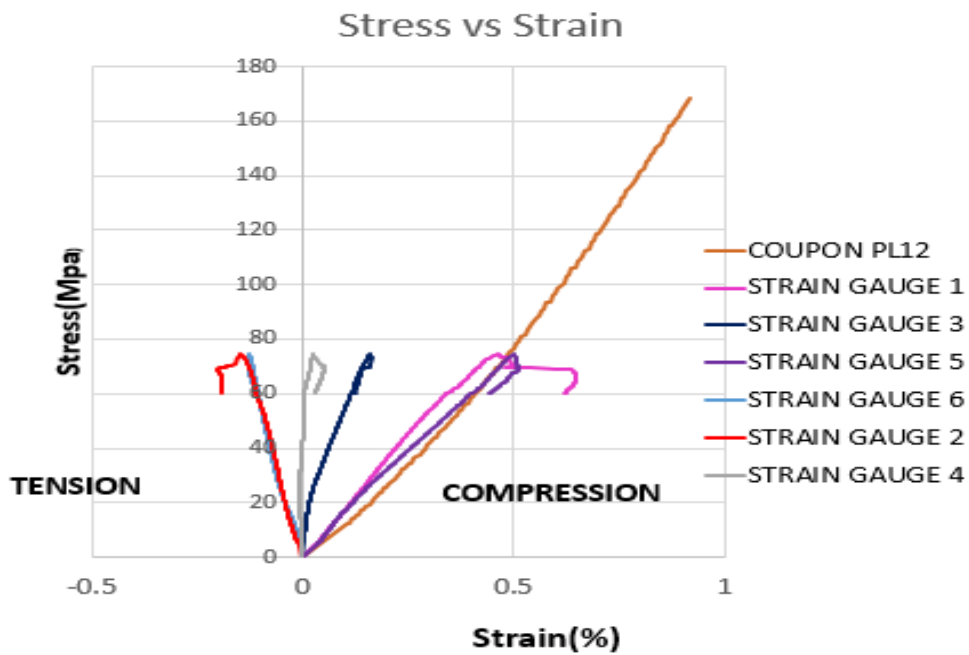


Figure 131 Comparison with coupon specimen PL12

As seen in the above Figure 131 strain gauge 1 and strain gauge 5 have almost equal stiffness as that of coupon result. While Strain gauge 3 and strain gauge 4 have higher stiffness than that of coupon specimen. Strain gauges 2 and 6 showed negative (tensile stress) stress and have almost equal stiffness that is greater than that of coupon specimen. Failure occurred near the imperfection area that is present near strain gauge 1 and 2. Delamination occurred near to strain gauge 1 and 2.

Strain gauge 4 and Strain gauge 5 strains differ, that shows uneven load distribution. This is caused due to bending happening in fixture plates. Strain observed in strain gauge 4 is significantly less than that of strain gauge 5. Strains recorded by strain gauge 3 and strain gauge 5 varied because of similar reason



Figure 132 Delamination occurring in Specimen2

Delamination was observed near strain gauge 1 and 2 (inside view) and imperfection was also present near strain gauge 1 and 2. It is believed that presence of material imperfection triggered failure in that area.

5.5.3 Axial compression test on specimen3

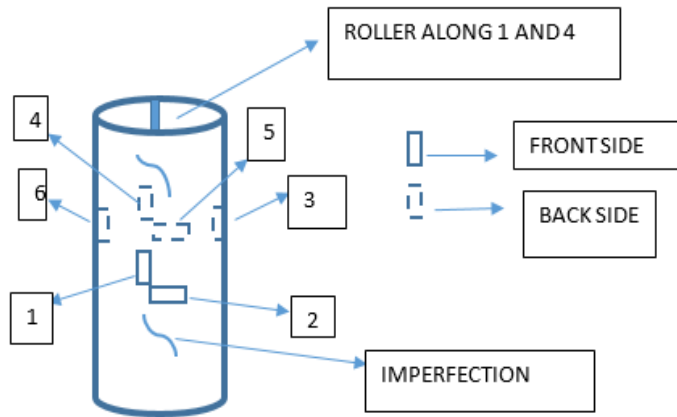


Figure 133 Orientation of strain gauges on specimen 3

Strain gauges were positioned at diametrically opposite points 1 and 4 along roller. At 1, a perpendicular strain gauge 2 was also provided to measure lateral strain. Similarly, at 4, 5 was provided. Roller is provided along the straight line between strain gauge 1 and 4. 3 and 6 were provided perpendicular to roller (along sides). Imperfection area was near to both 1,2 and 4,5 strain gauge area.

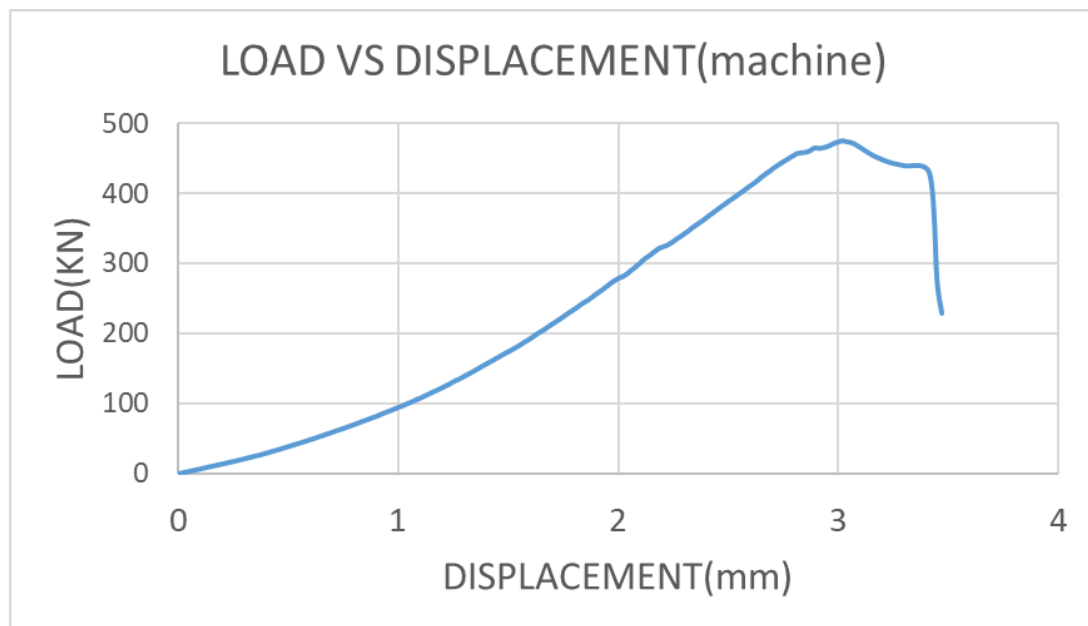


Figure 134 Load vs displacement graph for specimen3

Failure load of 475.25 KN was observed and failure stress of 112.62 Mpa was observed. Experiment was performed in displacement control mode with a rate of 1.3 mm/min.

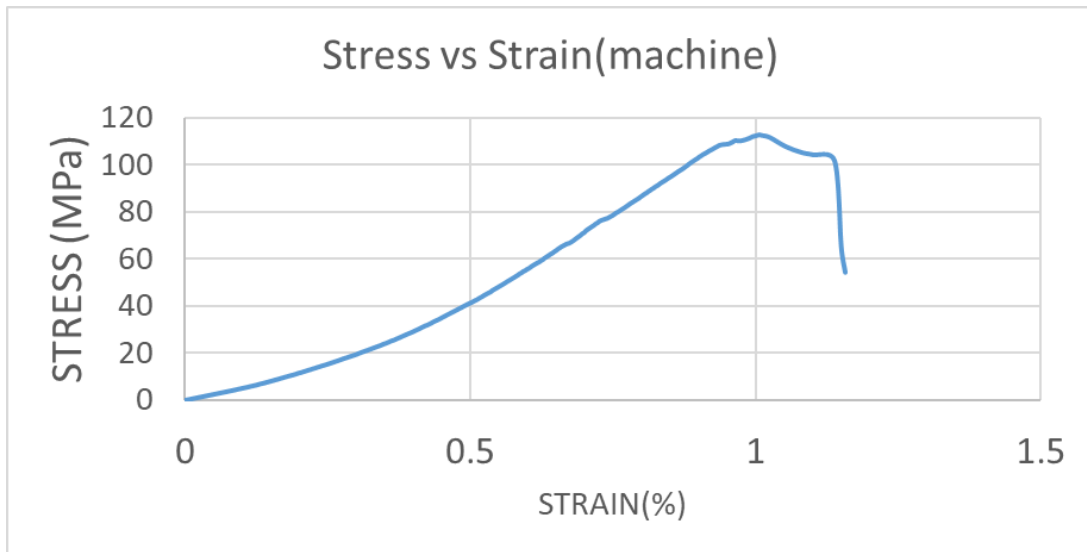


Figure 135 Stress vs strain graph for specimen 3

Stress vs strain graph for specimen 3 was also plotted. Stress was calculated by dividing the maximum load taken by specimen by cross sectional area of specimen. Strain was measured using strain gauges arranged according to orientation shown in Figure 5.55.

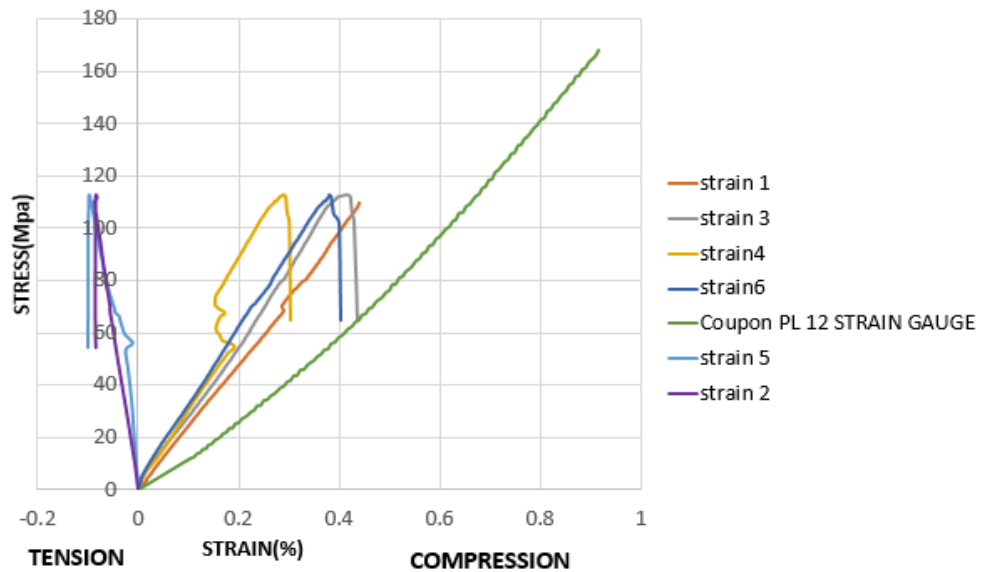


Figure 136 Comparison with coupon specimen PL12

As seen in the above Figure 136 all the strain gauges have higher stiffness than that of coupon. Strain gauges 2 and 5 showed negative (tensile stress) stress and have almost equal stiffness that is greater than that of coupon specimen. Failure occurred through strain gauge 4. Failure occurred in the imperfection area present near strain gauge 4 and 5. Failure also

occurred in imperfection area present near strain gauge 1 and 2. Some failure was also observed near strain gauge 3.

Strain gauge 3 and Strain gauge 4 strains differ, that shows uneven load distribution. This is caused due to bending happening in fixture plates. Strain observed in strain gauge 4 is significantly less than that of strain gauge 3. Strains recorded by strain gauge 4 and strain gauge 6 varied because of similar reason.



Figure 137 Failure through strain gauge 4 (left) and through strain gauge 3 (Right)

There was presence of material imperfection near strain gauge 4 and 5 area in specimen 3. Specimen 3 failed near the area with material imperfection. Even cracks and rupture occurred through strain gauge 4 as seen in Figure 137.

Failure near strain gauge 3 was also observed. Brooming occurred on top surface of specimen that can be caused because of two reasons. One can be because of presence of unevenness in specimen that caused improper alignment of specimen between platens of machine. Hence applied compressive load was not evenly distributed throughout the specimen and it started brooming in some areas. Another reason can be bending happening in fixture plates that were placed on top of specimen. Bending caused uneven distribution of load in specimen that caused brooming in some areas.



Figure 138 Presence of material imperfection and failure near stain gauge 4 and 5 (inside view)



Figure 139 Presence of material imperfection and failure near stain gauge 1 and 2 (inside view)

In inside view of specimen 3 there were cracks present in area having material imperfection This was present near strain gauge 4, 5 area and strain gauge 1,2 area and it triggered failure in that area and during the test delamination occurred in these areas.

5.6 Validation study of two H beams in abaqus

5.6.1 Comparison of deflection at midspan for H beam 1

The deflection in the y direction in H beam1 was calculated. It is validated with the experimental result that is given in Barbero et.al. For H beam1 the deflection at midspan (given by experiments) is 0.112 inch while the deflection at midspan given by Abaqus is 0.1155 inch.

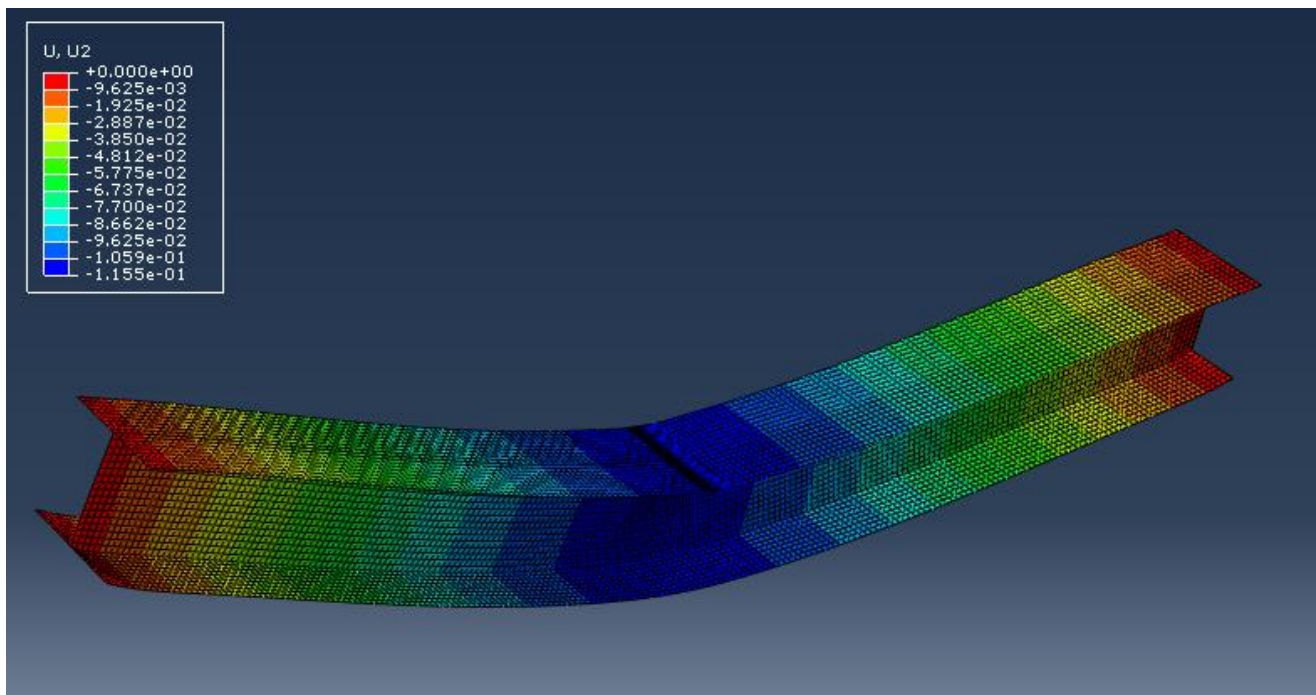


Figure 140 Deflection at midspan (abaqus) for H beam 1

Table 16 Comparison of deflection values for H beam 1

EXPERIMENTAL VALUE	OBTAINED VALUE
Deflection (in)	Deflection(in)
0.112	0.1155

As it can be seen in above table 17 obtained value of midspan deflection from abaqus matches closely with the experimental value. Variation between both is 3.125% that is quite acceptable.

5.6.2 Comparison of deflection at midspan for H beam 2

The deflection in the y direction in H beam2 was calculated. It is validated with the experimental result that is given in Barbero et.al. For H beam2 the deflection at midspan (given by experiments) is 0.3150 inch while the deflection at midspan given by Abaqus is 0.3401 inch.

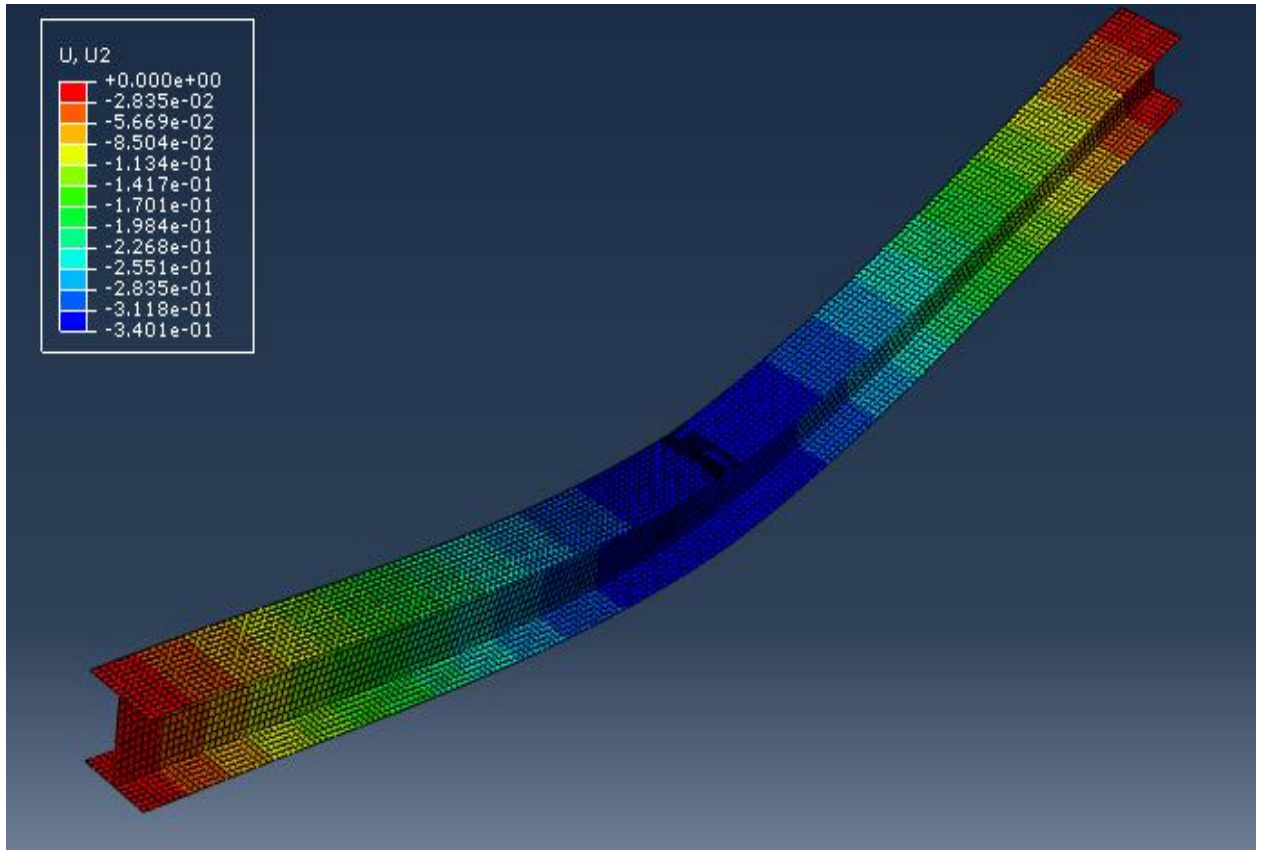


Figure 14 Deflection at midspan (abaqus) for H beam 2

EXPERIMENTAL VALUE	OBTAINED VALUE
Deflection (in)	Deflection (in)
0.3150	0.3401

Table 17 Comparison of deflection values for H beam 2

As it can be seen in above table18 obtained value of midspan deflection from abaqus matches closely with the experimental value. Variation between both is 7.968 % that is quite acceptable.

5.7 Reaction force for different mats

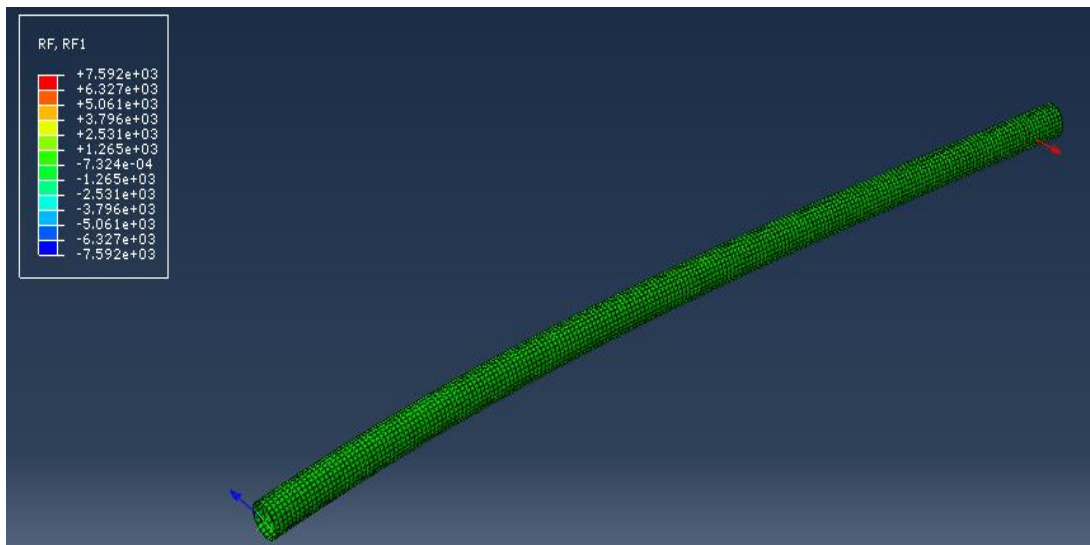


Figure 142 Reaction force determined at fixed end for MAT1

As seen in above figure 142, a reaction force of 7.592 KN was determined at fixed end, for a constant displacement of 1050 mm that was applied at the free end.

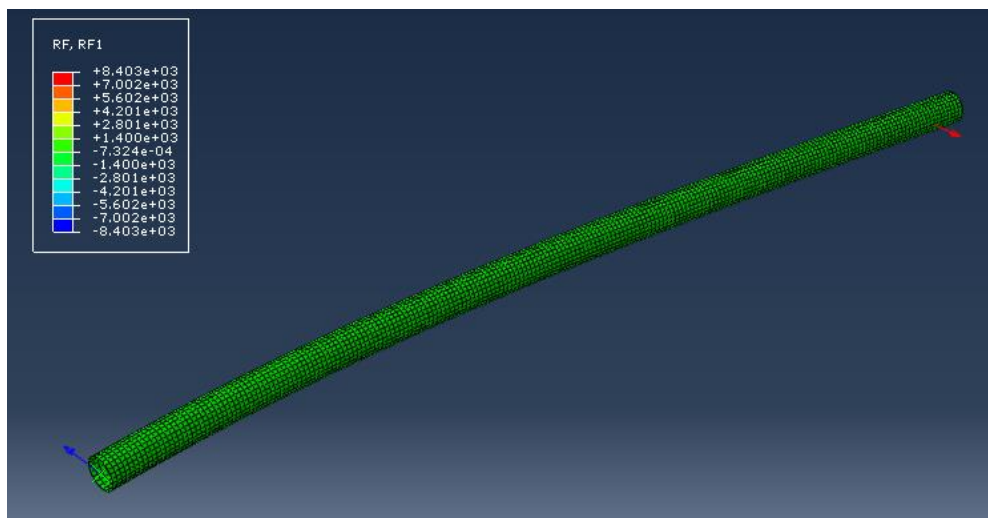


Figure 143 Reaction force determined at fixed end (90-0 mat) MAT2

As seen in above figure 143 a reaction force of 8.403 KN was determined at fixed end, for a constant displacement of 1050 mm that was applied at the free end.

5 mats of 90-0-chop configuration with symmetric configuration with rovings in between was used to see possible optimization in pole stiffness

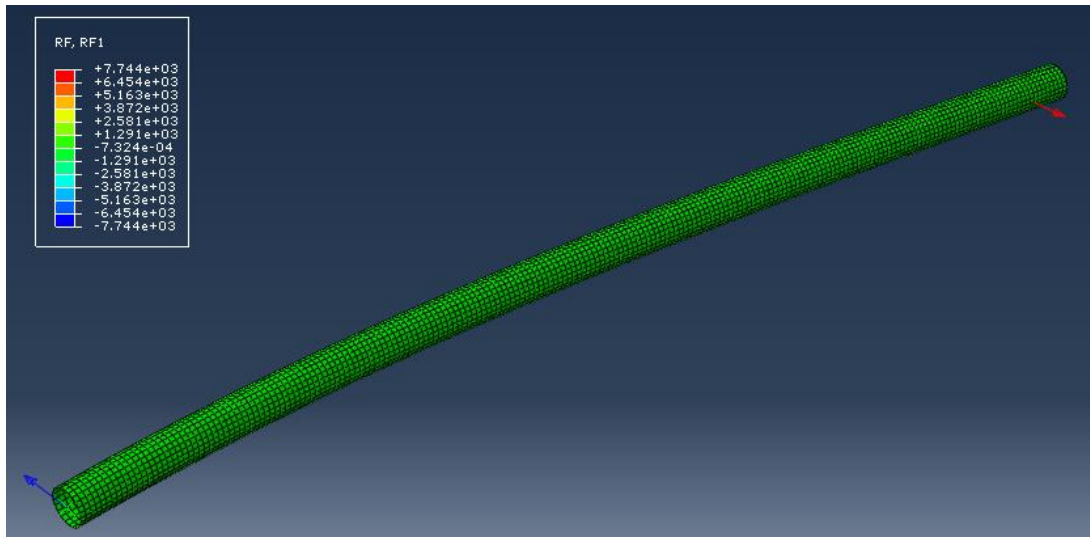


Figure 144 Reaction force determined at fixed end (0-90-chop mat) MAT3

As seen in above Figure 144 a reaction force of 7.744 KN was determined at fixed end, for a constant displacement of 1050 mm that was applied at the free end.

Number of mats were removed and additional rovings were added to maintain the same volume fraction. Results of these variations are summarized in below table

Stacking sequence	Load (KN)
MAT 1	7.592
MAT 2	8.403
MAT 3	7.744
MAT 4	8.045
MAT 5	8.486
MAT 6	8.703
MAT 7	8.898

Table 18 Comparison of load values for different mats

As it can be seen in the above table 19 Mat 7 with two 90-0 mats removed gives the highest load of 8.898 KN which means it will give highest stiffness. Hence it is preferred over all other mats.

5.8 Determination of stiffness for 0.5 m GFRP pole

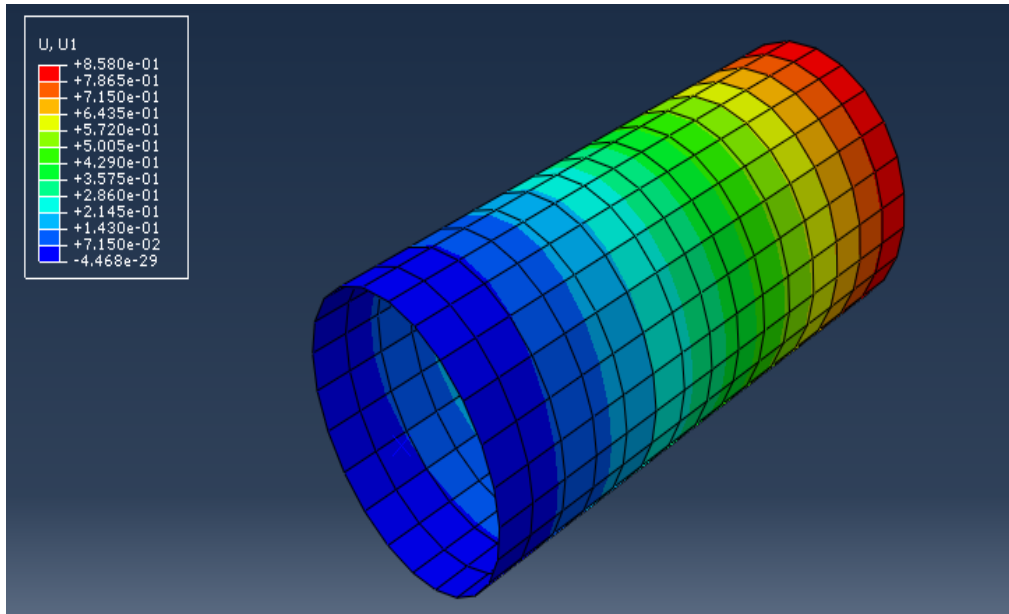


Figure 145 Deformation obtained from short pole

After dividing load of 7592 N with a deformation of 0.86 mm a stiffness value of 8827.91 N/mm was obtained.

Stacking sequence	Stiffness(N/mm)
MAT 1	8827.91
MAT 2	7031.79
MAT 3	8001.65

Table 19 comparison of stacking sequence (shear case)

As it can be seen in above table 20 MAT1 gave highest stiffness of 8827.91 N/mm that is expected because of presence of +45/-45 fibers which gives better stiffness performance under bending load when section length is reduced.

5.9 Analysis of plates for experimental setup

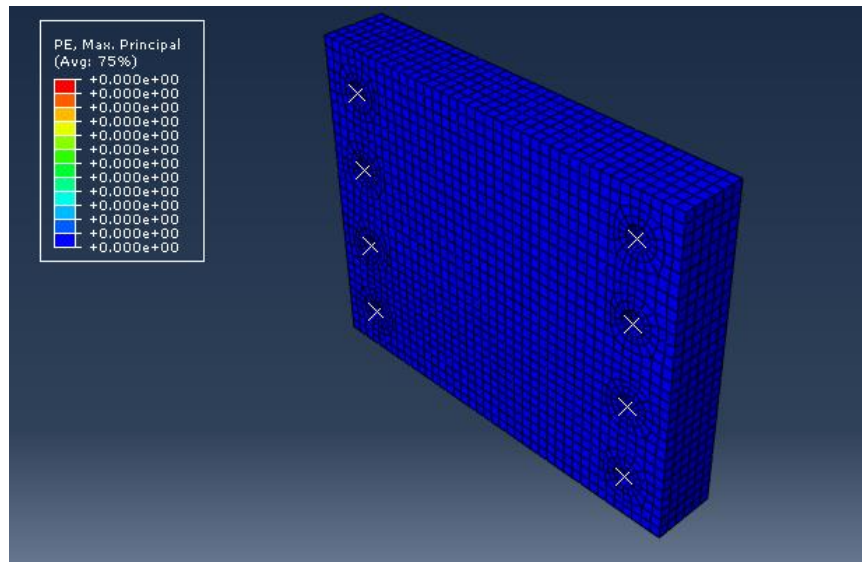


Figure 146No plastic strain for top plate

There was no plastic strain present in top plate. In material properties plasticity was given. Constant yield stress of 250 Mpa was given with plastic strain varying from 0 to 0.2. Since there was no presence of plastic strain which means that there is no bending in plate and it is safe to use it as support above GFRP pole.

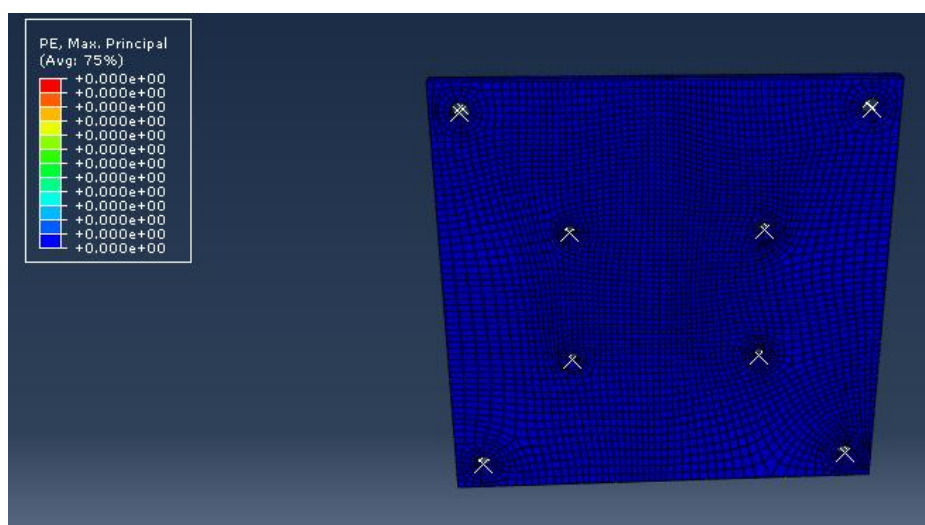


Figure 147No plastic strain for bottom plate

There was no plastic strain present in bottom plate. In material properties plasticity was given. Constant yield stress of 250 Mpa was given with plastic strain varying from 0 to 0.2. Since there was no presence of plastic strain which means that there is no bending in plate and it is safe to use it as bottom support.

5.10 Experimental results for compression test with jig

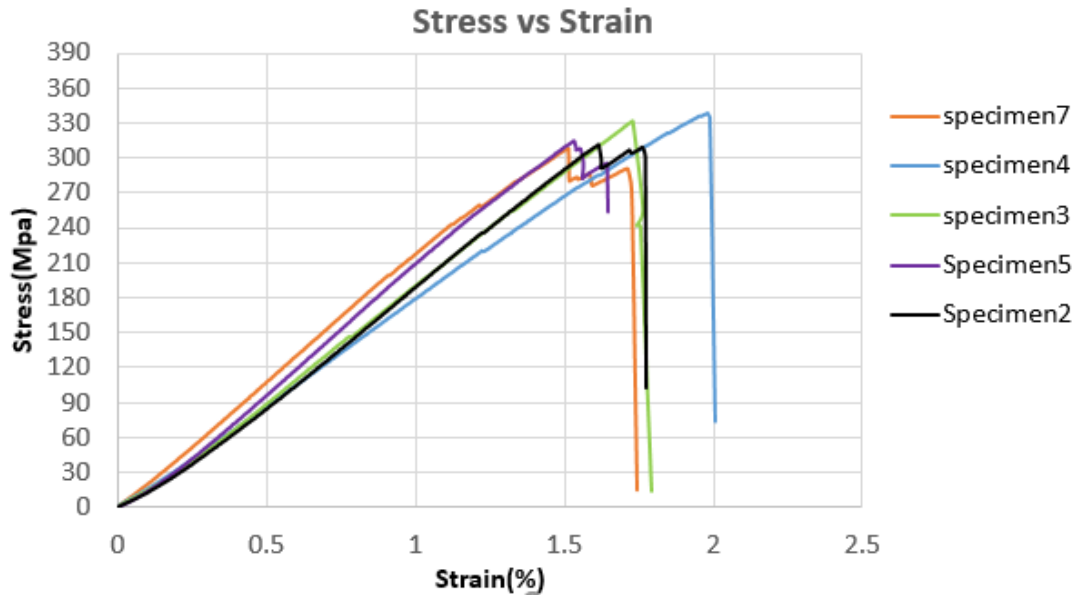


Figure 148 Stress vs strain results for coupons tested in compression with jig

Specimen 4 showed highest maximum stress of 339.05 Mpa while specimen 7 showed minimum maximum stress of 308.319 Mpa. Specimen3 also showed high maximum stress of 331.36 Mpa and specimen 5 showed maximum stress of 315.28 Mpa. Specimen 2 showed maximum stress of 311.39 Mpa.

Standard deviation of stress values was found out to be 13.41 Mpa. Average maximum stress came out to be 321.08 Mpa. Coefficient of variation was determined to be 4.17%.

5.10 Modeling of coupon specimen under tension

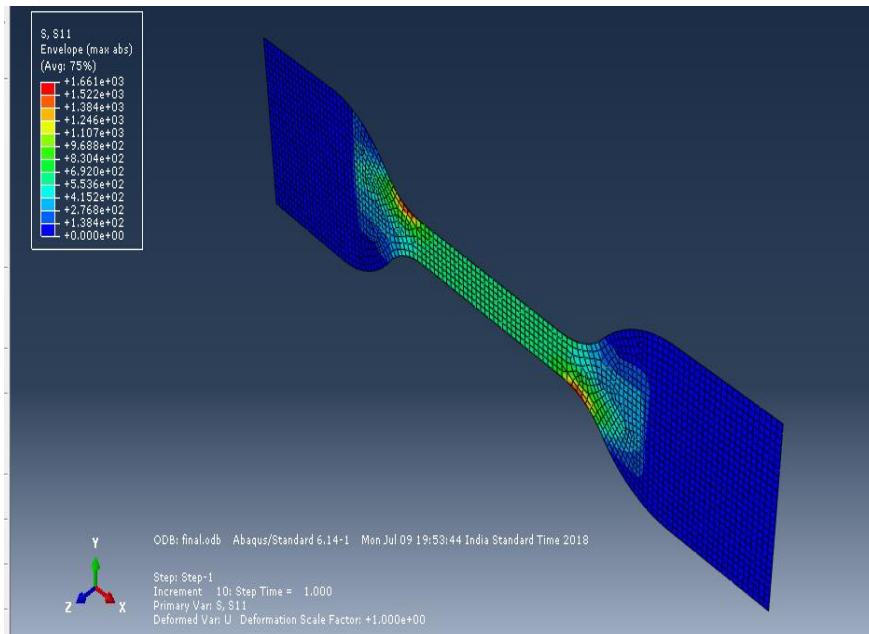


Figure 149 Stress determination for coupon specimen

Tension stress value of 166.1 Mpa was determined. S11 stress in direction of loading along x direction was determined.

5.11 Modeling of coupon specimen under Compression

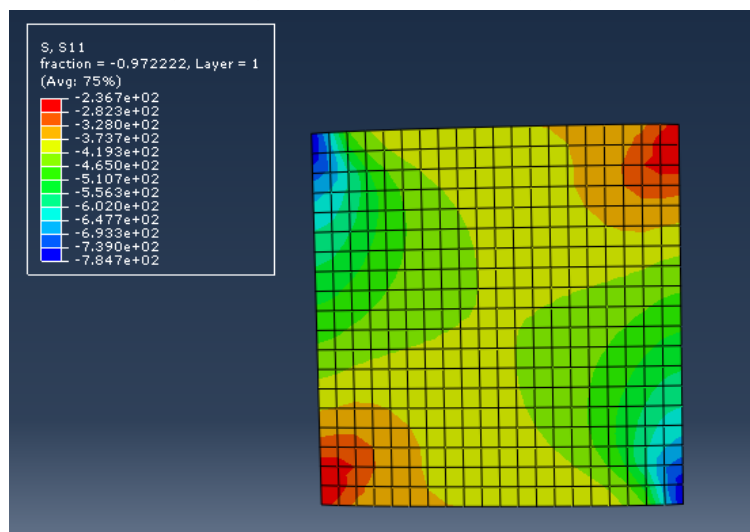


Figure 150 Compressive stress determined for coupon specimen

Compression stress value of 236.7 Mpa was determined. S11 stress in direction of loading along x direction was determined.

5.12 Modeling of coupon specimen under Compression

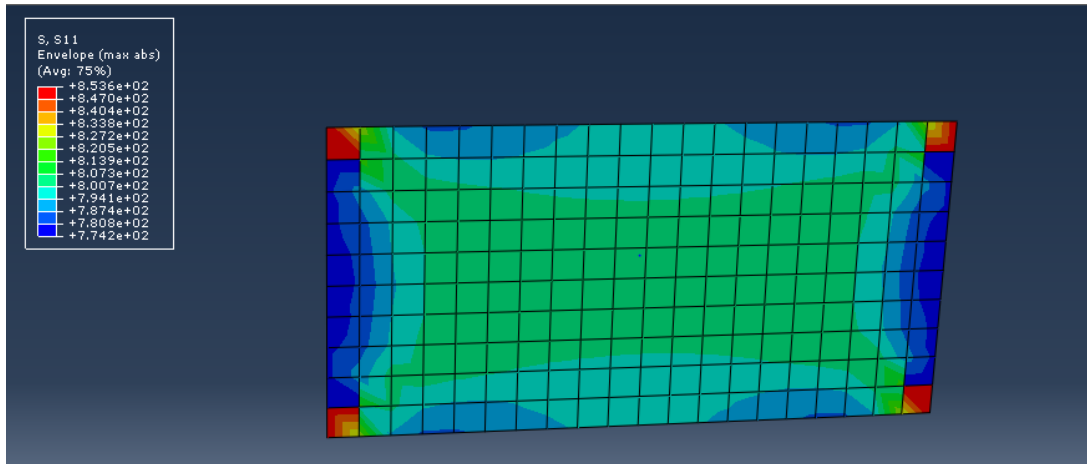


Figure 151 Compressive stress determined for coupon specimen

Compression stress value of 853.6 Mpa was determined. S11 stress in direction of loading along x direction was determined.

CHAPTER 6

6.CONCLUSIONS

Experimental testing of GFRP coupons were performed under tension, compression and bearing. Specimens cut from channel and pipe sections behaved differently under tension as well as under compression. Channel sections took more stresses because of better confinement of fibers. Under tension and compression specimens behaved linearly elastic up to failure. Failure modes under tension were shear plane fracture, delamination and debonding was also observed. For specimens tested under compression delamination and shear plane fracture of specimens were observed. Later delamination was minimized by use of prepared fixture (jig) to provide lateral confinement to specimens, because of which specimens failed in shear plane fracture. Under bearing specimens failed by shear out failure as well as under bearing failure mode. Specimens behaved almost linear elastic up to failure.

In experimental testing of short hollow GFRP tubes under axial compression delamination and crushing were observed. Brooming failure on top surface of specimens was also observed. Later it was realized that brooming occurred because of uneven distribution of load which was caused because of uneven distribution of load. Uneven load distribution happened because of two reasons. One is bending happening in fixture plates which caused load to be distributed not in a uniform manner and is because of manufacturing defects, which caused material imperfections in specimen and specimens failed near imperfections. There was premature failure in specimens.

Modeling of H beams was performed in abaqus. Results for mid span deflection for numerical model were compared with that from experiments. For H beam 1 variation between mid-span deflections from abaqus and experiments was 3.125%. For H beam 2 variation between mid-span deflections from abaqus and experiments was 7.968%. These variations are within the limits and are quite acceptable.

Optimization studies for seven-meter-long GFRP pole were performed. Out of different stacking sequence tried for optimization of pole, one having more number of longitudinal

fibers behaved better under bending load. It gave the highest stiffness, also when mats were removed and longitudinal fibers were increased more increase in stiffness value was observed.

To study shear effects on GFRP pole, a 0.5 meter GFRP cylinder was modeled having the same stacking sequence as that of 7-meter-long GFRP pole. It was observed that with reduced length now +45 and -45 fibers behaved better as compared to other fibers and increased stiffness was now observed for mats having more number of +45 and -45 fibers.

Four composite plates were prepared by hand layup technique. Keeping the volume fraction same one plate was made with 10 number of mats without any rovings. Other plates were made by varying the number of mats and rovings.

REFERENCES

1. Ernesto Guades, Thiru Aravinthan, Md Mainul Islam. Characterization of the mechanical properties of pultruded fiber-reinforced polymer tube. *Materials and design* (2014).
2. Slimane Metiche and Radhouane Masmoudi. Analysis and design procedures for the flexural behavior of glass fiber-reinforced polymer composite pole. *Journal of composite materials* (2012).
3. Girum Urgessa and Sara Mohamadi. Structural Assessment of Fiber-reinforced Polymer Composite Electric Poles (2016).
4. J. F. Davalos, H. A. Salim, P. Qiao, R. Lopez-Anido and E. J. Barbero. Analysis and design of pultruded FRP shapes under bending (1996).
5. J.G. Teng, Y.M. Hu. Behavior of FRP-jacketed circular steel tubes and cylindrical shells under axial compression. *Construction and building materials* (2007).
6. d. polyzois, s. ibrahim, v. burachynsky, and s. k. hassan. Glass fiber-reinforced plastic poles for transmission and distribution lines.
7. P. Sangeetha, R. Sumathi. Behavior of glass fiber wrapped concrete columns under uniaxial compression. *International Journal of Advanced Engineering Technology* (2010).
8. Rami Haj-Ali and Hakan Kilic. Nonlinear behavior of pultruded FRP composites (2002).
9. Togay Ozbakkaloglu, Deric J. Oehlers. Manufacture and testing of a novel FRP tube confinement system. *Engineering structures* (2008).
10. Fabio Minghini, Nerio tullini, Ferdinando laudiero. Full-section properties of pultruded frp profiles using bending tests.
11. Ferdinando laudiero, Fabio minghini, Nicola ponara, Nerio tullini. Buckling resistance of pultruded frp profiles under pure compression or uniform bending numerical simulation.
12. ASTM D 638, Standard Test Method for tensile Properties of Plastics (2003).
13. ASTM D 695, Standard Test Method for Compressive Properties of Rigid Plastics (2015).
14. ASTM D 953, Standard Test Method for bearing Strength of Plastics (2002).
15. ASTM D 4923, Standard Specification for Reinforced Thermosetting Plastic Poles (1992).

16. Alexandre Landesmann, Carlos Alexandre Serutia, Eduardo de Miranda Batistaa. Mechanical Properties of Glass Fiber Reinforced Polymer members for Structural Applications (2015).
17. NPTEL lecture 5, 7, 10 and 4.